2. SITES 1033 AND 1034[1]

Shipboard Scientific Party[2]

HOLE 1033A

Date occupied: 19 August 1996

Date departed: 19 August 1996

Time on hole: 3.75 hr

Position: 48°35.437′N, 123°30.205′W

Bottom felt (drill pipe measurement from rig floor, m): 238.0 m

Distance between rig floor and sea level (m): 11.2

Water depth (drill pipe measurement from sea level, m): 226.8

Total depth (from rig floor, m): 247.5

Penetration (m): 9.5

Number of cores: 1

Total length of cored section (m): 9.5

Total core recovered (m): 9.09

Core recovery (%): 95.7

Oldest sediment cored:
    Depth (mbsf): 9.5
    Nature: laminated diatomaceous mud
    Age: Holocene

HOLE 1033B

Date occupied: 19 August 1996

Date departed: 19 August 1996

Time on hole: 6.5 hr

Position: 48°35.439′N, 123°30.200′W

Bottom felt (drill pipe measurement from rig floor, m): 239.9

Distance between rig floor and sea level (m): 11.2

Water depth (drill pipe measurement from sea level, m): 228.7

Total depth (from rig floor, m): 345

Penetration (m): 105.1

Number of cores: 12

Total length of cored section (m): 105.1

Total core recovered (m): 106.35

Core recovery (%): 101.2

Oldest sediment cored:
    Depth (mbsf): 105.1
    Nature: silty clay
    Age: Pleistocene

HOLE 1033C

Date occupied: 19 August 1996

Date departed: 20 August 1996

Time on hole: 4.75 hr

Position: 48°35.445′N, 123°30.200′W

Bottom felt (drill pipe measurement from rig floor, m): 237.3

Distance between rig floor and sea level (m): 11.2

Water depth (drill pipe measurement from sea level, m): 226.1

Total depth (from rig floor, m): 310

Penetration (m): 72.7

Number of cores: 8

Total length of cored section (m): 72.7

Total core recovered (m): 75.87

Core recovery (%): 104.4

Oldest sediment cored:
    Depth (mbsf): 767
    Nature: silty clay
    Age: Pleistocene

HOLE 1033D

Date occupied: 20 August 1996

Date departed: 20 August 1996

Time on hole: 4.75 hr

Position: 48°35.434′N, 123°30.200′W

Bottom felt (drill pipe measurement from rig floor, m): 237.8

Distance between rig floor and sea level (m): 11.3

Water depth (drill pipe measurement from sea level, m): 226.5

Total depth (from rig floor, m): 307.5

Penetration (m): 69.7

Number of cores: 8

Total length of cored section (m): 69.7

Total core recovered (m): 73.78

Core recovery (%): 105.9

Oldest sediment cored:
    Depth (mbsf): 69.7
    Nature: silty clay
    Age: Pleistocene

HOLE 1034A

Date occupied: 20 August 1996

Date departed: 20 August 1996

Time on hole: 4.0 hr

Position: 48°38.000′N, 123°30.000′W

Bottom felt (drill pipe measurement from rig floor, m): 215.0

Distance between rig floor and sea level (m): 11.3

Water depth (drill pipe measurement from sea level, m): 203.7

Total depth (from rig floor, m): 224.5

Penetration (m): 9.5

Number of cores: 1

Total length of cored section (m): 9.5

Total core recovered (m): 10.05

Core recovery (%): 105.8

Oldest sediment cored:
    Depth (mbsf): 9.5
    Nature: laminated diatomaceous mud
    Age: Holocene

HOLE 1034B

Date occupied: 20 August 1996

Date departed: 20 August 1996

Time on hole: 5.75

Position: 48°38.000′N, 123°30.000′W

Bottom felt (drill pipe measurement from rig floor, m): 214.3

Distance between rig floor and sea level (m): 11.3

Water depth (drill pipe measurement from sea level, m): 203.0

Total depth (from rig floor, m): 332.5

Penetration (m): 118.2

Number of cores: 13

Total length of cored section (m): 118.2

Total core recovered (m): 117.22

Core recovery (%): 99.2

Oldest sediment cored:
    Depth (mbsf): 118.2
    Nature: silty clay
    Age: Pleistocene

HOLE 1034C

Date occupied: 20 August 1996

Date departed: 20 August 1996

Time on hole: 5.0 hr

Position: 48°38.005′N, 123°30.000′W

Bottom felt (drill pipe measurement from rig floor, m): 212.5

Distance between rig floor and sea level (m): 11.3

Water depth (drill pipe measurement from sea level, m): 201.2

Total depth (from rig floor, m): 315.5

Penetration (m): 103.0

Number of cores: 11

Total length of cored section (m): 103.0

Total core recovered (m): 97.38

Core recovery (%): 94.5

Oldest sediment cored:
    Depth (mbsf): 103.0
    Nature: silty clay
    Age: Pleistocene

HOLE 1034D

Date occupied: 20 August 1996

Date departed: 21 August 1996

Time on hole: 5.5 hr

Position: 48°37.996′N, 123°30.000′W

Bottom felt (drill pipe measurement from rig floor, m): 212.8

Distance between rig floor and sea level (m): 11.3

Water depth (drill pipe measurement from sea level, m): 201.5

Total depth (from rig floor, m): 313.5

Penetration (m): 100.7

Number of cores: 11

Total length of cored section (m): 103.77

Total core recovered (m): 103.77

Core recovery (%): 103.0

Oldest sediment cored: 100.7

    Depth (mbsf): 100.7
    Nature: silty clay
    Age: Pleistocene

HOLE 1034E

Date occupied: 21 August 1996

Date departed: 21 August 1996

Time on hole: 6.5 hr

Position: 48°37.997′N, 123°29.996′W

Bottom felt (drill pipe measurement from rig floor, m): 212.5

Distance between rig floor and sea level (m): 11.2

Water depth (drill pipe measurement from sea level, m): 201.3

Total depth (from rig floor, m): 302.0

Penetration (m): 89.5

Number of cores: 10

Total length of cored section (m): 89.5

Total core recovered (m): 92.5

Core recovery (%): 103.4

Oldest sediment cored:

Depth (mbsf): 89.5
Nature: silty clay
Age: Pleistocene

Principal Results: Late Pleistocene through Holocene sediments were cored (APC) at two sites in Saanich Inlet, an anoxic fjord located on southern Vancouver Island, British Columbia. The sites were located along the axis of the inlet at 238 and 200 m water depth, separated by ~4.8 km. Three holes were cored at the deeper, southern site, and four holes were cored at the northern site. The southern site was drilled to 105.1 meters below seafloor (mbsf) and the northern to 118.2 mbsf.

The uppermost 40−50 m consist of very well-laminated diatomaceous muds deposited over the past ~7000 yr. These sediments are characterized by lamina "triplets" made up of gray silty mud, deposited during late fall to early spring; olive diatomaceous ooze, deposited in late spring to early summer; and dark olive-gray diatomaceous mud, deposited in late summer and early fall. These triplets (varves) range in thickness from ~3 to 15 mm, averaging ~6 mm. Well-preserved plant debris and charcoal are plentiful throughout this interval, and macroscopic fish remains are common.

Below the very well-laminated interval, sediments become progressively less distinctly laminated and contain abundant whole bivalves and shell fragments, reflecting better oxygenated bottom-water conditions between ~12,000 and 7,000 calendar (cal) yr BP. At this time, relative sea level is believed to have been at least 15 m below that of today; the sill would thus have stood at 55 m water depth or less compared to 70 m today.

The Holocene laminated diatomaceous muds are interrupted by occasional massive intervals, a few centimeters to several decimeters in thickness. These are essentially structureless diatomaceous muds, commonly with a basal zone of discontinuous or fragmented laminae and a capping of diatomaceous ooze.

A 1.0- to 1.5-cm-thick, light gray ash layer, interpreted to be the Mazama Ash (7645 cal yr BP), based on accelerator mass spectrometry (AMS) radiocarbon dates, was cored in most holes, providing an invaluable stratigraphic datum.

The earliest Holocene is marked by a nearly structureless 40-cm-thick gray mud unit with an extremely sharp basal contact and gradational upper contact. It was cored in all holes at both sites and has been dated at ~11,000 cal yr BP. It apparently represents an abrupt discharge event.

The olive-gray diatomaceous muds are gradationally underlain by more massive gray silty mud containing graded sand units, dropstones, and contorted silt and sand laminae. This late Pleistocene glaciomarine unit is older than ~12,000 cal years BP; the oldest AMS date obtained from this unit is ~14,500 cal years BP, ~25 m above the base of the drilled section at the more northerly Site 1034.

The upper parts of the sediment section at both sites were highly disturbed due to gas expansion resulting in generally poor quality acoustic velocity data. The bulk density in the upper well-laminated interval is generally low (1−1.3 Mg/m³), with short intervals of higher bulk density characterized by high magnetic susceptibility; shear strengths are low in this unit (~10 kPa).

The underlying late Pleistocene unit of gray mud has significantly higher bulk densities (1.9−2.1 Mg/m³) and shear strengths (~40 kPa) than the Holocene well-laminated unit. Despite the higher shear strengths in this interval, there is no indication of any ice loading or erosion.

The organic geochemistry of the sediments segregate into two clear diagenetic zones at 50 mbsf (Site 1033) and 80 mbsf (Site 1034). The combination of changes in organic supply and oxygenation in the overlying water column are likely responsible for this situation.

The uppermost zone has anaerobic, organic-rich sediments (1−2.5 wt% C_{org}) and enhanced remineralization. This is indicated by the intense enrichment of nutrient concentrations and extensive bacterial sulfate reduction to sulfide and methanogenesis. The toxic sulfide accumulations preclude infauna in the upper zone, and as a result, the sediments are laminated and not bioturbated.

In the deeper zone, the organic matter is largely refractory and an order of magnitude lower than in the shallower zone (~0.2 wt% C_{org}). The limited diagenesis is indicated by dissolved sulfate close to full marine concentrations (26 mM), low nutrient levels, and an absence of methane. The clearly oxidized conditions support benthic communities that can bioturbate the sediments and destroy any record of lamination.

Preliminary diatom analyses from the well-laminated Holocene show similar species, abundances, and compositions to previous sediment studies and phytoplankton investigations. Dominant species include *Paralia sulcata, Thalassionema nitzschoides, Skeletonema costatum, Thalassiosira gravida, Chaetoceros radicans* (spores), and *Thalassiosira eccentrica*.

Bivalves in the lowermost part of the Holocene are dominated by *Macoma calcarea* and *Axinopsida serricata*. Identified wood samples include Western Red Cedar (*Thuja plicata*) and Pacific Yew (*Taxus brevifolia*).

BACKGROUND AND SCIENTIFIC OBJECTIVES

Introduction

Saanich Inlet, a fjord in southeastern Vancouver Island 25 km north of Victoria, British Columbia (Figs. 1, 2), varies from 0.4 km to 7.6 km over its 26 km length. The average depth of the inlet is 120 m and its maximum depth is 238 m. Two sites along the axis of the fjord were sampled (using the advanced hydraulic piston corer) to obtain as complete a record as possible through the Holocene. Site 1033 was in 238 m water depth in the southern, narrower (~2-km-wide) part of the fjord (48°35.438′N, 123°30.201′W) and was drilled to 105.1 mbsf. Site 1034 (48°38.000′N, 123° 30.000′W) was located in 200 m water depth, 4.8 km to the north of Site 1033, where the inlet is ~4 km in width; this site was drilled to 118.2 mbsf.

Saanich Inlet consists of a single basin separated by a bedrock sill at the north end of the fjord, in Satellite Channel, from open ocean waters in Haro Strait (Fig. 1). This sill rises to within 70 m of the surface, thereby restricting deep-water circulation. As a result, the lower part of the water column, particularly below 200 m, is anoxic. The abundance of freshwater in Haro Strait (Fig. 1) beyond the sill, principally from the Fraser River, plus the high primary productivity in the inlet in spring and summer, and the sluggish estuarine circulation,
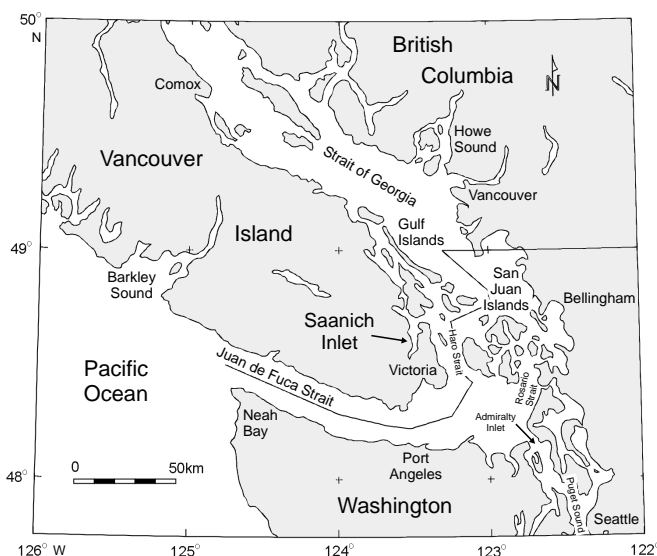

Figure 1. Location map of southwestern British Columbia and northern Washington state showing the location of Saanich Inlet on southernmost Vancouver Island.
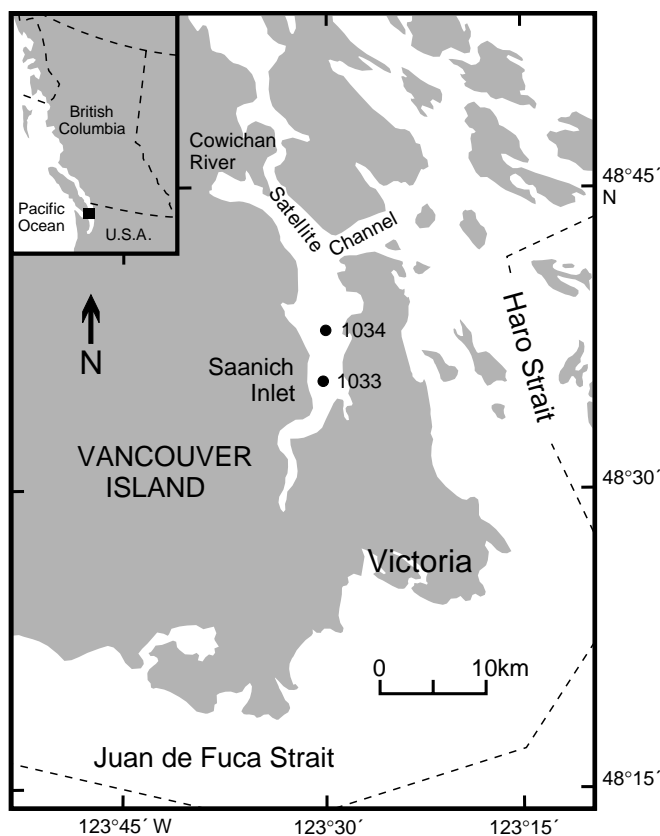
Figure 2. Location map showing the location of Sites 1033 and 1034 in Saanich Inlet.

all contribute to anoxia of bottom waters, a condition that exists virtually throughout the entire year. This anoxia leads to an absence of benthic fauna and the preservation of the seasonal record of deposition as fine laminae of organic-rich and terrigenous sediments.

Holocene sediments in Saanich Inlet consist primarily of dark silt and clay layers deposited during fall and spring freshets and light-colored diatom laminae deposited during spring and summer blooms. Sediments are rhythmically laminated; individual couplets have been shown to be annual deposits and are thus termed varves (Gross et al., 1963; Sancetta and Calvert, 1988; Bobrowsky and Clague, 1990; Blais, 1995). Varved sequences are interbedded with occasional massive beds from a few centimeters to tens of centimeters thick (Buddemeier, 1969; Powys, 1987; Bobrowsky and Clague, 1990; Bobrowsky et al., 1993; Blais, 1995). These beds are somewhat coarser than the laminated sequence and contain sparse brackish, shallow-water benthic foraminifers; they have been interpreted as the products of sediment gravity flows (Bobrowsky and Clague, 1990; Blais, 1995).

There is a trend from more organic-rich basinal sediments in the southern part of the inlet to less in the north, reflecting the greater influence of terrigenous sediment coming from the Cowichan River to the northwest of the mouth of Saanich Inlet and, possibly, from the Fraser River (Figs. 1, 2). Between latitudes 48°34′ and 48°38′N, Brown et al. (1972) reported a decrease in average organic C in the upper 2.5 m of sediment from 4.57% to 2.56%. The greater contribution of terrigenous sediment in the northern part of the inlet is reflected in the 20% to 25% greater thickness of Holocene sediments compared to the southern part. The two sites drilled were chosen, in part, to allow a comparison of diagenetic processes.

Unlike most other fjords in British Columbia and Alaska, the drainage basin for the Saanich Inlet is relatively small and contains no significant rivers. Although a very small amount of sediment enters from the south, at the head of the inlet through the Goldstream River, most of the 9×10^4 tons of terrigenous sediment deposited annually in the fjord comes from the sediment plume of the Cowichan River that enters Satellite Channel to the northwest of the head of the inlet (Gross et al., 1963; Drinnan et al., 1995; British Columbia Ministry of Environment, Lands and Parks, 1996); a minor amount comes from the Fraser River plume, which, on rare occasions, penetrates the inlet.

Sedimentation rates for varved sediments were estimated, based primarily on relatively short piston and gravity cores (representing at most 4600 yr), to be between 4 and 6 mm per year (e.g., Gucluer and Gross, 1964; Blais, 1995). These authors estimate that between 0.24 and 0.36 g/cm^3 of dry sediment is deposited annually. Bobrowsky and Clague (1990) report average varve thicknesses over the past 1400 yr of 4 mm; overall sedimentation rates during this period, including the intercalated more massive silty units, averaged ~8.84 mm/yr. Gucluer and Gross (1964) present radiocarbon data for the past 3100 yr that yield sedimentation rates of 4.1 to 6.3 mm/yr. Buddemeier (1969), from a core located somewhat closer to the Goldstream River delta at the southern end of the inlet, obtained average varve thicknesses (i.e., annual accumulation) of 5.7 mm at ~18 m depth in the core to ~14.2 mm at 3 m depth; this difference was found to be in general accord with sediment compaction. He determined average accumulation rates based on radiocarbon dating over the past 3860 yr to be 4.89 mm/yr. Blais (1995) shows that uncompacted varves range from ~4.5 mm in the southern inlet to 12.71 in the north, whereas compacted varves range from 4.4 to ~9.0 mm.

Geologic Setting

Saanich Inlet lies in the Nanaimo Lowlands physiographic region (Holland, 1964). The terrain surrounding the inlet ranges from gently rolling in the north to steeply sloping in the south. Relative to much of Vancouver Island, the area has generally low relief. The fjord is underlain by volcanic, plutonic, and sedimentary rocks, as well as their metamorphic equivalents, ranging in age from Devonian/Carboniferous through middle and possibly Late Cretaceous (Muller, 1981). Lithologies include meta-andesite, gneissic diorite, greenschist, amphibolite, argillite, dacite, tuff, breccia, quartz diorite, basalt, diabase, gabbro, andesite, rhyolite, granodiorite, quartz monzonite, and limestone. Prominent basement faults (45 Ma), trending northeast-southwest, cut through the area.

Surficial sediments surrounding Saanich Inlet were deposited during the last (Wisconsinan) glaciation and the Holocene; they were mapped in detail most recently by Blyth and Rutter (1993) and Blyth et al. (1993). Maximum ice thicknesses in the area are estimated to have been between 1100 and 1500 m at ~15,000 ^{14}C yr BP with most of southern Vancouver Island ice free by 13,000 ^{14}C yr BP (Alley and Chatwin, 1979). Three principal sedimentary units are found in the region. The oldest, Vashon Drift, consisting of till, sand, and gravel, was deposited by a lobe of Cordilleran ice during the Fraser Glaciation (Clague, 1994). Capilano sediments, deposited in the sea at the end of the Fraser Glaciation (Clague, 1994), consist of sand, gravel, silt, and clay. Holocene sediments consist of fluvial, marine, lacustrine, and organic deposits (Clague, 1994).

Holocene Climatic Record

Prior to ~13,000 ^{14}C yr BP, Vancouver Island was characterized by a cool to cold and possibly dry climate (Hebda, 1983, 1995) as ice retreated rapidly from the region. Soon after retreat, between ~12,000 and 10,000 ^{14}C yr BP, highly mixed forest assemblages, with no extensive modern equivalents, appeared along the coast from Oregon to the Queen Charlotte Islands. These assemblages have made it difficult to ascertain precisely the nature of climate in this interval (Hebda and Whitlock, 1997). Mathewes (1993) has suggested that these

unusual combinations of species may be related to Younger Dryas cooling.

Between ~10,000 and 7,000 ^{14}C yr BP, the vegetation types are indicative of an interval of severe summer drought conditions, reflecting greater-than-present summer solar radiation and less-than-present winter solar radiation (Mathewes, 1985; Hebda and Whitlock, 1997). Temperatures are estimated to have been from 2° to 4°C warmer than today for much of this interval, reaching a maximum between ~9000 and 7500 ^{14}C yr BP. The abundance of charcoal at various sites during this time period suggests that fires were more frequent than today (Cwynar, 1987; Hebda and Whitlock, 1997).

A transition, taking 3000 to 4000 yr, from a warm, dry climate to moderate, moist conditions began shortly before 7000 ^{14}C yr BP (Hebda and Whitlock, 1997). Considerable attention by several researchers has been devoted to the study of conditions at ~6000 ^{14}C yr BP (summarized by Hebda, 1995). Hebda (1995) concludes that at this time southern Vancouver Island was warmer (by perhaps 1°C) than today, but it had comparable precipitation and was relatively moist compared to the early Holocene.

Conditions warmer than today persisted until ~5000 ^{14}C yr BP, with the clearest indications of cooling occurring at ~4000 ^{14}C yr BP. Temperatures have been essentially equivalent to those of today since ~4000 ^{14}C yr BP (Hebda, 1995).

Sea-level position in this region throughout the late Quaternary has been governed by both eustatic lowering and isostatic depression and rebound. At ~12,000 ^{14}C yr BP, the sea level is estimated to have been ~15 m above present (Clague et al., 1982). Between 11,000 and ~4,000 ^{14}C yr BP, it had fallen to as much as 15 m below the modern position; dating and elevation controls on this part of the sea-level curve are, however, limited. There is some suggestion from elsewhere in the area (Linden and Schurer, 1988) that sea levels during this interval could have been as much as 55 m below present at ~9000 ^{14}C yr BP. The sea level over the past 4000 yr has been within a few meters of present day. An important implication of the significantly lowered sea levels immediately following deglaciation is that the sill depth at the entrance to Saanich Inlet would have been much less than the 70 m depth of today. It is in the early part of this interval that sediments at both Sites 1033 and 1034 reflect well-oxygenated bottom waters, as evidenced by the absence of laminated sediments and the presence of a rich bivalve community.

Oceanography

The oceanography of the southern Strait of Georgia region, including Saanich Inlet, is governed by surface freshwater discharge from the Fraser River, intrusion of partially mixed high salinity water from the Pacific through the Strait of Juan de Fuca and Haro Strait, and by the strength and direction of the prevailing winds in the area at various times of year (Thomson, 1994). The Fraser River plume has a particularly strong influence on mixing. In winter, intense cooling can lead to strong vertical convection and a near-homogeneous upper layer. During the summer, when Fraser discharge is highest, the upper layer becomes highly stratified, a combination of runoff and higher ambient temperatures. In summer, this upper layer is from 2 to 10 m thick and is pushed southward in the Strait of Georgia (and towards Saanich Inlet) under the influence of the prevailing northwest winds.

Deep water renewal in all seasons involves a mixture of higher salinity offshore waters and waters originating in the Strait of Georgia. It is essentially a continuous process that varies because of changing conditions both offshore (intensity of upwelling-downwelling) and in the Strait (volume and duration of Fraser freshet). The water that spills into various basins of the Strait of Georgia, including Saanich Inlet, is strongly modulated by processes on the outer coast. "Long-term changes in the strength and duration of upwelling off the coast, such as those associated with strong El Niño–Southern Oscillation events will impact on the water properties of the channels adjoining Juan de Fuca Strait. Movement of higher salinity water into the strait

at depth in summer as a result of upwelling on the adjacent continental shelf also will affect the generation of internal tides in the vicinity of sills or marked topographic features" (Thomson, 1994). These would include the sill at the entrance to Saanich Inlet.

Near-surface circulation patterns in Saanich Inlet are highly variable, the product of both tidal fluctuations and wind (British Columbia Ministry of Environment, Lands and Parks, 1996). Currents generally move southward along the western side of the inlet on flood tides and northward along the eastern shore during ebbs (D. Stucchi, pers. comm., 1997). In the northern part of the inlet, currents above the sill depth are products of tidal and estuarine circulation from Satellite Channel, with freshwater inputs largely from the Cowichan River. The currents typically are slow (e.g., mean at 14 m depth, 4.9 cm/s), but can reach maximum values at 44 m depth of >25 cm/s. In the southern part of the inlet, below sill depth, currents are sluggish (mean at 88 m depth, 5.7 cm/s; EnviroEd Consultants Ltd., 1995). A central counterclockwise surface gyre is apparent during at least the summer season, when estuarine circulation is weakest (British Columbia Ministry of Environment, Lands and Parks, 1996).

There is evidence from sediment trap studies of a strong control on primary productivity exerted by tidal cyclicity (F. Whitney, pers. comm., 1997) and may be seen in fine sediment laminae of shallow cores (M. McQuoid, pers. comm., 1997). The possibility that the tidal regime may also affect terrigenous inputs to the inlet and that these fluctuations in both biogenic and terrigenous sediment components may be recorded in sediment cores is being investigated.

The estuarine circulation affects only the waters above the sill, which acts a barrier limiting exchange of bottom waters in the fjord with those of the open ocean in Haro Strait. Minimum salinities in Haro Strait occur between May and early July, related to the freshet of the Fraser River (Anderson and Devol, 1973; Stucchi and Giovando, 1983; Fig. 3). Renewal of bottom waters in Saanich Inlet can only occur when surface salinities in Haro Strait exceed those of the bottom waters (i.e., when freshwater input to the southern Strait of Georgia is at a minimum). This bottom water renewal occurs at the ends of August, September, and October, driven by and limited by fortnightly tidal mixing (Herlinveaux, 1962; Anderson and Devol, 1973; Stucchi and Giovando, 1983; Fig. 3). Renewal events typically last 8 to 10 days each month and, to a depth of 100 m, occur annually, though to varying degrees. Renewal events reaching 200 m are less frequent, occurring in only about half of the years during which measurements have been made (Anderson and Devol, 1973; Pickard, 1975; Stucchi and Giovando, 1983). It has been suggested that interannual variability in deep water and its renewal may depend to a very great extent on variability in the source waters (Stucchi and Giovando, 1983). The deep-water renewal events would bring well-oxygenated waters into the bottom of the fjord and displace the existing anoxic waters upward, with relatively minor mixing along the interface between the two (R.E. Thomson, pers. comm., 1997). The depth differences and separation of the two drilling sites should permit an assessment of the basinal extent of past flushing events.

Water temperatures in the fjord fall within the expected range for fjords in British Columbia (Pickard, 1975). At <50 m depth, temperature changes are seasonal, ranging from ~5°C in January to ~18°C in July. Below 50 m, temperatures are stable at 8°–9°C. Surface-water salinities range widely, depending on precipitation and drainage (Herlinveaux, 1962).

Several studies of the species composition and seasonality of phytoplankton assemblages have been undertaken over the past 20 yr and are summarized in Hobson and McQuoid (1997). A well-developed diatom bloom occurs in April or May, composed of the genera *Minidiscus* sp. (Sancetta, 1989) and *Thalassiosira,* including the species *pacifica, eccentrica, gravida, nordenskiöldii,* and *rotula,* and, in some instances, a small form of *Skeletonema costatum.* Later in the bloom, this early assemblage is replaced by *Chaetoceros compressus, C. radicans, C. socialis,* and a large form of *S. costatum.* The end of the bloom, because of decreasing nutrient fluxes as stratification increases, is marked by a shift in taxonomic composition to a diverse
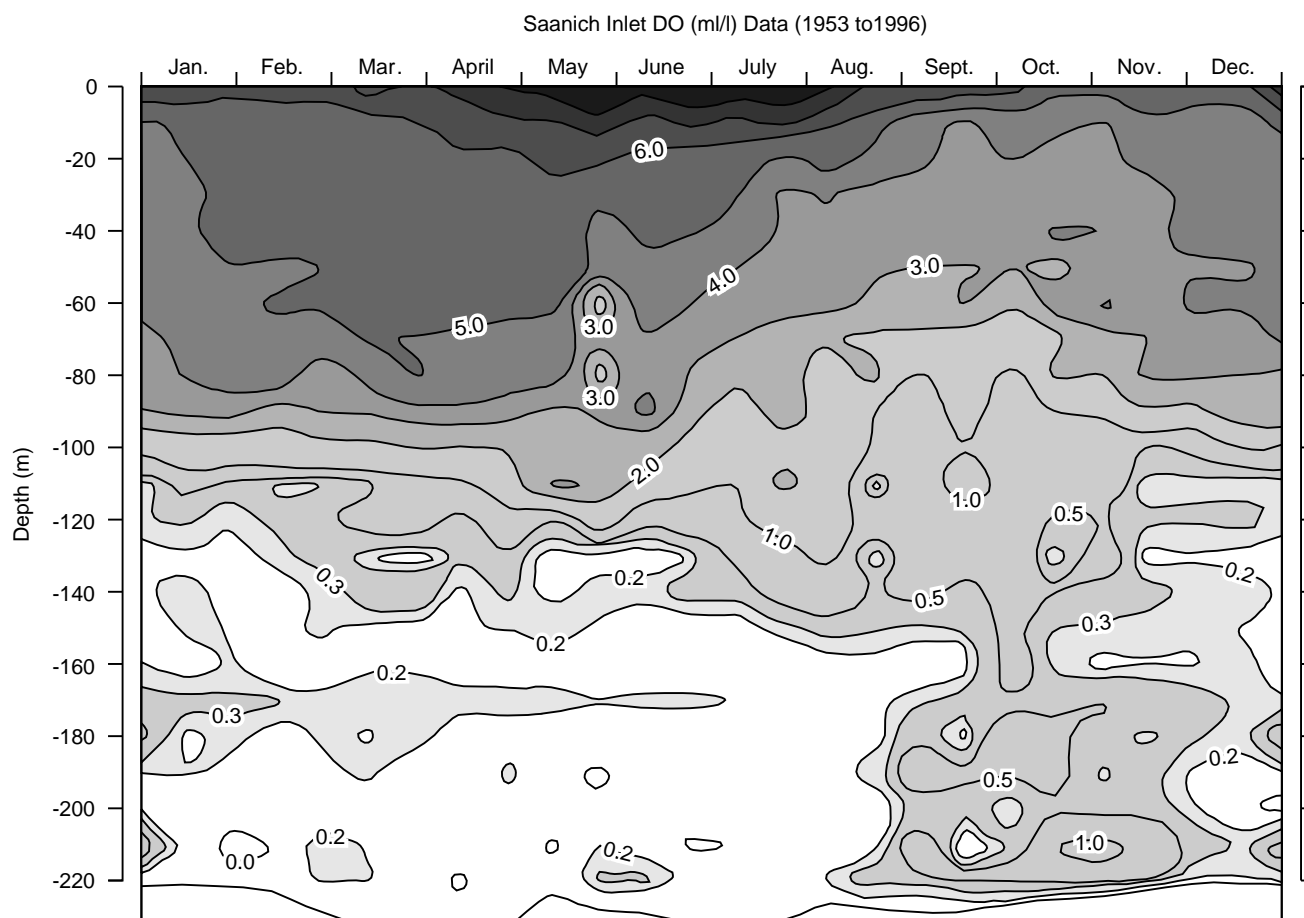
Saanich Inlet DO (ml/l) Data (1953 to 1996)

Figure 3. A summary of dissolved oxygen content (mL/L) in Saanich Inlet waters throughout the year. The diagram is a composite of all data collected from 1953 to 1996. (D. Stucchi, Institute of Ocean Sciences, unpubl. data).

group of nanoflagellates and dinoflagellates through June, July, and August. Nutrient fluxes can occasionally increase through the summer, resulting in short-lived diatom blooms, caused by storms or tidal advection of nutrient-rich water. These blooms are dominated by *Corethron criophilium, Ditylum brightwellii, Detonula pumila, Eucampia zoodiacus, Leptocyclindrus danicus, Nitzschia pungens,* and *S. costatum.* Mixing and advection become more intense in fall, resulting in blooms of *Chaetoceros compressus, concavicornis, debilis, diadema, didymus, lorenzianus,* and *vanheurkii, Corethron criophilium, Rhizosolenia setigera, S. costatum,* and *Thalassionema nitzschoides.* Most diatoms disappear in October or early November.

These annual changes have occurred, in general, over the past century or so in the inlet. An exception, however, is the appearance of *Rhizosolenia setigera* (probably) after 1942. Also, low abundances of *S. costatum* correlate well with El Niño events.

OBJECTIVES

Paleoenvironments

Continuous coring through the Holocene sediments in Saanich Inlet offers the rare opportunity of sampling, at a seasonal resolution, both terrestrial and oceanographic temperate latitude changes over the past 8,000–10,000 yr and at a lower resolution into the late Pleis-

tocene. There has been considerable interest expressed in being able to continue these investigations back through to deglaciation to better understand the succession of floras in this wet temperate region following deglaciation, climatic cyclicity during the Holocene, and the links among oceanographic, climatic, and terrestrial environmental conditions. Previous studies have examined modern processes controlling diatom accumulation in Saanich Inlet (Sancetta, 1989), at the annual cycle of sedimentation in the fjord (Sancetta and Calvert, 1988), and various other aspects of faunal (e.g., changes in fish communities; V. Tunnicliffe, pers. comm., 1995), and terrestrial flora (R. Hebda, pers. comm., 1995). Other signals, such as the prevalence of fire and the human occupation of coastal sites, have also been detected in piston cores.

The objective of the interdisciplinary investigations is to develop an ultra-high resolution paleoecologic record of the inshore northeast Pacific for the last 8,000–10,000 yr or so using organic remains preserved in Saanich Inlet sediments. This sequence will be related year by year to a 9000-yr tree-ring climate record and regional terrestrial environmental framework that has been developed for a lake site only 5 km distant on climatically sensitive southeast Vancouver Island. Heusser's (1983) study of Saanich Inlet, Hebda's (1995) regional summary, and other investigations (e.g., Allen, 1995) have established a sound, low-resolution palynological framework and have shown that the vegetation in the area is highly sensitive to climate change. In particular, attention will be focused on several critical

intervals of rapid climate change: the Pleistocene/Holocene transition; the Younger Dryas (or similar episodes of cooling and landscape instability in the early Holocene), the ~9 ka warm, dry interval, the ~7.5–6.8 ka transition to a moist climate, and the 4.5–4 ka cooling. Other intervals that have been the focus of intensive interdisciplinary investigations elsewhere (e.g., 6,000 yr BP) will also be studied (Hebda, 1995).

The lower part of the cored section of gray, inorganic sediments older than ~12,000 cal yr BP, offers the opportunity of studying sedimentary processes associated with deglaciation in the region. These glaciomarine sediments, sampled at both Sites 1033 and 1034, have been dated at more than 14,500 cal yr BP.

Paleoseismicity

Driven by the concern that a great subduction earthquake or major crustal earthquake in southwestern British Columbia or northwestern Washington could cause widespread damage, several investigators focused their attention on the geologic record for evidence of past events that could provide insights into the frequency and magnitude of future earthquakes. The paucity of large earthquakes within historical time in the region has required researchers to search for proxy data to ascertain whether such events have, in fact, occurred, and, if so, with what frequency. Because of the remarkable stratigraphic preservation and resolution in Saanich Inlet sediments, several recent studies have been undertaken focusing on the more silty massive units in the sequence as possible indicators of past earthquake events (e.g., Bobrowsky and Clague, 1990; Bobrowsky et al., 1993; Blais, 1992). These units have been interpreted as seismically triggered sediment gravity flows and, in the uppermost part of the sediment column (last 1500 yr), would indicate an average of one flow every 100 yr (Blais, 1995); this estimate appears compatible with projections made from historical seismicity data and are compatible with the rate of liquefaction events seen in Pleistocene lake deposits 100 km to the south in Washington state (Sims, 1975). Based on other evidence from the region, larger earthquakes (greater than magnitude 8 and believed to be of subduction origin) have a return period of ~600 yr. However, to date, neither the historical nor geological record is sufficiently long to determine confidently the frequency of great subduction earthquake events or major crustal events.

Considerable more work is required to improve the confidence in this set of proxy data; much would be added by demonstrating that this rate has been consistent over a longer time interval, such as throughout the Holocene. A continuous record of seismically induced events over a long period would be an extremely valuable contribution to seismic hazard assessment in the region.

Sediment Diagenesis

Saanich Inlet has long been recognized as a model environment for studies of organic diagenesis and low-temperature remineralization reactions in a shallow, temperate, isolated anoxic basin. The combination of restricted water circulation, seasonal stratification, and moderate rates of organic matter accumulation have led to dysaerobic bottom waters and anoxic sediments. This proposal is a good companion and comparative site to the Ocean Drilling Program (ODP) drilling of Santa Barbara Basin during Leg 146.

Benchmark studies were undertaken more than 20 yr ago (e.g., Gross et al. 1963; Gucluer and Gross, 1964; Nissenbaum et al., 1972; Presley et al., 1972; Brown et al., 1972). Saanich Inlet was selected for these studies for many reasons: (1) the sediments contain significant amounts of organic carbon (up to 5%), making it a possible recent analogue of black shales; (2) very high sedimentation rates (4–5 times faster than in Santa Barbara Basin, for example) enable very detailed studies of early diagenetic processes; and (3) two very distinct sources of organic material exist, mainly humus-rich soil from highly forested areas around the inlet and phytoplankton, primarily diatoms. Previous studies in Saanich Inlet looked at major, minor, and trace element concentrations in interstitial waters and various sediment fractions, dissolved carbon dioxide, phosphate, sulfate, methane and ammonia, carbon isotopes, various hydrocarbons, and amino, humic, and fulvic acids. Most of these investigations, however, focused only on the upper 2 to 3 m of the sediment column.

Several geochemical factors make Saanich Inlet particularly attractive as a drilling site. The broad spectrum of diagenetic stages, including aerobic to sulfate reduction and methanogenic fermentation, are represented and well characterized in the various Saanich Inlet sediments. Climatic variations during the Holocene (see above) are intricately recorded in the sediments (V. Tunnicliffe and M. Whiticar, pers. comm., 1997). In addition to the sedimentologic evidence, initial organic and stable isotope geochemical investigations suggest that the signals of seasonal and climatic changes are faithfully recorded in the sediments. Significant climatic and redox shifts are recorded in Saanich Inlet sediments, enabling isotopic and molecular biomarker studies of proxy signals. Furthermore, long-term geochemical and ocean chemical measurements in Saanich Inlet have been made of the dissolved and particulate constituents in the water column and in the uppermost 3 m of sediment. These determinations, which include nutrients, gases, inorganic solids as well as intensive surveys of biological populations, are distinct advantages of the location. Analysis of sediments from Saanich Inlet affords a unique opportunity for microbiologists and geochemists to provide detailed work on diagenesis of deeper seated sediments. Previously, most of the microbial work has been severely restricted by standard ODP operating conditions such as (1) long periods at sea without shore lab contact (difficult to send critical fresh samples to shore-based labs); (2) insufficient facilities available or accessible aboard the *JOIDES Resolution* for specialized work-up of bacterial cultures and unstable compounds; and (3) constraints on the use of radiotracers.

These reasons make Saanich Inlet extremely well suited for advanced research in marine biogeochemistry. This is especially true for investigating and applying molecular and stable isotope techniques to biomarker molecules as proxy signals to assess climatic changes. The drilling at this site is also a superb biogeochemical opportunity to investigate the bacterial processes of methanogenesis and methylotrophy. Again, the site offers a unique chance to investigate organic compound classes, such as lipids and amino acids, and their response to changing redox and climatic conditions.

Saanich Inlet is also a rare and fundamental opportunity for marine microbial ecologists to obtain deeper sediment samples with which they can investigate the activities and processes of bacterial and viral assemblages.

Site Surveys

Single-channel seismic surveys (Figs. 4, 5) were undertaken from the *John P. Tully* using a 40-in^3 air gun with a wave-shaping kit and a 3-s firing rate at 2000 psi. The streamer was a 30-m array consisting of 50 elements in a 16-m active section situated between two 7-m dead sections. The air gun was towed at a 1-m depth, 15 m astern of the vessel.

The analog signal was digitally sampled at 4 kHz for 1 s. The raw signal was first passed through a 40- to 5000-Hz bandpass filter with a 20 dB gain. Processing involved bottom picking (mute to water bottom), predictive deconvolution for multiple removal, linear time-varying gain (TVG) to enhance basement, and a 40- to 1000-Hz bandpass filter.

Based on previous piston coring experience in Saanich Inlet, it was anticipated that the Holocene was represented by the highly stratified uppermost ~100 ms (two-way traveltime) part of the section (Fig. 5). The sites were therefore selected to penetrate completely this interval and to sample the uppermost part of the underlying nearly structureless interval, anticipated to be stiff, Pleistocene glaciomarine muds.
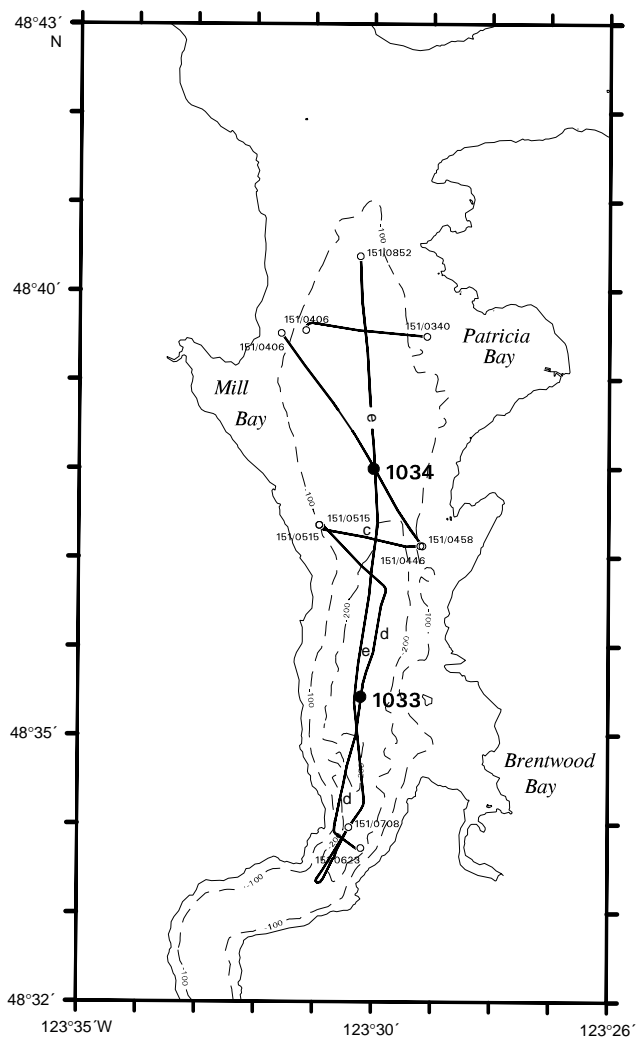
Figure 4. Shiptrack of single-channel air gun seismic site survey undertaken from *John P. Tully*. Seismic profiles are presented in Figure 5.

OPERATIONS

Port Call in Victoria, B.C.

Leg 169S began with the first line ashore in Victoria, B.C., at the Ogden Point, WestCan Terminal, Pier A, at 1900 hr on 15 August (local time). Normal port call activities and unloading and loading were completed on 16 and 17 August. Extensive tours were conducted for the public, media, and officials with ~1400 people touring the ship in 2 days. Meetings were held to review the shallow-water coring guidelines and operating procedures. The 500-ton elevators were used to save time in case a drive off occurred with little warning. H_2S and gassy pressured-core-liner safety procedures were reviewed. Two chiefs from the Tsartlip and Tseycum villages welcomed the ship to their waters and presented the ship with a beaded eagle feather.

Transit From Victoria To Site SI-1B (Site 1033)

The last line ashore was at 0615 hr on 19 August, and the ship departed for Saanich Inlet. The ship was stopped twice to adjust the main magnetic compass magnets. The 48-nmi transit from Victoria to proposed site SI-1B required 6.25 hr at an average speed of 7.36 kt. The Pilots Association required a full time pilot aboard ship for Saan-

ich Inlet operations, including coring in dynamic positioning systems (DPS) mode. A small boat therefore brought three pilots out to work their 8-hr shifts each day.

The Canadian Coast Guard buoy tender Tsekoa II and a Fast Response Craft were met at proposed site SI-1B at 1200 hr on 19 August and immediately started enforcing the 300-m safety zone around the ship, as numerous pleasure craft were in the area.

Hole 1033A

The beacon was dropped at proposd site SI-1B on differential global positioning system (dGPS) mode coordinates: 48°35.433′N, 123°30.201′W. A Benthos shallow-water beacon was dropped on a long 7-m tether (because of 5 m of very soft, soupy mud at the sediment/water interface) at 1253 hr on 19 August; however, the Benthos beacon had an erratic signal and was unusable. A modified low power (190–196 dB) Datasonics 354M retrievable commandable beacon was dropped at 1305 hr to evaluate its performance in shallow water and to provide a backup in the narrow inlet. The ship was offset 50 m (9°) from the Datasonics beacon to test signal strength for a shallow water drill, and all four hydrophones were still effective. The offset warning lights were set at 4% (yellow) and 8% (red) of water depth.

The corrected precision depth recorder (PDR) water depth was 241.4 meters below rig floor (mbrf). Core 169S-1033A-1H was taken with the bit at 238 mbrf, but the gassy core was blown out of both the top and bottom of the core liner, and several large gas voids were present in the liner. The calculated water depth was 238.0 mbrf; however, the actual seafloor depth and driller's core depths are probably deeper. The 9.09 m of core that remained in the liner was archived as Core 169S-1033A-1H, 0–9.5 mbsf.

Hole 1033B

The ship remained at the site, and Hole 1033B was spudded with the bit at 231 mbrf. Although the very soupy and gassy core was falling out of the core liner when retrieved, 0.62 m of sediment was recovered for a calculated seafloor depth of 239.9 mbrf. Because core was lost out of the barrel, the actual seafloor depth and driller's core depths are probably deeper by several meters. APC Cores 169S-1033B-1H through 12H were taken from 0 to 105.1 m with 88%–100% recovery (Table 1). No orientation or temperature measurements were taken in any holes at Site 1033. H_2S was detected to 100+ ppm in the upper three sections of Core 169S-1033A-1H, but negligible H_2S was noted below that. The hole bottomed in gray mud, and the base of laminated sediments was found at roughly 54 m, much shallower than expected; therefore, Holes 1033C and 1033D were terminated earlier than predicted.

Cores 169S-1033B-7H, 9H, 11H, and 12H appeared to be "partial strokes," but recovered full cores ("partial strokes" are indicated when the pressure in the pipe does not bleed off quickly at the end of the stroke, which may indicate less than a 9.5-m APC core barrel stroke). Some core suck-in (syringe effect) therefore is possible, with core disturbance at the bottom of those cores. The hole was plugged with gel mud.

Hole 1033C

The ship was moved 10 m north of Hole 1033A and 1033B. Hole 1033C was spudded with the bit at 234 mbrf and had good recovery; therefore, the sea floor depth is 237.3 mbrf. APC Cores 169S-1033C-1H through 8H were taken from 0 to 72.7 m with 100% recovery. The hole was plugged with gel mud.

Hole 1033D

The ship was moved 20 m south of Hole 1033C. APC Cores 169S-1033D-1H through 12H were taken from 0 to 105.1 m with 100% recovery. The seafloor depth is 237.8 mbrf. Core 169S-1033D-
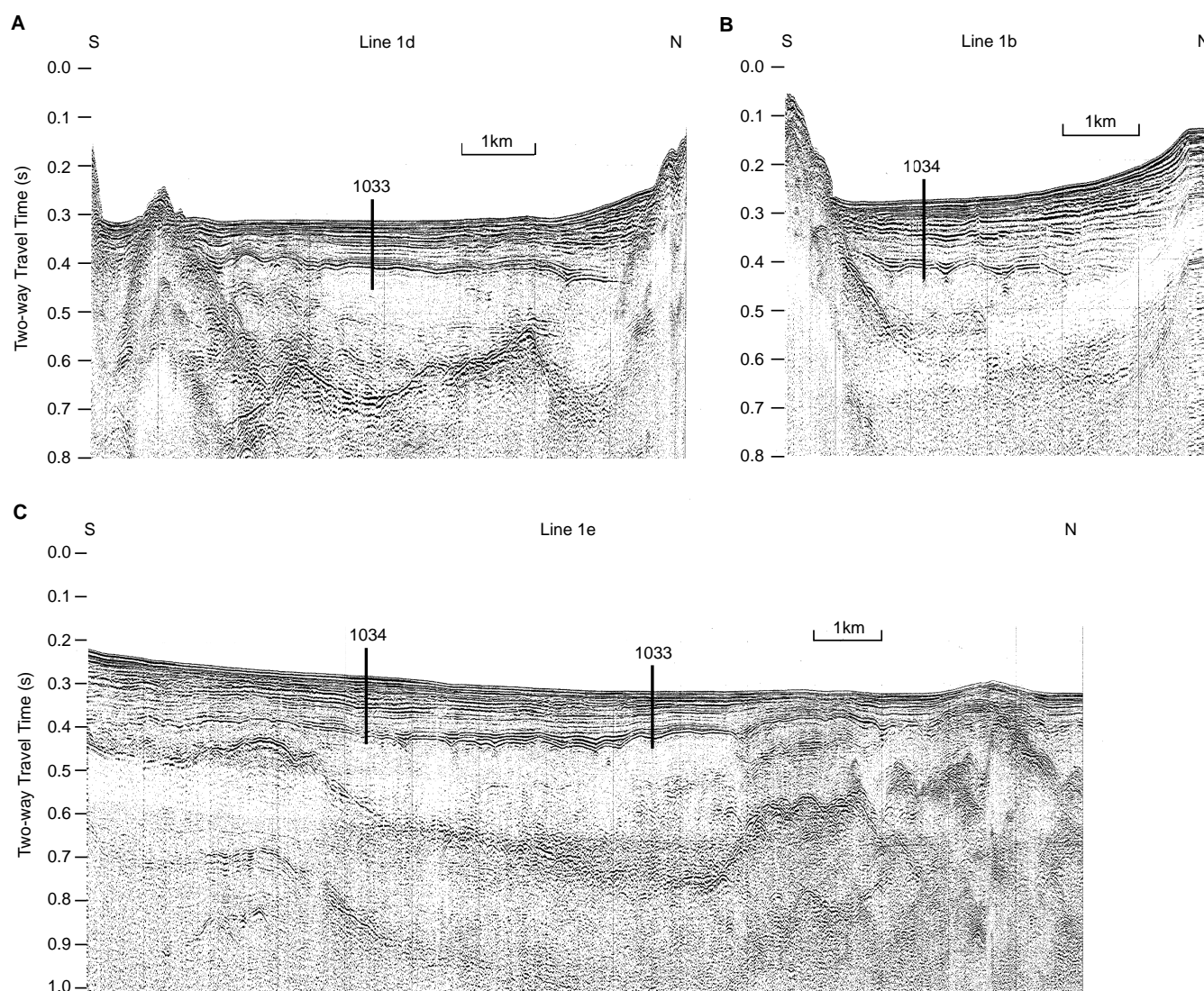
Figure 5. **A.** Single-channel seismic Profile d (151/0623-0852) through Site 1033 (see Fig. 4 for location). **B.** Single-channel seismic profile b (151/0406-0458) through Site 1034 (see Fig. 4 for location). **C.** Single-channel seismic Profile e (151/0708-0852) through Sites 1033 and 1034 (see Fig. 4 for location).

7H appeared to be a partial stroke with full recovery. The bit cleared the seafloor at 0830 hr on 20 August. The Datasonics beacon was recovered. The hole was plugged with gel mud.

There was no constant current in the inlet, and tidal currents up to 1 kt produced less than 2 m offset. There were numerous curious pleasure boats and water taxis in the area, and the assistance of the Canadian Coast Guard was invaluable in maintaining adequate clearance.

Transit to Site SI-2B (Site 1034)

The bit was pulled to 125 mbrf for the transit in DPS mode to Site 1034. The 2.6 nmi transit was completed in 2.5 hr. A modified low power (190–196 dB) Datasonics 354M retrievable commandable beacon was dropped at 1035 hr on 20 August on dGPS coordinates: 48°38.000′N, 123°30.000′W.

Hole 1034A

Hole 1034A was spudded at 1200 hr on 20 August. APC Core 169S-1034A-1H had gassy core extruding from the top of the liner. The calculated water depth was 215.0 mbrf; however, the actual seafloor depth (and driller's core depths) should probably be the same for Hole 1034B. The 10.05 m of core that remained in the liner was archived as Core 169S-1034A-1H (0–9.5 m; see Table 2).

Hole 1034B

The ship was not moved. Core 169S-1034B-1H provided a good seafloor measurement of 215.0 mbrf. APC Cores 169S-1034B-1H through 13H were taken from 0 to 118.2 m, with recovery from 84% to 100%. No cores were oriented at Hole 1034B. Temperature measurements were taken only on Hole 1034E. The last three cores were

Table 1. Coring summary for Site 1033.

Core	Date (August 1996)	Time (UTC)	Depth (mbsf)	Length cored (m)	Length recovered (m)	Recovery (%)
169S-1033A-						
1H	19	2310	0.0–9.5	9.5	9.09	95.7
Coring totals:				9.5	9.09	95.7
169S-1033B-						
1H	19	2340	0.0–0.6	0.6	0.62	100.0
2H	20	0005	0.6–10.1	9.5	9.88	104.0
3H	20	0025	10.1–19.6	9.5	10.31	108.5
4H	20	0040	19.6–29.1	9.5	10.24	107.8
5H	20	0110	29.1–38.6	9.5	10.11	106.4
6H	20	0130	38.6–48.1	9.5	10.25	107.9
7H	20	0155	48.1–57.6	9.5	9.59	101.0
8H	20	0235	57.6–67.1	9.5	9.61	101.0
9H	20	0335	67.1–76.6	9.5	9.46	99.6
10H	20	0350	76.6–86.1	9.5	9.44	99.3
11H	20	0430	86.1–95.5	9.4	8.51	90.5
12H	20	0510	95.5–105.0	9.5	8.33	87.7
Coring totals:				105.0	106.35	101.3
169S-1033C-						
1H	20	0655	0.0–6.2	6.2	6.13	98.9
2H	20	0710	6.2–15.7	9.5	10.11	106.4
3H	20	0735	15.7–25.2	9.5	10.23	107.7
4H	20	0755	25.2–34.7	9.5	10.16	106.9
5H	20	0820	34.7–44.2	9.5	9.86	104.0
6H	20	0855	44.2–53.7	9.5	9.77	103.0
7H	20	0920	53.7–63.2	9.5	9.99	105.0
8H	20	1000	63.2–72.7	9.5	9.62	101.0
Coring totals:				72.7	75.87	104.3
169S-1033D-						
1H	20	1140	0.0–3.2	3.2	3.17	99.0
2H	20	1210	3.2–12.7	9.5	10.09	106.2
3H	20	1230	12.7–22.2	9.5	10.14	106.7
4H	20	1250	22.2–31.7	9.5	10.15	106.8
5H	20	1310	31.7–41.2	9.5	10.15	106.8
6H	20	1335	41.2–50.7	9.5	10.09	106.2
7H	20	1355	50.7–60.2	9.5	10.08	106.1
8H	20	1420	60.2–69.7	9.5	9.91	104.0
Coring totals:				69.7	73.78	105.8

Table 2. Coring summary for Site 1034.

Core	Date (August 1996)	Time (UTC)	Depth (mbsf)	Length cored (m)	Length recovered (m)	Recovery (%)
169S-1034A-						
1H	20	1710	0.0–9.5	9.5	10.05	105.8
Coring totals:				9.5	10.05	105.8
169S-1034B-						
1H	20	1935	0.0–4.2	4.2	4.25	101.0
2H	20	1956	4.2–13.7	9.5	10.05	105.8
3H	20	2010	13.7–23.2	9.5	10.24	107.8
4H	20	2030	23.2–32.7	9.5	10.15	106.8
5H	20	2045	32.7–42.2	9.5	10.15	106.8
6H	20	2100	42.2–51.7	9.5	10.22	107.6
7H	20	2115	51.7–61.2	9.5	9.90	104.0
8H	20	2130	61.2–70.7	9.5	9.53	100.0
9H	20	2150	70.7–80.2	9.5	7.71	81.1
10H	20	2300	80.2–89.7	9.5	9.19	96.7
11H	20	2330	89.7–99.2	9.5	9.58	101.0
12H	20	2350	99.2–108.7	9.5	8.27	87.0
13H	21	0015	108.7–118.2	9.5	7.98	84.0
Coring totals:				118.2	117.22	99.2
169S-1034C-						
1H	21	0200	0.0–8.0	8.0	8.00	100.0
2H	21	0225	8.0–17.5	9.5	10.05	105.8
3H	21	0250	17.5–27.0	9.5	10.18	107.1
4H	21	0310	27.0–36.5	9.5	10.12	106.5
5H	21	0330	36.5–46.0	9.5	10.10	106.3
6H	21	0345	46.0–55.5	9.5	10.11	106.4
7H	21	0400	55.5–65.0	9.5	8.93	94.0
8H	21	0425	65.0–74.5	9.5	1.60	16.8
9H	21	0445	74.5–84.0	9.5	9.68	102.0
10H	21	0505	84.0–93.5	9.5	9.24	97.2
11H	21	0535	93.5–103.0	9.5	9.37	98.6
Coring totals:				103.0	97.38	94.5
169S-1034D-						
1H	22	0705	0.0–5.7	5.7	5.67	99.5
2H	22	0725	5.7–15.2	9.5	10.09	106.2
3H	22	0745	15.2–24.7	9.5	10.20	107.3
4H	22	0805	24.7–34.2	9.5	10.10	106.3
5H	22	0835	34.2–43.7	9.5	9.86	104.0
6H	22	0900	43.7–53.2	9.5	10.18	107.1
7H	22	0930	53.2–62.7	9.5	9.89	104.0
8H	22	0950	72.2–81.7	9.5	9.91	104.0
9H	22	1015	72.2–81.7	9.5	9.93	104.0
10H	22	1040	81.7–91.2	9.5	8.94	94.1
11H	22	1105	91.2–100.7	9.5	9.00	94.7
Coring totals:				100.7	103.77	103.1
169S-1034E-						
1H	22	1240	0.0–4.0	4.0	4.03	101.0
2H	22	1320	4.0–13.4	9.4	9.95	106.0
3H	22	1400	13.4–23.0	9.6	10.07	104.9
4H	22	1420	23.0–32.5	9.5	10.14	106.7
5H	22	1435	32.5–42.0	9.5	10.10	106.3
6H	22	1505	42.0–51.5	9.5	10.12	106.5
7H	22	1525	51.5–61.0	9.5	9.61	101.0
8H	22	1545	61.0–70.5	9.5	10.14	106.7
9H	22	1610	70.5–80.0	9.5	9.84	103.0
10H	22	1630	80.0–89.5	9.5	8.48	89.2
Coring totals:				89.5	92.48	103.3

partial strokes in stiff glacial clay. The hole was plugged with gel mud.

Hole 1034C

The ship was moved 10 m north of Holes 1034A and 1034B. APC Cores 169S-1034C-1H through 11H were taken from 0 to 103.0 m, with recovery from 94% to 100% except for Core 169S-1034C-8H, which had 17% recovery after it struck a hard concretion. The last two cores were partial strokes. The hole was plugged with gel mud.

Hole 1034D

The ship was moved 20 m south of Hole 1034C. APC Cores 169S-1034D-1H through 11H were taken from 0 to 100.7 m, with recovery from 94% to 100%. The last two cores were partial strokes. The hole was plugged with gel mud.

Hole 1034E

The ship was moved 10 m east of Hole 1034D. APC Cores 169S-1034E-1H through 10H were taken from 0 to 89.5 m with 100% recovery (except for 94% recovery on Core 169S-1034E-10H). Adara temperature measurements were taken on Cores 169S-1034E-3H, 6H, and 9H. The last two cores were partial strokes. The hole was plugged with gel mud. The Canadian Coast Guard Tsekoa II and the Fast Response Craft were released at 1115 hr on 21 August.

Transit to Victoria

The 39.0-nmi transit to Victoria required 4.0 hr at 9.75 kt. The first line ashore was at 1515 hr on 21 August 1966, ending Leg 169S.

LITHOSTRATIGRAPHY

The sediments recovered at Sites 1033 and 1034 consist of two lithologic units of distinctly different sediment types. Unit I comprises dominantly laminated diatomaceous muds (Fig. 6) with some decimeter-scale massive interbeds. The sediments of Unit II comprise mainly gray muds and sandy muds with pebbles. A schematic lithologic summary is provided in (Fig. 7) and more detailed summary figures for the two sites are given in Figures 8 and 9. Smear-slide data are presented in Table 3.

Site 1033: Description of Lithostratigraphic Units
Unit I

Intervals: 169S-1033A-1H; 169S-1033B-1H to 6H-5, 123 cm; 169S-1033C-1H to 6H-2, 114 cm; 169S-1033D-1H to 6H-4, 96 cm
Age: Holocene
Depth: Hole 893A: 0–9.5 mbsf; Hole 893B: 0–45.83 mbsf; Hole 893C: 0–46.84 mbsf; Hole 893D: 0–46.66 mbsf

The sediments of Unit I comprise olive-gray and gray diatomaceous muds. Terrigenous mineral constituents determined by smear-slide analysis include silt grade quartz, feldspar, mica, and clay. Biogenic constituents are dominated by diatoms, but also include silicoflagellates. Pollen and plant debris also are present. Macroscopic plant debris is common throughout and is often concentrated along particular laminae. Shell fragments and some intact shells occur occasionally in the upper 30 m, become more common from ~30 mbsf, and are abundant from ~43 mbsf to the base of the unit, although they are not present in the basal gray clay bed.

The sediment is mainly finely laminated on a millimeter- to centimeter-scale with interbedded massive intervals. Three main lamina components are observed including dark olive-gray (5Y 3/2) diatomaceous mud, olive (5Y 4/3) diatom ooze, and dark gray (N4) silty mud. These three components form an overall triplet in which the thicknesses of the individual components (particularly the diatom ooze and the silty mud) vary from lamina to lamina. The overall thickness of the triplets ranges from 3 to 10 mm with average thickness between 4 and 6 mm. The maximum thickness is 9−10 mm above 20 mbsf decreasing to 5 mm below this depth. With the exception of discrete massive (unlaminated) intervals, the sediment is well laminated to ~32 mbsf. Between 32 and 39 mbsf, the sediment varies from well to intermittently laminated, whereas between 39 and 42 mbsf, it is intermittently laminated and contains traces of lamination between 42 mbsf and the gray clay at 46 mbsf at the base of the unit.

The laminated sediments are interbedded with massive intervals that decrease in abundance and thickness downhole. These are commonly a few centimeters to a few decimeters thick, but range up to 1 m between 0 and 15 mbsf. A thin, millimeter- to centimeter-thick, zone of discontinuous laminae is commonly present at the base of massive intervals, and a thick diatom ooze lamina often forms the cap (Fig. 10).

A 2-cm-thick, light gray volcanic ash horizon (Fig. 11) occurs at intervals 169S-1033B-5H-6, 52−54 cm (37.12 mbsf), 169S-1033C-5H-3, 91−93 cm (38.61 mbsf), and 169S-1033D-5H-5, 41−43 cm (38.13 mbsf). Rare carbonate concretions occur in the deeper part of the core, the shallowest observed at 26 mbsf.

The base of the unit is marked by a ~50-cm-thick, stiff gray structureless mud. This has a very sharp basal contact (Fig. 12), but has a transitional upper contact marked by color-grading from gray (5GY 4/1) clay to olive-gray (10Y 4/1) diatom-bearing mud. This unit is 56 cm thick in both intervals 169S-1033B-6H-5, 67−123 cm, and 169S-1033D-6H-4, 40−96 cm, and 45 cm thick in interval 169S-1033C-6H-2, 69−114 cm. A thinner, 10 cm-thick gray clay occurs ~40 cm above the basal clay.

Unit II

Intervals: 169S-1033B-6H-5, 123 cm through 12H-CC; 169S-1033C-6H-2, 114 cm through 8H-CC; 169S-1033D-6H-4, 96 cm through 8H-CC
Age: late Pleistocene
Depth: Hole 1033B: 45.83−105.1 mbsf; Hole 1033C: 46.84−72.7 mbsf; Hole 1033D: 46.66−69.7 mbsf

Unit II sediments are predominantly composed of rapidly accumulated dense, massive gray to olive-gray terrigenous silty clay.
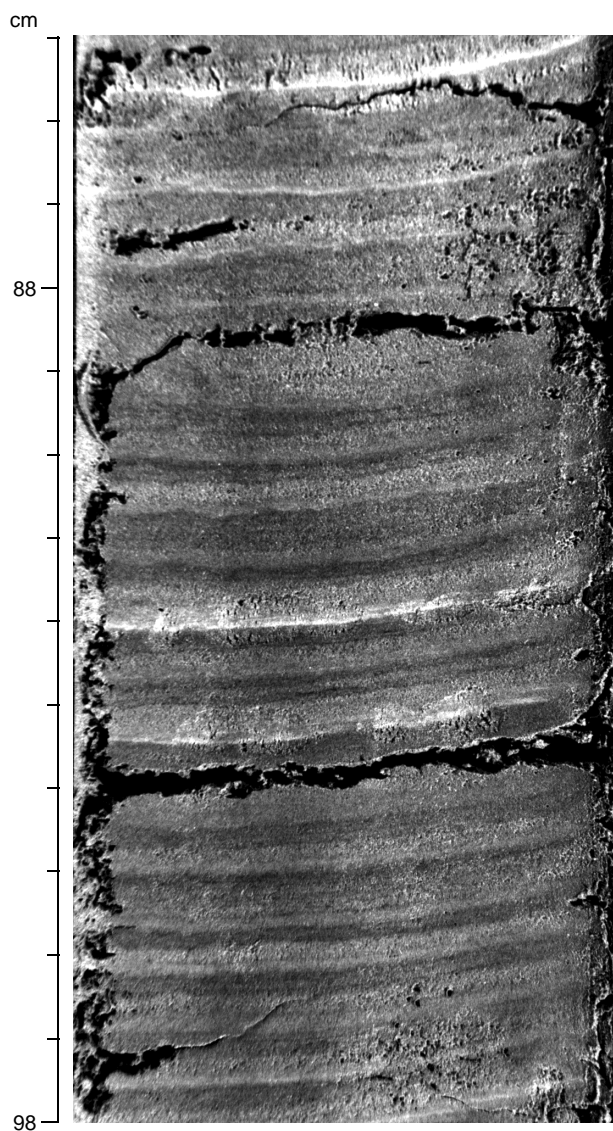

Figure 6. Photograph showing characteristic laminated muds of Unit I. The paler laminae are diatom ooze; the darker laminae are diatomaceous mud and the occasional very light sub-laminae are silty muds (interval 169S-1034B-3H-6, 85−98 cm).
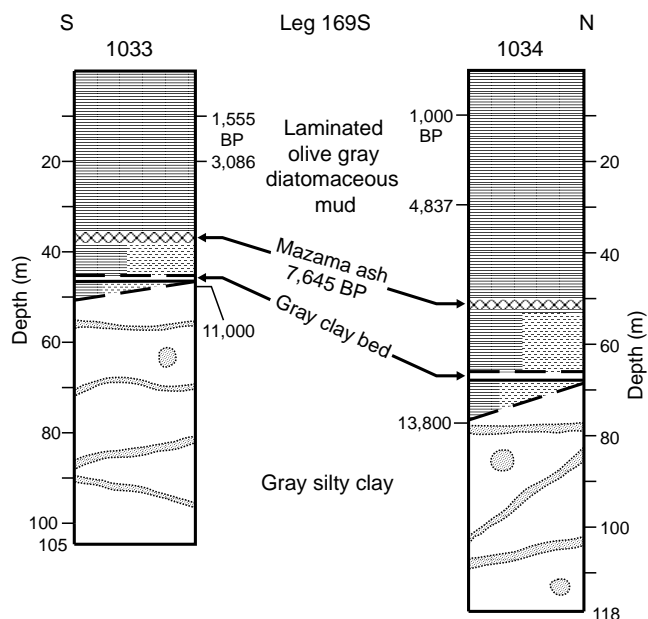

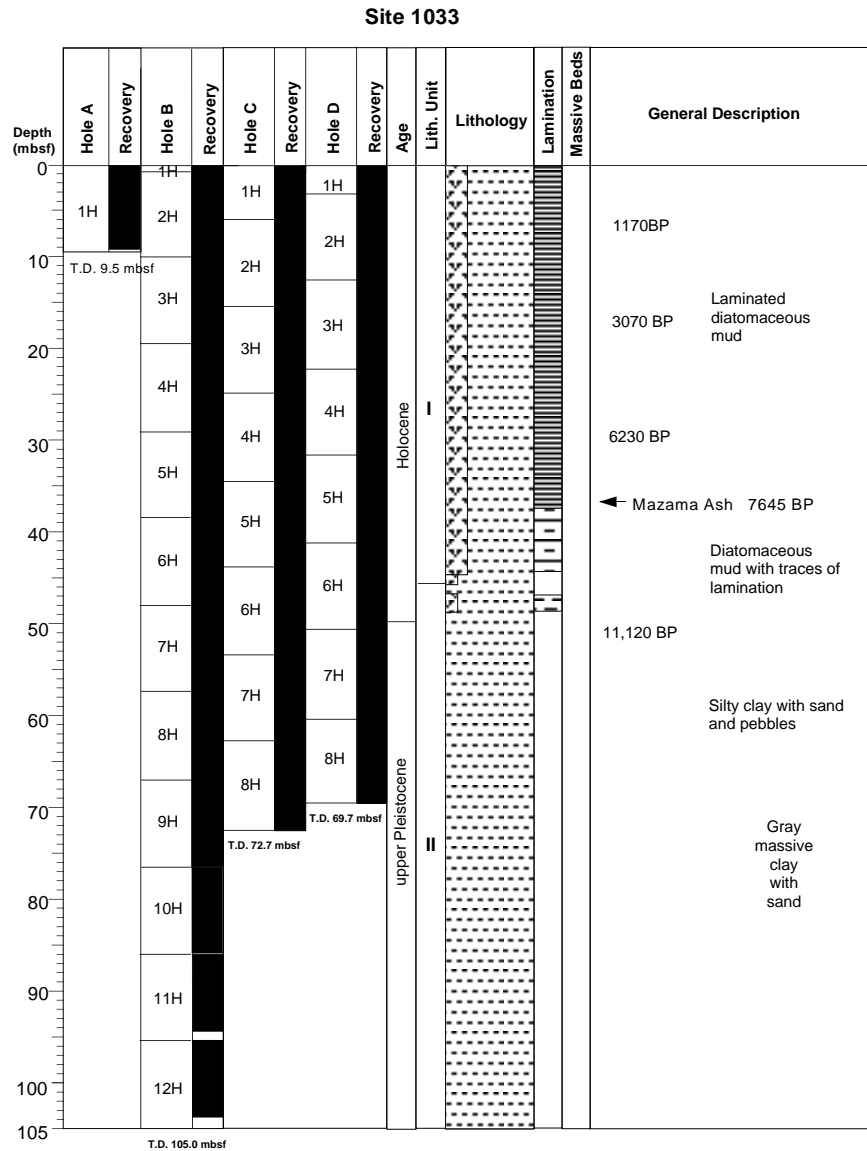Figure 7. Schematic lithologic summary showing Sites 1033 and 1034.

Site 1033

Figure 8. Lithologic summary of Site 1033.

Minor lithologies include sand beds (Fig. 13) and interlaminated very fine sand or silt with mud. Normally graded sand beds fine upward from coarse sand to silt and range in thickness from 3.5 to 88 cm. Sand beds occur at irregular intervals and decrease in thickness and grain size downhole. Thin silt or very fine sand laminae, individually less than 3 mm thick, typically occur in isolated, 5- to 55-cm-thick packets. Laminae are planar to discontinuous and generally less than 3 mm thick. In addition to the laminae, isolated pebbles, granules, and coarse sand grains in mud, and lenses of poorly sorted sand occur. The distribution, b-axis diameter, composition, and shape of pebbles sampled during the logging of Holes 1033C and 1034E are summarized in Table 4. Both of the pebbles sampled from Site 1033 are metamorphic rocks (Table 4). Debris is concentrated at discrete intervals. The uppermost debris-rich unit is 140 cm thick in interval 169S-1033C-7H-3, 10 cm, and 76 cm thick at interval 169S-1033D-7H-5, 12 cm (56.8 mbsf). Other debris-rich zones are 17 cm thick in interval 169A-1033C-8H-4, 51 cm (68.2 mbsf), and 15 cm thick in 169S-1033D-8H-2, 0 cm (61.7 mbsf).

Bioturbation is low to moderate and has resulted in the disruption of thin laminae and dark mottling of mud. Bivalves and bryozoans were observed at the top of the Unit II but do not occur below 51.7 mbsf (interval 169S-1033D-7H-2, 5 cm). There is also evidence of

contorted and inclined sand beds. In several sections sand beds dip steeply in opposite directions over a short distance downcore (e.g., Sections 169S-1033B-9H-4 and 9H-5, and 169S-1033B-12H-1 through 12H-3).

In the upper few meters of Unit II, the lithology is transitional to that of Unit I with a color gradation from gray to olive-gray and a transition from structureless, gray clay and mud to diatomaceous mud with traces of laminae.

Site 1034: Description of Lithologic Units

Unit I

Intervals: 169S-1034A-1H; 169S-1034B-1H to 8H-5, 124 cm; 169S-1034C-1H through 8H-CC; 169S-1034D-1H to 8H-4, 57 cm
Age: Holocene
Depth: Hole 1034A: 0–9.5 mbsf; Hole 1034B: 0–68.44 mbsf; Hole 1034C: 0–66.6 mbsf; Hole 1034D: 0–67.77 mbsf; Hole 1034E: 0–70.5 mbsf

Unit I comprises olive-gray and gray diatomaceous muds. The terrigenous and biogenic constituents are as described for Site 1033. Plant fragments are common in the upper 50 m. Whole and broken
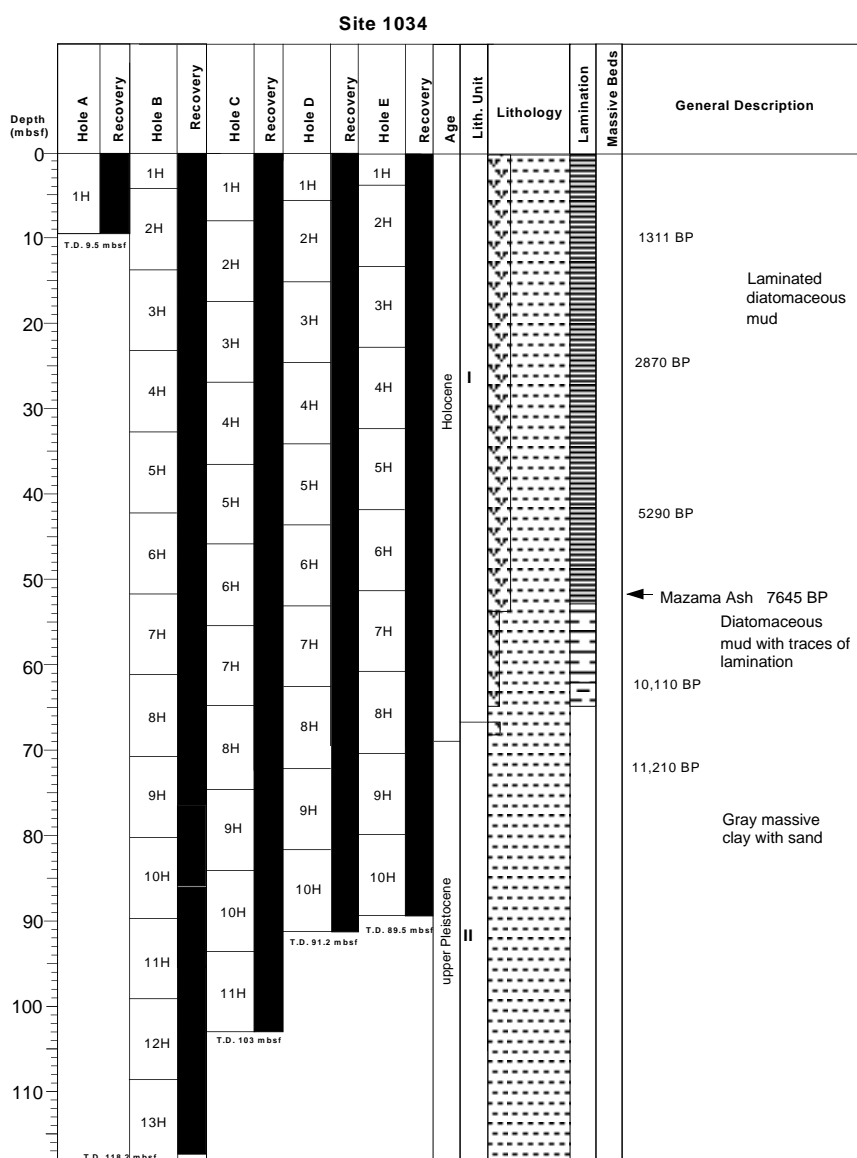
Figure 9. Lithologic summary of Site 1034.

shell fragments are common below ~54 mbsf and are abundant between 60 and 75 mbsf.

The sediment is well laminated between the surface and ~50 mbsf and is intermittently laminated with only a few distinct laminae between 50 and 65 mbsf with some traces of laminae between 65 and 70 mbsf. The major lamina subcomponents are similar to Site 1033, although the thicker laminae at Site 1034 contain as many as six sublaminae. Lamina thickness varies from a maximum of 15 mm in the top 20 m to 5–10 mm below this depth. Marked variations in laminae thickness (e.g., between 5 and 10 mm) occur on a decimeter scale.

A series of massive intervals ranging in thickness from a few centimeters to ~25 cm occur. Although thinner and less frequent than the massive intervals encountered at Site 1033, these intervals are similar in style with basal zones of discontinuous or fragmented laminae and with an uppermost prominent diatom ooze.

A 2-cm-thick, gray volcanic ash horizon occurs at intervals 169S-1034B-1H-1, 2–4 cm (51.74 mbsf), and 169S-1033D-5H-1, 86–88 cm (54.06 mbsf). Carbonate concretions are common between 55 and

65 mbsf. Aggregates of calcite (Fig. 14) and an isolated calcite crystal (Fig. 15) are thought to result from decomposition of hexahydrates (see "Organic Geochemistry" section, this chapter).

The base of the unit is marked by a ~40 cm-thick, stiff gray structureless mud that has a sharp basal contact with olive-gray mud. The unit is 40 cm thick in Hole 1034B (interval 169S-1034B-8H-5, 84–127 cm), although the actual thickness may be distorted by folding; the unit is 34 cm in Hole 1034D (interval 169S-1034D-8H-4, 25–59 cm). The mud is not observed in Hole 1034C (which caught on a concretion at the top of the core), and only the top 38 cm of the gray mud was recovered in interval 169S-1034E-8H-CC. Although this unit is similar to the gray mud at Site 1033, it is ~15 cm thinner at Site 1034.

Unit II

Intervals: 169S-1034B-8H through 13H; 169S-1034C-8H through 11H; 169S-1034D-8H through 11H; 169S-1034E-8H through 10H
Age: late Pleistocene

Table 3. Summary of smear slide results.

Core, section, interval (cm)	Lithology	Comment	Texture			Mineral constituents									Biogenic constituents						
			Sand	Silt	Clay	Quartz	Feldspars	Mica	Volcanic glass	Clay	Opaques	Accessory	Rock fragments	Carbonate	Diatoms	Silicoflagellates	Sponge spicules	Pollen	Plant debris	Organic debris	Radiolarians
169S-1033B-																					
2H-1, 90	D		<1	50	50	P	F	P							A	R	C	P		F	
2H-6, 118	D	Light lamina	<1	70	30	P	P	P							A	R	C	P		R	
2H-6, 118	D	Light lamina; diatom	<1	60	40	F	F	P							A	F	C			F	
2H-7, 30	D		<1	60	40	C	C	R							A		A	P		F	
3H-1, 44	D	Dark lamina	<1	60	40	C	C			C					A	R	A	R		F	
3H-1, 44	D	Light lamina	<1	65	35	P	P								A	R	A	P	R	R	
3H-6, 37	D		<1	50	50		F	F			P				A	R	C	P	R	R	
3H-7, 21	D		<1	40	60	C	F	R		R	R				A	P	A	A		R	
4H-1, 128	D		<1	40	60	F	F	R							A	R	A	C	R	R	
4H-2, 133	D		1	59	40	C	C	C		C					A	R	A		F	F	
4H-3, 31	D		0	50	50	P	P	P							A	R	A		P	C	
5H-1, 74	D		<1	40	60	C	R	P		R					A	R	F	P			
5H-1, 120	D		<1	50	50	F	F	F							A	P	A	R		P	
5H-1, 140	D		<1	60	40	C	C	F		F	P				A	P	C		C	R	
5H-5, 18	D		50	25	25	C	C	C			P	P			P	P	R	P		P	
5H-5, 55	M		<1	30	70	C	C	C							A	P	C	P		P	
5H-6, 53	M		30	50	20	P		P	A		P						P	P			
6H-1, 105	M	Carbonate concretion	30	50	20			F			P		A	F	P	F	P		P		
6H-5, 121	D		5	55	40	C	C	C		C	R	F			A	P	R			R	
6H-5, 126	D		1	59	40	F	F	F			R	R			A	R	C			R	
7H-2, 32	D		40	30	30	A	A	A			R	R	R		P	P	P				
7H-2, 60	M		5	50	45	C	C	C			F	F			A		A	P			
8H-4, 68	D		45	45	10	A	A				F	R									
8H-4, 112	D		10	30	60	A	A	A			F	F									
9H-2, 80	D		10	40	50	C	C	C		C	R	R									
9H-2, 92	D		40	30	30	C	C	C		C	R	R									
10H-6, 20	D		20	40	40	C	C	C			F	A									
10H-6, 65	D		90	10	0	C	C	C			F	F	F								
169S-1034B-																					
1H-2, 20	D		5	60	35	F	F	F			P				A	P	F	R		R	
2H-6, 32	D	Light lamina	<1	50	50	R	R	R							A	P	A	R		R	
2H-6, 32	D	Dark lamina	<1	50	50	F	C	F			R	R			A	P	C			R	
4H-4, 84	D	Dark lamina	<1	35	65	R	F	F		C	R	R			A	R	C	P		R	
4H-6, 9	D	Light lamina	<1	40	60	R	F	F		C	P	R			A	R	F	F		F	
6H-3, 111		White parting	<1	50	50	P	P	P			F	P	P		A	F	F	F		P	A
8H-5, 124		Gray clay	<1	40	60	F	C	F			C	P	F		C	P	F	F			
8H-4, 14	D	Clay-silt lamina	40	40	20	C	C	C			P	P	F		P	P	P	P			
9H-1, 47		Sand	70	30	10	C	C	C			P	F	F		P			P			

Note: D = laminated diatomaceous mud, M = massive interval, P = present (<1%), F = few (5%−10%), A = abundant (>30%), R = rare (1%−5%), and C = common (10%−30%).

Depth: Hole 1034B: 68.44−118.2 mbsf; Hole 1034C: 66.6−103.0 mbsf; Hole 1034D: 67.77−100.7 mbsf; Hole 1034E: 70.5−89.5 mbsf.

Unit II is dominated by dense, massive gray to olive-gray terrigenous silty clay. Thick graded sand beds and thin laminae of fine sand and silt form minor lithologies. The thickness of sand beds varies greatly between holes; it is most commonly <2 cm, but ranges up to 25 cm. In Hole 1034B, graded sand beds occur irregularly in Cores 169S-1034B-10H and 11H. One bed is 25 cm thick in Section 169S-1034B-10H-1, but most are <2 cm thick. However, sand is the dominant lithology in Core 169S-1034C-10H. Sections 169S-1034B-10H-1 through 10H-3 consist of two normally graded sand beds. The upper bed fines upward from fine sand to silt, and the lower fines upward from coarse to fine sand. Between these units there is 23 cm of cross-bedded fine sand (Section 169S-1034C-10H-1). Cores 169S-1034D-10H and 169S-1034E-10H were highly disturbed. Section 169S-1034E-10H-1 contained a lithified laminated concretion at 54 cm that disrupted the rest of Core 169S-1024E-10H below this depth during coring. Bioturbation, recognized by disruption of thin laminae, horizontally infilled burrows and black mottles, is minimal to moderate in Unit II and decreases with depth. Bivalves, bryozoans, and charcoal occur near the top of Unit II. Scattered dropstones, clus-

ters of pebbles, and irregularly shaped pods of sand and granules in mud are common (examples in Sections 169S-1034C-11H-4 and 11H-5 and 169S-1034D-11H-1 through 11H-3, 11H-5 and 11H-6). A light brown silt clast is observed in Section 169S-1034E-9H-4. Eight pebbles are described from Core 169S-1034E-10H (Table 4). Five different lithologies are present, representing plutonic igneous and volcanic rock types.

At Site 1034 the top of Unit II is marked by a structureless gray terrigeneous mud similar to that in Unit II of Site 1033. This distinctive gray unit was not recovered in 1034C.

Summary of Depositional Environments

The laminae triplets of Unit I are thought to represent marine varves. Initial X-ray radiography shows that up to 10 intra-annual sublaminae are present (Fig. 16). Shore-based research will assess the origins of the massive intervals that interrupt the laminated sediments that are believed to be either mass-flow deposits or oxygenated intervals. The general degree of preservation of laminae indicates that intermittent bottom-water oxygenation in early Holocene times was sufficient to pervasively disrupt lamina fabrics; however the degree of oxygenation progressively lessened, resulting in more dominant anaerobic conditions with concomittant lamina preservation. The
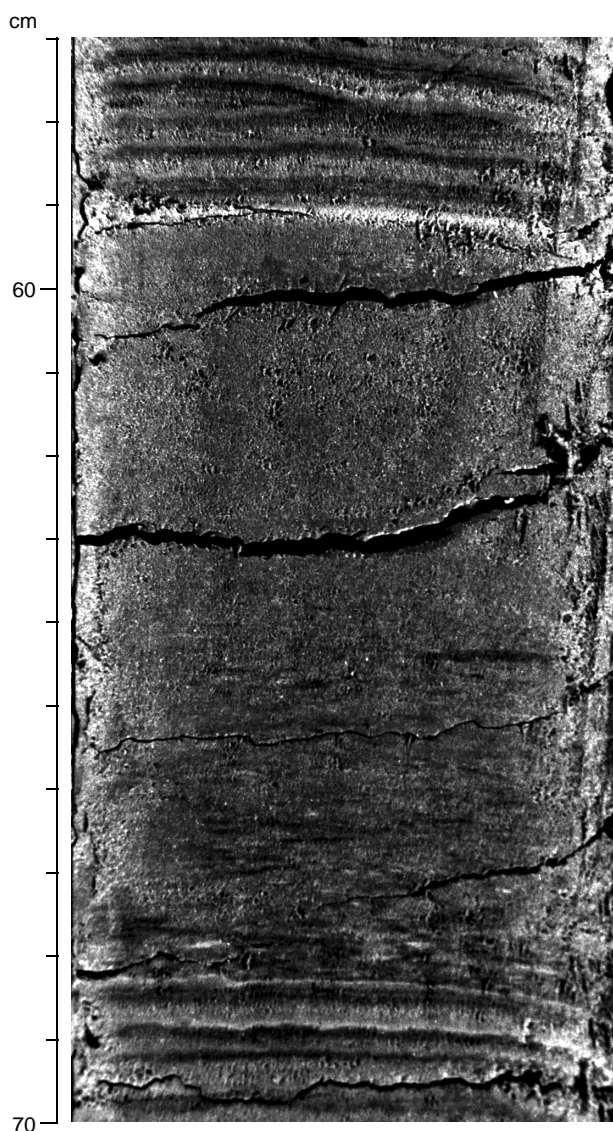
Figure 10. Photograph of a thin massive interval within laminated sediment showing discontinuous/disrupted laminae at the base, grading to entirely homogenous mud. A characteristic pale diatom ooze lamina marks the top (interval 169S-1033B-4H-4, 56–70 cm).

Figure 11. Photograph of the distinctive ash horizon thought to represent the Mazama Ash (interval 169S-1033B-5H-6, 48–60 cm).

sediments of Unit II are interpreted to result from glaciomarine deposition. The various pebbles and pods of sand within Unit II are interpreted as dropstones originating from melting icebergs. The pebble lithology and characteristics may be used to identify sources of debris in icebergs.

Inter-Hole Correlation

Lithologic correlation between holes was primarily based on the matching of distinctive massive (unlaminated) intervals between holes (Figs. 17, 18), the Mazama Ash horizon, the clay at the base of Unit I, sand beds in Unit II, and distinctive laminae or packets of laminae. Detailed correlations of massive intervals are given in Tables 5 and 6.

Chronology

Results from the ^{14}C determinations show that ages vary from 286 to 507 cal yr BP, to 14,280 to 14,958 cal yr BP (Table 7). Based on

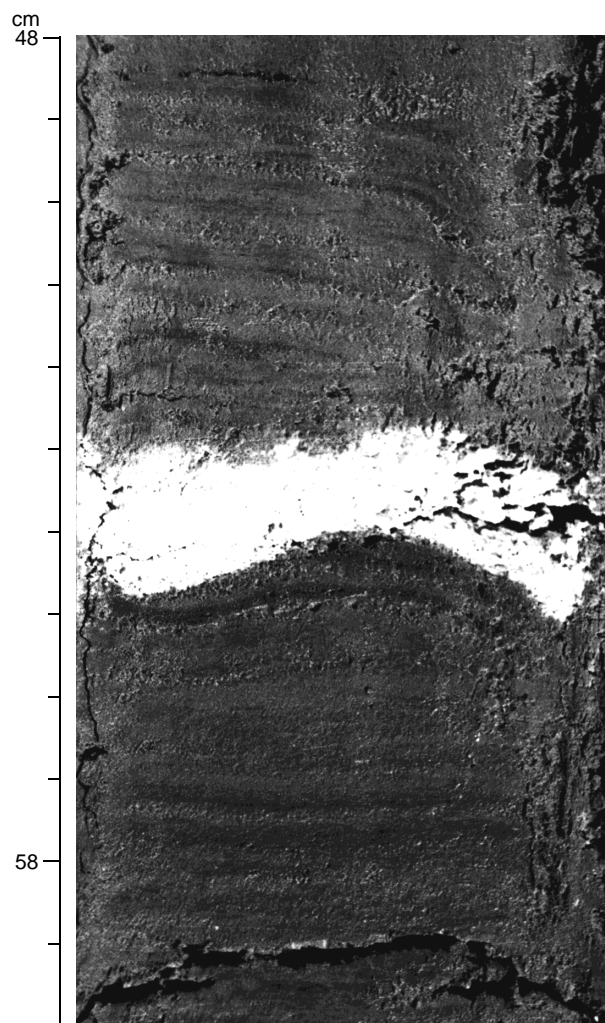an average sedimentation rate of 7 mm/yr at Hole 1033C down to the first ^{14}C age, there is roughly 1.5 m of sediment missing from the sediment/water interface to the top of the core. Similarly, based on an average sedimentation rate of 11 mm/yr at Holes 1034B and 1034C down to the first ^{14}C age, there is ~0.6–2.1 m of sediment missing from the sediment/water interface to the top of the sediment core. However, there is over 500 yr of sediment overlap with eight piston cores collected in the central part of Saanich Inlet (Blais, 1995) that contained the shallowest part of the sediment column.

[14]C ages from the ODP cores are shown in Table 7 and Figure 19 (for an expanded version of Figure 19, please see the back-pocket foldout for this chapter). These ^{14}C ages confirm that most of the Holocene and latest Pleistocene sediments have been recovered.

Reservoir Age Determination

A possibility exists that the reservoir correction for Saanich Inlet is not exactly 801 ± 23 yr as determined by Robinson and Thomson (1981). Reservoir corrections made by Robinson and Thomson (1981) were determined with samples collected in Sooke, B.C., on the south-southwest coast of Vancouver Island. Saanich Inlet, located on the southeast coast, may receive old carbon from sources different from those determined from samples located in Sooke. To verify this, a comparison was made of ^{14}C ages from a wood/shell pair (Samples
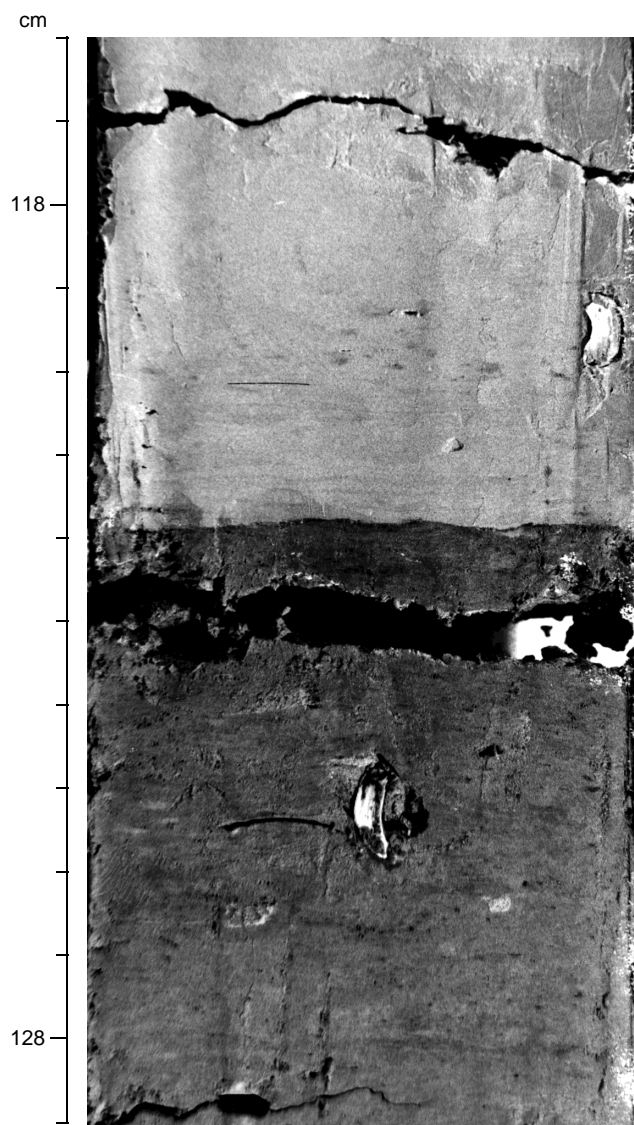
Figure 12. Base of structureless 40-cm thick, gray mud unit dated at ~11,000 cal yr BP (interval 169S-1033B-6H-5, 116–129 cm).
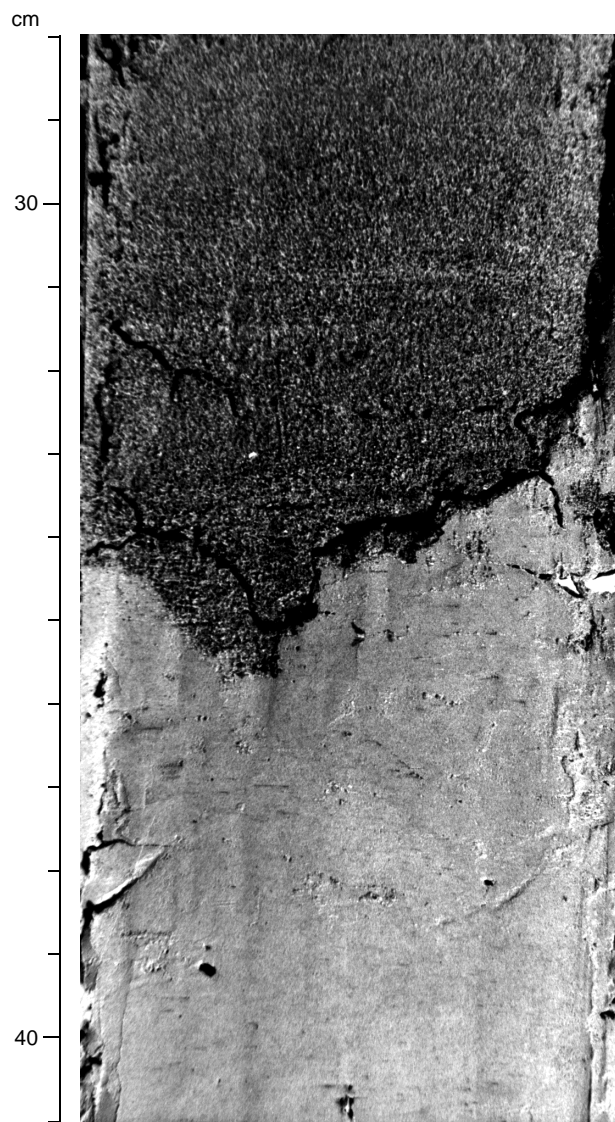

Figure 13. The irregular erosive base to a sand layer in Unit II (interval 169S-1033B-7H-2, 27–41 cm).

169S-1033C-2H-6, 125 cm, and 2H-16, respectively), ~82 yr apart. The reservoir correction calculated from this wood/shell pair is 798 ± 50 yr. This is very close to the literature value of 801 ± 23 yr (Robinson and Thomson, 1981). The literature value therefore has been used for the reservoir correction of all marine radiocarbon ages in this study.

Age of Major Stratigraphic Units

The youngest age for the distinctly laminated diatomaceous mud intercalated by massive mud layers is 286–507 cal yr BP and the oldest 6409–6741 cal yr BP (Fig. 19). Below this distinctly laminated diatomaceous mud is a transition zone of indistinctly laminated diatomaceous mud, which contains numerous paired bivalve shells and is bioturbated. This indistinctly laminated mud unit contains a transitional basal contact with Pleistocene gray glaciomarine mud. The oldest age found within the Pleistocene sediments is 14,280–14,958 cal yr BP.

Table 4. Details of pebbles found within Unit II.

| Core, section, interval (cm)	Depth (mbsf)	Size (cm)	Rock type	Shape	Notes
169S-1033C-					
7H-3, 60	57.30	1.7	Gneissic marble	Rounded	
7H-5, 18	59.88	2.0	Hornfels	Rounded	Striated
169S-1034E-					
10H-3, 78	83.78	0.9	Diorite	Rounded	
10H-3, 90	83.90	1.8	Porphoritic basalt	Rounded	Striated
10H-3, 100	84.00	1.8	Granodiorite	Angular	
10H-3, 102	84.02	1.0	Banded rhyolite	Subrounded	
10H-3, 102	84.02	0.6	Banded rhyolite	Subrounded	
10H-3, 131	84.31	0.7	Gabbro	Subrounded	
10H-3, 146	84.46	2.2	Diorite	Rounded	
10H-CC, 20	88.48	3.2	Granodiorite	Angular	
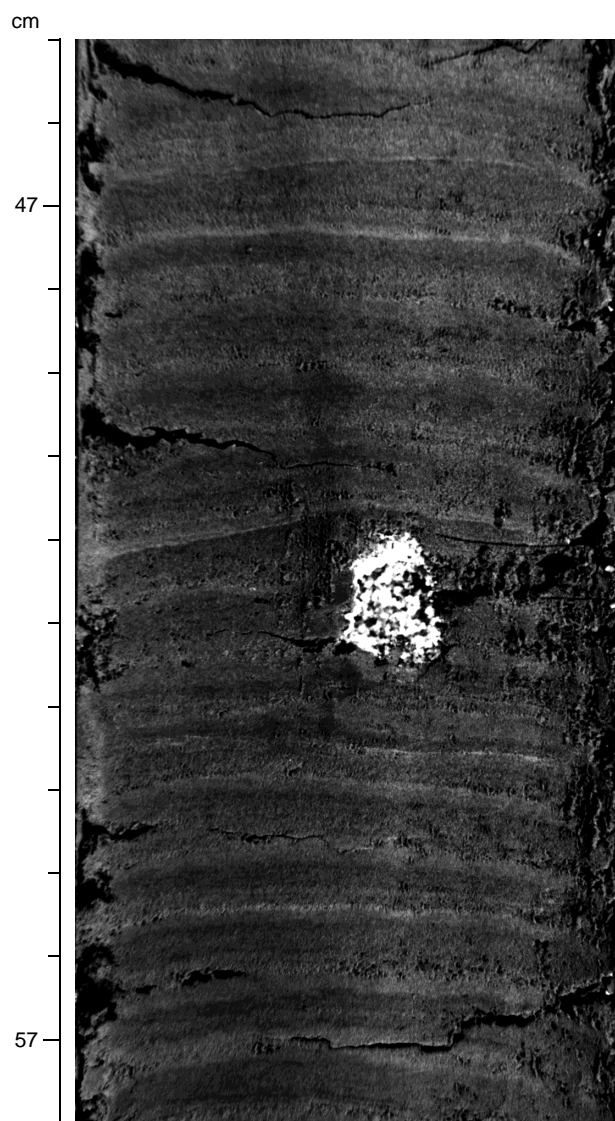
Figure 14. Pale yellow aggregate of granular calcite within laminated sediment in interval 169S-1034B-5H-2, 45–58 cm. This is thought to result from the decomposition of a calcium carbonate hexahydrate crystal (ikaite).
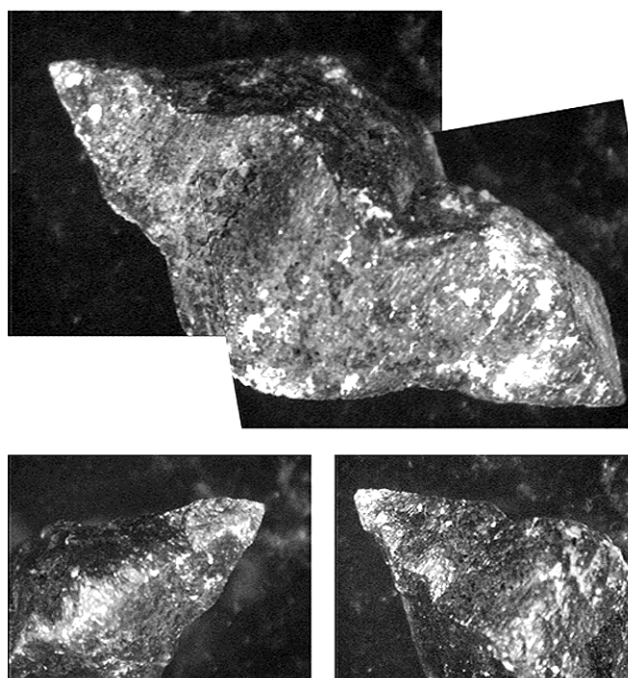

Figure 15. Angular, biterminated calcite crystal thought to represent a glendonite pseudomorph of calcium carbonate hexahydrate (ikaite; Sample 169S-1034D-7H-1, 76 cm).

Within the indistinctly laminated Holocene mud a volcanic ash is observed. A wood fragment found a few centimeters above this volcanic ash in Hole 1033D yielded an age range of 7392–7547 cal yr BP (or 6650 ± 50 yr BP), which roughly corresponds with the literature value of 6900 ^{14}C yr BP (Bacon, 1983) and 6800 ^{14}C yr BP (Abella, 1988) for the Mazama Ash.

Below the volcanic ash, but still within the indistinctly laminated diatomaceous mud, lies a stiff gray clay with a transitional upper contact and a very sharp basal contact. Its age range in Hole 1033B is bracketed at ~1 m above at 10,355–10,894 cal yr BP and just below at 10,952–11,452 cal yr BP and in Hole 1034B, above at 10,098–11,944 cal yr BP and below at 10,870–11,083 cal yr BP and in Hole 1034D, above at 10,998–11,614 cal yr BP and below at 10,965–11,445 cal yr BP.

PHYSICAL PROPERTIES

Site 1033

Physical properties measurements at Site 1033 were conducted on both whole-round core sections and on discrete samples from split cores. The whole-round measurements include GRAPE bulk density, acoustic compressional wave velocity, and magnetic susceptibility. MST measurements were completed for Hole 1033B during Leg 169S and for Holes 1033A, 1033C, and 1033D during Leg 169. Color reflectance was measured on split cores in all holes. Undrained shear strength was measured on split cores in Hole 1033B.

Composite Stratigraphy

MST and color reflectance data are used to correlate cores from each hole at this site and to construct a composite stratigraphic section. Cores recovered from Site 1033 suffered from a small amount of gas expansion in the upper 30 to 40 mbsf. This resulted in poor-quality acoustic velocity data that could not be used for correlation purposes. Cores were analyzed by independent cross-correlation using GRAPE bulk density, magnetic susceptibility, and L*, the ratio of black to white reflectance from color measurements. In general, the data show enough variability for correlation. There are differences in the measured values of all parameters between the cores immediately measured after recovery (Hole 1033B) and the cores measured weeks later (Holes 1033A, 1033C, 1033D, and 1033E). These differences could be a result of sediment consolidation over the intervals where gaps in the core occurred from gas expansion or from core drying.

The correlation for Site 1033 is shown in Figure 20. Cores are offset from the measured depth (mbsf) and plotted with their offsets in meters composite depth (mcd). Table 8 lists the offset depths that reflect the depth (mcd) shifts. The top core in each hole was very disturbed, resulting in poor correlations in the upper 8–10 m. Below this very soft, disturbed, black silty clay interval, the sediment varves are clearly visible, and the correlations are good. Based on the quality of the MST GRAPE bulk density, cores were selected to represent a composite (spliced) stratigraphic section for Site 1033. The cores selected for the composite are identified in Table 8.
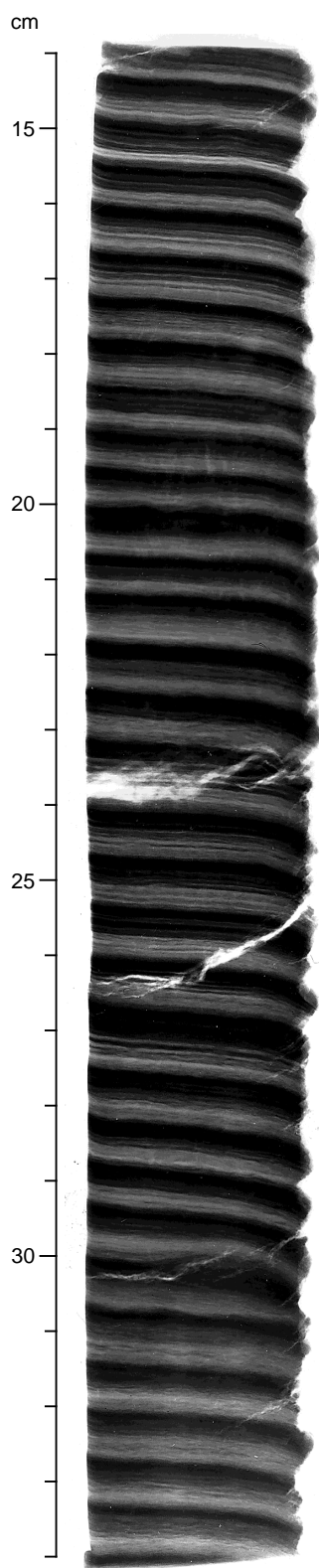
Figure 16. Print of X-ray radiograph of laminated sediments from interval 169S-1034B-4H-3, 14−34 cm. The centimeter-scale pale (diatom-rich) dark (terrigenous sediment-rich) alternations represent annual "varves." Within these annual varves, up to 10 intra-annual sub-laminae are present.

Index Properties

Bulk density, measured using the composite MST GRAPE, is shown in Figure 21A. The bulk density at Site 1033 is very low and shows only small increases with depth (1.1 to 1.3 Mg/m³) in the upper 45 m (37−38 mbsf). At ~45 mcd, bulk density begins to increase with depth (0.6 Mg/m³ increase over a 20-m interval). The bulk density change at 45 mcd corresponds with the change in visual core description from laminated diatomaceous mud to gray structureless clay. At ~65 mcd (56.5 mbsf), bulk density values again begin to show only small increases with depth, increasing from 1.9 to 2.1 Mg/m³ at 110 mcd (101.6 mbsf).

Small intervals of higher bulk density that overprint the generally increasing trends with depth are observed in the upper 65 mcd (56.5 mbsf). These correspond to intervals of high magnetic susceptibility (Fig. 21B), suggesting a source change rather than a change in stress history. These intervals occur at a frequency of 7 to 12 m (~1−1.5 ka) downhole.

Acoustic Velocity

Acoustic velocity was measured using the digital sound velocimeter (DSV) at selected intervals within the gray clay unit in Hole 1033B. The P-wave logger on the MST did not produce quality data because of small core-expansion intervals that attenuated the sound signal in all cores (Table 9).

Undrained Shear Strength

Shear strength was measured at Site 1033 using a motorized miniature vane shear device. Measurements were made on cores from Hole 1033B. Shear strength at Site 1033 shows small increases with depth (~10 kPa) in the upper 42 mcd (33 mbsf; Fig. 22). Although these strengths are low, the ratio of undrained shear strength to effective overburden stress ($S_u/P_o' = 0.2$) suggests that these sediments are normally consolidated. From 42 to 55 mcd (33 to 55 mbsf), shear strength increases at a higher rate with depth than the surficial sediment interval. However, the S_u/P_o' ratio decreases over this interval, suggesting an underconsolidated interval. The interval above 42 mcd corresponds with the very well-laminated diatomaceous mud unit. Another change in the shear strength profile occurs at 68 mcd (58 mbsf), with a sharp increase to 40 kPa, and then an increasing profile with depth to the bottom of the hole. Although shear strength shows large increases with depth, the S_u/P_o' ratio decreases with depth to a low of 0.12 at the base of the hole, suggesting an underconsolidated sediment section. It is unlikely that these sediments at the base of the hole, interpreted as glaciomarine, experienced any ice loading or erosion.

Site 1034

At Site 1034, physical properties were measured on both whole-round core sections with the multisensor track and with discrete samples from split cores. The whole-round measurements include GRAPE density, acoustic compressional wave velocity, and magnetic susceptibility. MST measurements were completed for Hole 1034B during Leg 169S and for Holes 1034A, 1034C, 1034D, and 1034E during Leg 169. Color reflectance was measured on split cores in all holes. Undrained shear strength was measured on split cores in Hole 1034B.

Composite Stratigraphy

MST and color reflectance data are used to correlate cores from each hole at this site and to construct a composite stratigraphic section. Cores recovered from Site 1034 suffered from gas expansion in
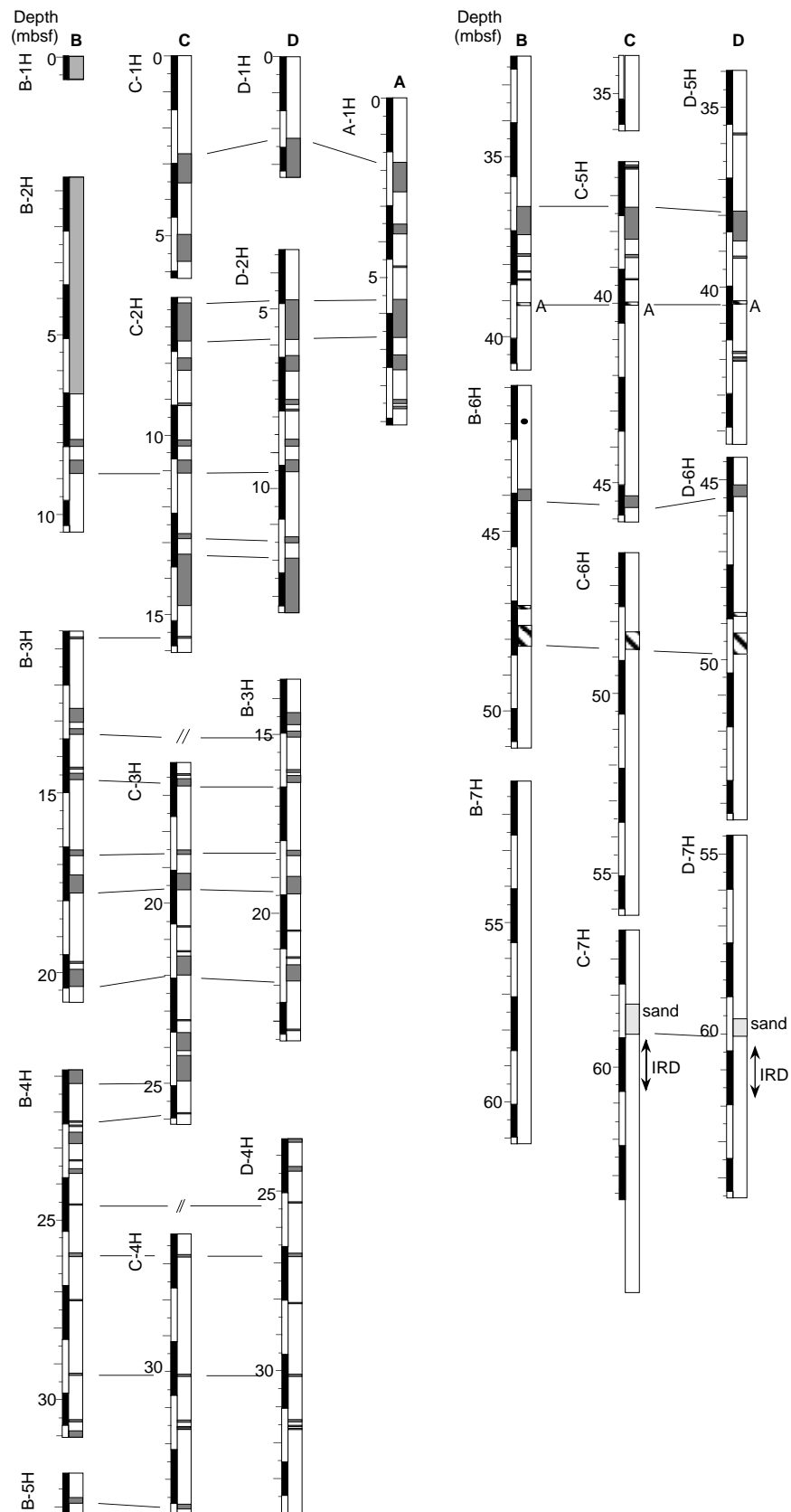
Figure 17. Composite summary of Site 1033 showing inter-hole correlation based on occurrence of massive intervals, distinctive ash, and clay beds.
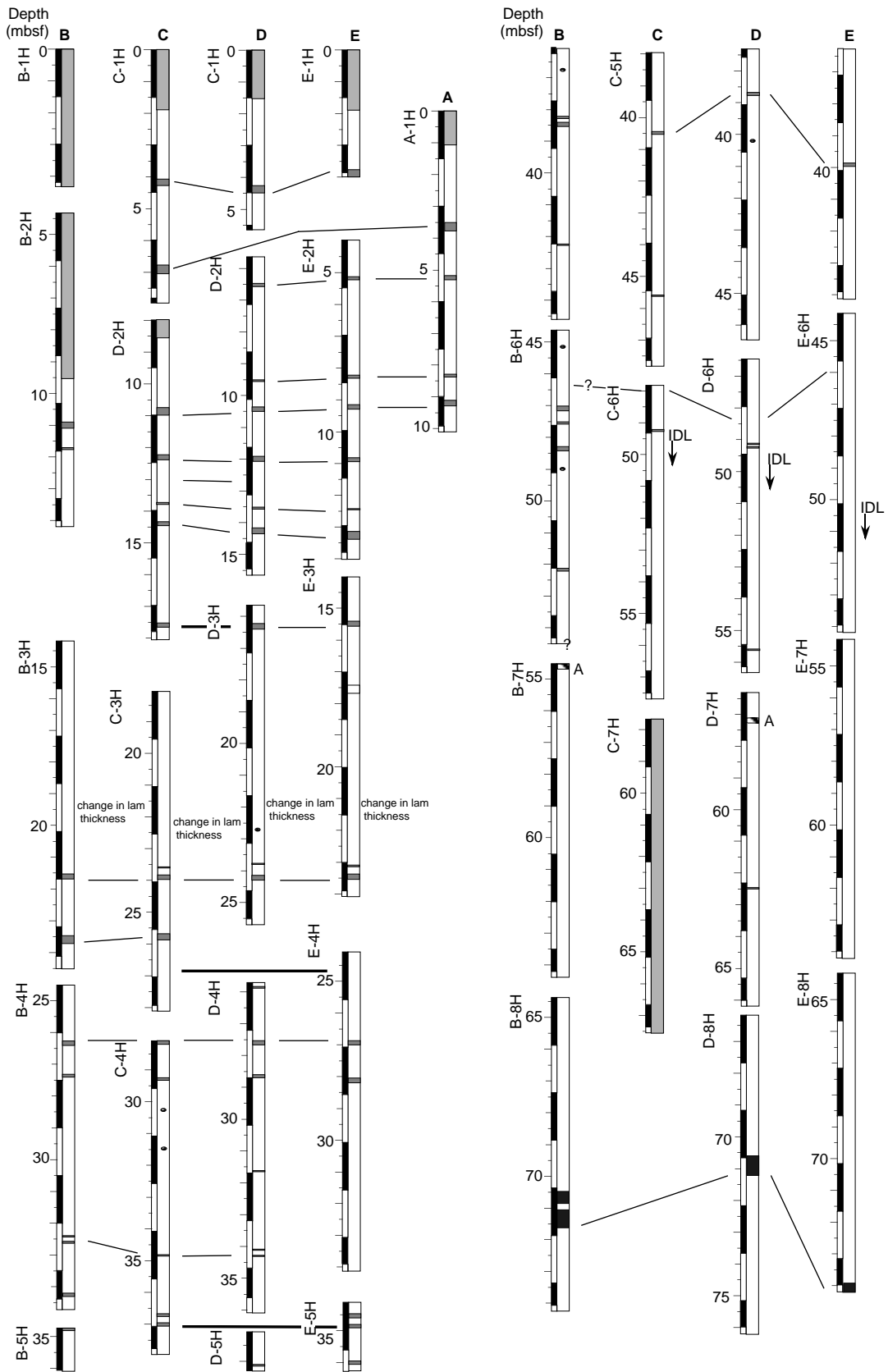
Figure 18. Composite summary of Site 1034 showing inter-hole correlation based on occurrence of massive intervals, distinctive ash, and clay beds.

Table 5. Correlation of massive intervals at Site 1033.

Massive interval number	Hole 1033A Core, section, interval (cm)	Depth (mbsf)	Hole 1033B Core, section, interval (cm)	Depth (mbsf)	Hole 1033C Core, section, interval (cm)	Depth (mbsf)	Hole 1033D Core, section, interval (cm)	Depth (mbsf)
1	1H-2, 27–110	1.77–2.60			1H-2, 123, to 1H-3, 54	2.73–3.54	1H-2, 76-CC, through 1H-CC	2.26–3.2
2	1H-3, 48–76	3.48–3.76	Not recognized		1H-4, 48–137	4.98–5.87		
3	1H-4, 17–20	4.67–4.70	Not recognized					
4	1H-4, 108, to 1H-5, 64	5.58–6.64	Not recognized		2H-1, 15–121	6.35–7.41	2H-1, 139, to 2H-2, 99	4.59–5.69
5	1H-5, 112, to 1H-6, 5	7.12–7.55	Not recognized		2H-2, 11–57	7.81–8.27	2H-2, 144, to 2H-3, 34	6.14–6.54
6	1H-6, 87–98	8.37–8.48	Not recognized		2H-2, 141–150	9.11–9.20	2H-3, 119–130	7.39–7.50
7	1H-6, 107–112	8.57–8.62	Not recognized		Not recognized		2H-3, 139–144	7.59–7.64
8			2H-5, 132–150	7.92–8.10	2H-3, 95–113	10.15–10.33	2H-4, 76–93	8.46–8.63
9			2H-6, 33–73	8.43–8.83	2H-4, 2–29	10.72–10.99	2H-4, 133, to 2H-5, 19	9.03–9.39
10					2H-5, 56–71	12.76–12.91	2H-6,49–65	11.19–11.35
11					2H-5,112, to 2H-6, 103	13.32–14.23	2H-6, 109, through 2H-CC	11.79–12.7
12			3H-1, 17–22	10.27–10.32	2H-7, 0–49	15.20–15.69		
13			3H-2, 64–100	12.24–12.60			3H-1, 93–129	13.63–13.99
14			3H-2, 102–109	12.62–12.69			Not recognized	
15			3H-2, 119–136	12.79–12.96			3H-2, 0–11	14.20–14.31
16			3H-3, 78–83	13.88–13.93	3H-1, 33–37	16.03–16.07	3H-2, 102–109	15.22–15.29
17			3H-3, 94–111	14.04–14.21	3H-1, 47–66	16.17–16.66	3H-2, 118–138	15.38–15.58
18			3H-5, 5–20	16.15–16.30	3H-2, 93–105	18.13–18.25	3H-4, 24–41	17.44–17.61
19			3H-5, 75–126	16.85–17.36	3H-3, 9–56	18.79–19.36	3H-4, 97–148	18.17–18.68
20			Not recognized		3H-4, 4–6	20.24–20.26	3H-5, 99–101	19.69–19.71
21			3H-7, 16–20	19.26–19.30	3H-4, 75–79	20.95–20.99	3H-6, 21–25	20.41–20.45
22			3H-7, 37–86	19.47–19.96	3H-4, 97–141	21.17–21.61	3H-6, 43–89	20.63–21.09
23					3H-5, 115–117	22.85–22.87	3H-7, 74–77	22.44–22.47
24					3H-6, 0–53	23.20–23.73		
25			4H-1, 0–48	19.60–20.08	3H-6, 65–137	23.85–24.57		
26			4H-2, 5–9	21.15–21.19	3H-7, 77–79	25.47–25.49		
27			4H-2, 22–54	21.32–21.64			4H-1, 0–8	22.20–22.28
28			4H-2, 99–101	22.09–22.11			Not recognized	
29			4H-2, 126–139	22.36–22.49			4H-1, 77–90	22.97–23.10
30			4H-3, 72–75	23.32–23.35			4H-2, 24–28	23.94–23.98
31			4H-4, 59–66	24.69–24.76	4H-1, 64–72	25.84–25.92	4H-3, 16–25	25.36–25.45
32			4H-5, 39–42	25.99–26.02	Not recognized		4H-4, 4–7	26.74–26.77
33			4H-6, 92–98	28.02–28.08	4H-3, 89–96	29.09–29.16	4H-5, 54–60	28.74–28.80
34			4H-7, 73–79	29.33–29.39	4H-4, 66–72	30.36–30.42	4H-6, 30–37	30.00–30.07
35			5H-CC, 11–35	29.60–29.84	4H-4, 83–87	30.53–30.57	4H-6, 47–50	30.17–30.20
36					4H-4, 90–91	30.60–30.61	4H-6, 55–57	30.25–30.27
37			5H-1, 70–85	29.80–29.95	4H-6, 0–15	32.70–32.85		
38			Not recognized				5H-2, 23–28	33.43–33.48
39			Not recognized		5H-1, 9–15	34.79–34.85	Not recognized	
40			Not recognized		5H-1, 16–20	34.86–34.90	Not recognized	
41			5H-4, 81, to 5H-5, 18	34.41–35.28	5H-1, 123, to 5H-2, 65	35.93–36.85	5H-3, 90, to 5H-4, 22	35.60–36.42
42			5H-5, 64–72	35.74–35.82	5H-2, 107–115	37.27–37.35	5H-4, 66–72	36.86–36.92
43			5H-5, 113–116	36.23–36.26	Not recognized		Not recognized	
44			5H-5, 133–136	36.43–36.46	5H-3, 23–27	37.93–37.97	Not recognized	
Mazama Ash			5H-6, 52–54	37.10–37.12	5H-3, 91–93	38.59–38.61	5H-5, 41–43	38.11–38.13
45			6H-2, 138, to 6H-3, 17	41.48–41.77	5H-7, 30–60	44.00–44.30	6H-1, 76–106	41.96–42.26

Note: Because of recoveries exceeding 100%, inaccuracies in the precise depths (mbsf) of some massive intervals are apparent in this table.

the upper 30 to 40 mbsf. This disturbance resulted in poor quality acoustic velocity data that could not be used for correlation purposes. Cores were analyzed by independent cross-correlation using GRAPE bulk density, magnetic susceptibility, and L*, the ratio of black to white reflectance from color measurements. In general, the data show enough variability for correlation. There are differences in the measured values of all parameters between the cores immediately measured after recovery (Hole 1034B) and the cores measured weeks later (Holes 1034A, 1034C, 1034D, and 1034E). These differences could be caused by consolidation of the sediment over the intervals, where gaps in the core occurred from gas expansion or from drying of the core.

The correlation for Site 1034 is shown in Figure 23 A–C. Cores are offset from the measured depth (mbsf) and plotted with their offsets in modified core depth (mcd). Table 10 lists the offset depths that reflect the depth (mcd) shifts. The top core in each hole was very disturbed resulting in poor correlations in the upper 8−10 m. Below this very soft, disturbed organic-rich, black silty clay interval, the thin annual sediment beds are clearly visible and the correlations are reasonable. Based on the quality of the MST Grape bulk density, cores were selected to represent a composite (spliced) stratigraphic section for Site 1034. The cores selected for the composite are identified in Table 10.

Index Properties

Bulk density, measured using the composite MST GRAPE, is shown in Figure 24A. The bulk density for the upper 70 m at Site 1034 is very low and shows only small increases with depth (1 to 1.3 Mg/m^3). At ~70 mcd, bulk density begins to increase with depth with a 0.5 Mg/m^3 increase over 15 m. This change at 70 mcd (65 mbsf) corresponds to a change in sediment type according to the visual core descriptions from laminated diatomaceous mud to gray structureless clay. At ~95 mcd (94 mbsf), bulk density values again begin to show only small increases with depth, increasing from ~1.9 to 2.2 Mg/m^3 at 115 mcd.

Small intervals of higher bulk density overprint the generally low values in the upper 70 mcd. These denser intervals correspond to intervals of high magnetic susceptibility (Fig. 24B), suggesting lithologic changes rather than a change in stress history.

Acoustic Velocity

Acoustic velocity was measured using the DSV at selected intervals within the gray clay unit in Hole 1034B. The P-wave logger on the MST did not produce quality data because of core gaps and cracks caused by gas expansion. Gaps and cracks cause rapid attenuation of

Table 6. Correlation of massive intervals at Site 1034.

Massive interval number	Hole 1034A Core, section, interval (cm)	Depth (mbsf)	Hole 1034B Core, section, interval (cm)	Depth (mbsf)	Hole 1034C Core, section, interval (cm)	Depth (mbsf)	Hole 1034D Core, section, interval (cm)	Depth (mbsf)	Hole 1034E Core, section, interval (cm)	Depth (mbsf)
1	1H-3, 49–75	3.49–3.75			1H-3, 106–130	4.06–4.30	1H-3, 126–150	4.26–4.50	1H-3, 73–84	3.73–3.84
2	1H-4, 66–76	5.16–5.26			1H-5, 77–103	6.77–7.03	2H-1, 83–94	6.53–6.64	2H-1, 117–123	5.17–5.23
3	1H-6, 73–76	8.23–8.26					2H-3, 88–92	9.58–9.62	2H-3, 127–136	8.27–8.36
4	1H-7, 9–30	9.09–9.30	Not recognized		Not recognized		2H-4, 22–39	10.42–10.59	2H-4, 69–83	9.19–9.33
5			2H-6, 63–82	12.33–12.52	2H-2, 129–150	10.79–11.00	2H-5, 28–44	11.98–12.14	2H-5, 83–97	10.83–10.97
6			2H-6, 142–144	13.12–13.14	2H-3, 124–140	12.24–12.40	2H-6, 39–44	13.59–13.64	2H-6, 97–99	12.47–12.49
7					2H-4, 126–130	13.76–13.80	2H-6, 103–123	14.23–14.43	2H-7, 17–41	13.17–13.41
8					2H-5, 35–45	14.35–14.45				
9					2H-7, 56–69	17.56–17.69	3H-1, 57–73	15.77–15.93	3H-1, 138, to 3H-2, 0–5	14.78–14.95
10										
11					3H-4, 102–104	23.02–23.04	3H-6, 63–65	23.33–23.35	3H-7, 9–13	22.49–22.53
12			3H-5, 136–150	21.06–21.20	3H-4, 127–141	23.27–23.41	3H-6, 90–106	23.60–24.06	3H-7, 37–53	22.77–22.93
13			3H-7, 28–48	22.98–23.18	3H-6, 11–31	25.11–25.31				
14					Not recognized		4H-1, 16–19	24.86–24.89	Not recognized	
15			4H-2, 26–40	24.96–25.10	4H-1, 0–12	27.00–27.12	4H-2, 33–47	26.53–26.67	4H-2, 128–142	25.78–25.92
16			4H-2, 132–141	26.02–26.11	4H-1, 114–121	28.14–28.21	4H-2, 142–150	27.62–27.70	4H-3, 96–110	26.96–27.10
17			Not recognized		Not recognized		4H-4, 146–148	30.66–30.68		
18			4H-6, 40–42	31.10–31.12	Not recognized		4H-6, 90–92	33.10–33.12		
19			4H-6, 58–62	31.28–31.32	4H-5, 72–73	33.72–33.73	4H-6, 108–111	33.28–33.31		
20			4H-7, 74–84	32.94–33.04	4H-6, 108–117	35.58–35.67			5H-1, 37–49	32.87–32.99
21					4H-6, 139–148	35.89–35.98			5H-1, 70–78	33.20–33.28
Correlation uncertain			5H-1, 0–7	32.70–32.77	4H-7, 6–8	36.06–36.08				
Correlation uncertain			5H-3, 49–54	36.19–36.24			5H-1, 102–105	35.22–35.25	5H-2, 36–47	34.36–34.47
Correlation uncertain			5H-3, 66–79	36.36–36.49	5H-2, 101–111	39.01–39.11	5H-2, 110–119	36.80–36.89	5H-4, 127–137	38.27–38.37
Correlation uncertain			5H-7, 0–4	41.70–41.74	5H-6, 13–17	44.13–44.17				
Correlation uncertain										
Correlation uncertain			6H-2, 89–102	44.59–44.72	6H-1, 138–143	47.38–47.43	6H-2, 116–118	46.36–46.38		
Correlation uncertain			6H-2, 141–144	45.11–45.14	Not recognized		6H-2, 125–129	46.45–46.49		
Correlation uncertain			6H-7, 3–9	51.23–51.29	6H-6, 30–34	53.80–53.84	6H-7, 10–17	52.80–52.87		
Correlation uncertain					6H-6, 103–105	54.53–54.55				
Mazama Ash			7H-1, 3–5	51.73–51.75			7H-1, 86–88	54.06–54.08		

Note: Because of recoveries exceeding 100%, inaccuracies in the precise depths (mbsf) of some massive intervals are apparent in this table.

the acoustic signal. Acoustic *P*-wave velocity in the lower gray clay unit varies from 1.5 to 1.6 km/s (Table 11).

Undrained Shear Strength

Shear strength was measured on split cores from Hole 1034B using a motorized miniature vane shear device. Shear strength at Site 1034 shows small increases with depth over the top 70 m, increasing from ~5 to 20 kPa over this interval (Fig. 25). Although these strengths are low, the ratio of undrained shear strength to effective overburden stress ($S_u/P_o' = 0.2$) suggests that these sediments, as at Site 1033, are normally consolidated. Below ~70 mcd (65 mbsf), the shear strength profile shows a change in slope, with shear strengths increasing with depth at a greater rate than before and with higher variability. This lower section corresponds with the gray clay unit in the visual core descriptions. The variability is likely related to changing sediment types in massively bedded deposits. The S_u/P_o' ratios decrease with depth, similar to the same unit at Site 1033, suggesting that ice loading at this site was unlikely.

ORGANIC GEOCHEMISTRY

Overview

The organic geochemistry of the sediments in the Saanich Inlet clearly shows a diagenetic segregation into two major compartments.

The boundary between these two zones occurs at ~50 mbsf at Site 1033 and at 80 mbsf at Site 1034.

The uppermost zone distinguishes itself as organic-rich sediments (1–2.5 wt% C_{org}). Enhanced remineralization of this organic matter leads to anaerobic conditions in these sediments. This is indicated by the intense enrichment of nutrient concentrations, such as alkalinity up to 106 mM. The bacterial exhaustion of free oxygen, nitrogen, and metal oxides in the interstitial fluids, according to the typical diagenetic sequence (Claypool and Kaplan, 1974), has lead to the utilization of sulfate by sulfate-reducing bacteria (SRBs) as terminal electron acceptors. The SRBs effectively remove dissolved sulfate to trace or non-detectable levels in the shallow anaerobic zone. The exhaustion of sulfate leads to intense methanogenesis in the upper zone of Saanich Inlet sediments. Furthermore, the toxic sulfide accumulations preclude the population of the surface sediments by infauna. As a result, the sediments are not bioturbated and retain their original laminated deposition.

In the deeper diagenetic zone, the organic matter is an order of magnitude lower than in the shallower zone (~0.2 wt% C_{org}). This organic material is largely refractory and does not support extensive diagenesis. As a consequence, the dissolved sulfate is close to full marine concentrations (26 mM), methane is absent, and the nutrient levels are low (e.g., alkalinities ~4 mM). The clearly oxidized conditions support benthic communities that can bioturbate the sediments and destroy any record of lamination.

Table 7. Summary of accelerator mass spectrometer (AMS) radiocarbon ages of material taken from Sites 1033 and 1034.

Core, section, interval (cm)	Sample	Taxon	^{14}C age (yr BP)	Calibrated ^{14}C age (yr BP)
169S-1033B-				
2H-7, 28	Shell	Bivalvia *Compsomyax subdiaphana*	2,420 ± 60	1,407−1,715
3H-5, 144	Charcoal		2,940 ± 50	2,892−3,316
5H-1, 8	Charcoal		5,430 ± 50	6,059−6,389
6H-2, 15	Shell	Bivalvia *Macoma calcarea*	8,880 ± 50	8,929−9,226
6H-2, 60	Shell	Bivalvia *Axinopsida serricata*	9,030 ± 50	9,078−9,388
6H-2, 90	Shell	Bivalvia *Axinopsida serricata*	9,150 ± 50	9,246−9,474
6H-4, 110	Shell	Bivalvia *Axinopsida serricata*	10,190 ± 70	10,304−10,879
6H-5, 135	Shell	Bivalvia *Macoma calcarea*	10,600 ± 60	10,952−11,452
6H-5, 141	Shell	Bivalvia *Macoma calcarea*	10,700 ± 50	11,003−11,643
6H-6, 13	Shell	Bivalvia *Macoma calcarea*	10,710 ± 60	11,000−11,687
6H-6, 88	Shell	Bivalvia *Macoma calcarea*	11,050 ± 60	11,668−12,336
169S-1033C-				
2H-2, 116	Wood		1,240 ± 50	973−1,286
2H-6, 125	Wood		1,770 ± 50	1,536−1,819
2H-7, 16	Shell fragment		2,650 ± 50	1,704−1,960
3H-1, 37	Wood	Pacific Yew *Taxus brevifolia*	2,460 ± 50	2,347−2,735
4H-5, 71	Charcoal		5,900 ± 50	6,568−6,886
5H-6, 51	Shell	Cirripedia *Balanus nubilus*	8,810 ± 50	8,766−9,154
5H-7, 56	Wood	Pacific Yew *Taxus brevifolia*	8,430 ± 50	9,269−9,491
6H-1, 134	Shell fragment		10,220 ± 60	10,355−10,894
169S-1033D-				
2H-1, 28	Shell fragment		1,620 ± 50	652−888
2H-4, 107	Wood		1,410 ± 50	1,193−1,406
4H-1, 124	Shell	Cirripedia *Balanus nubilus*	4,450 ± 50	3,894−4,224
4H-4, 34	Wood		4,500 ± 60	4,872−5,433
5H-5, 9	Wood		6,650 ± 50	7,392−7,547
6H-2, 52	Wood		8,890 ± 60	9,664−9,987
6H-4, 14	Shell fragment		10,480 ± 50	10,864−11,073
6H-4, 101	Shell fragment		10,630 ± 60	10,967−11,504
6H-4, 137	Shell	Bivalvia *Macoma carlottensis*	10,890 ± 60	11,383−12,102
7H-2, 5	Shell	Gastropoda *Cylichna alba*	13,080 ± 70	14,038−14,711
169S-1034B-				
2H-4, 118	Shell	Bivalvia *Mytilus edulis*	1,880 ± 80	868−1,199
3H-2, 113	Wood		1,880 ± 50	1,631−1,923
4H-2, 52	Wood		2,840 ± 50	2,781−3,156
4H-2, 108	Wood		2,810 ± 60	2,762−3,156
4H-4, 56	Wood		4,260 ± 50	4,554−4,977
6H-4, 3	Wood		5,670 ± 50	6,303−6,632
6H-CC, 0	Shell	Bivalvia *Macoma calcarea*	7,320 ± 50	7,271−7,471
7H-4,107	Shell	Bivalvia *Macoma calcarea*	8,590 ± 50	8,469−8,891
7H-6, 129	Shell	Bivalvia *Macoma calcarea*	9,060 ± 50	9,148−9,419
7H-CC, 0	Shell	Bivalvia *Macoma calcarea*	11,070 ± 70	11,677−12,377
8H-2, 57	Shell	Bivalvia *Macoma calcarea*	9,790 ± 50	9,914−10,185
8H-3, 53	Shell		10,280 ± 60	10,429−10,927
8H-5, 16	Shell	Bivalvia *Macoma calcarea*	10,800 ± 70	11,098−11,944
8H-5, 134	Shell		10,490 ± 50	10,870−11,083
8H-6, 66	Shell		10,710 ± 50	11,009−11,662
8H-7, 10	Shell		11,070 ± 60	11,702−12,361
9H-5, 21	Shell	Bivalvia *Nuculana fossa*	12,630 ± 60	13,557−14,067
169S-1034C-				
1H-4, 146	Wood		330 ± 50	286−507
2H-3, 51	Wood		1,350 ± 50	1,173−1,344
3H-6, 69	Shell		3,330 ± 50	2,552−2,777
4H-5, 71	Fish bones		6,130 ± 50	5,577−5,840
6H-3, 110	Wood	Western Red Cedar *Thuja plicata*	5,790 ± 50	6,417−6,741
6H-6, 72	Shell	Bivalvia *Axinopsida serricata**	7,160 ± 50	7,152−7,349
9H-5, 60	Shell	Scaphopoda *Rhabdus rectius*	13,250 ± 50	14,266−14,917
10H-7, 49	Shell	Bivalvia *Yoldia martyria*	13,270 ± 60	14,280−14,958
169S-1034D-				
1H-CC, 2	Wood		390 ± 50	305−521
2H-4, 20	Wood		1,030 ± 50	796−1,053
2H-6, 62	Wood		1,440 ± 50	1,262−1,411
6H-4, 24	Wood		5,770 ± 60	6,409−6,741
7H-4, 30	Shell fragment		8,420 ± 70	8,302−8,581
7H-4, 136	Wood		7,910 ± 60	8,504−8,960
8H-1, 44	Shell fragment		9,900 ± 60	9,983−10,339
8H-3, 143	Shell	Bivalvia *Nuculana fossa*	10,690 ± 50	10,998−11,614
8H-4, 96	Shell fragment		10,610 ± 50	10,965−11,445
169S-1034E-				
5H-6, 40	Wood		4,270 ± 50	4,590−4,960
6H-6, 96	Shell fragment		7,070 ± 60	7,009−7,268
7H-4, 12	Shell fragment		8,210 ± 60	8,082−8,354
8H-1, 12	Shell	Bivalvia *Macoma calcarea**	9,450 ± 60	9,491−9,870
9H-1, 19	Wood	Pacific Yew *Taxus brevifolia*	10,110 ± 50	11,086−12,105
9H-1, 69	Wood		10,410 ± 60	12,038−12,509
9H-1, 133	Shell	Bivalvia *Macoma calcarea*	11,450 ± 60	12,385−12,748
9H-4, 64	Shell	Bivalvia *Nuculana fossa*	12,660 ± 50	13,597−14,091

Notes: * = cores not used in composite splice. Ages are in both radiocarbon years and corrected calendar years (see text for explanation).
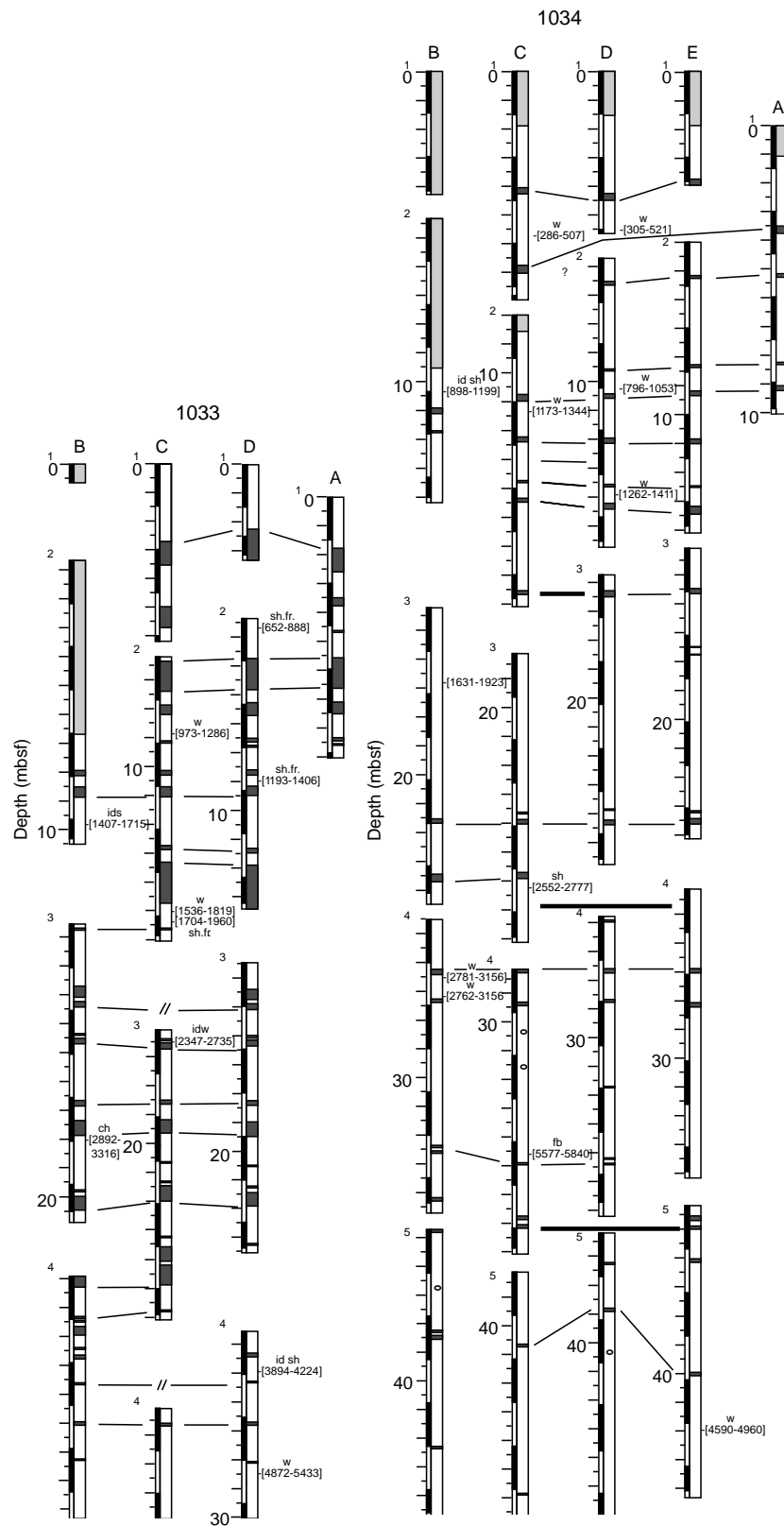
Figure 19. Accelerator mass spectrometer ^{14}C ages in calendar years BP for Sites 1033 and 1034. For an expanded version of this figure, please see the back-pocket foldout, this volume.
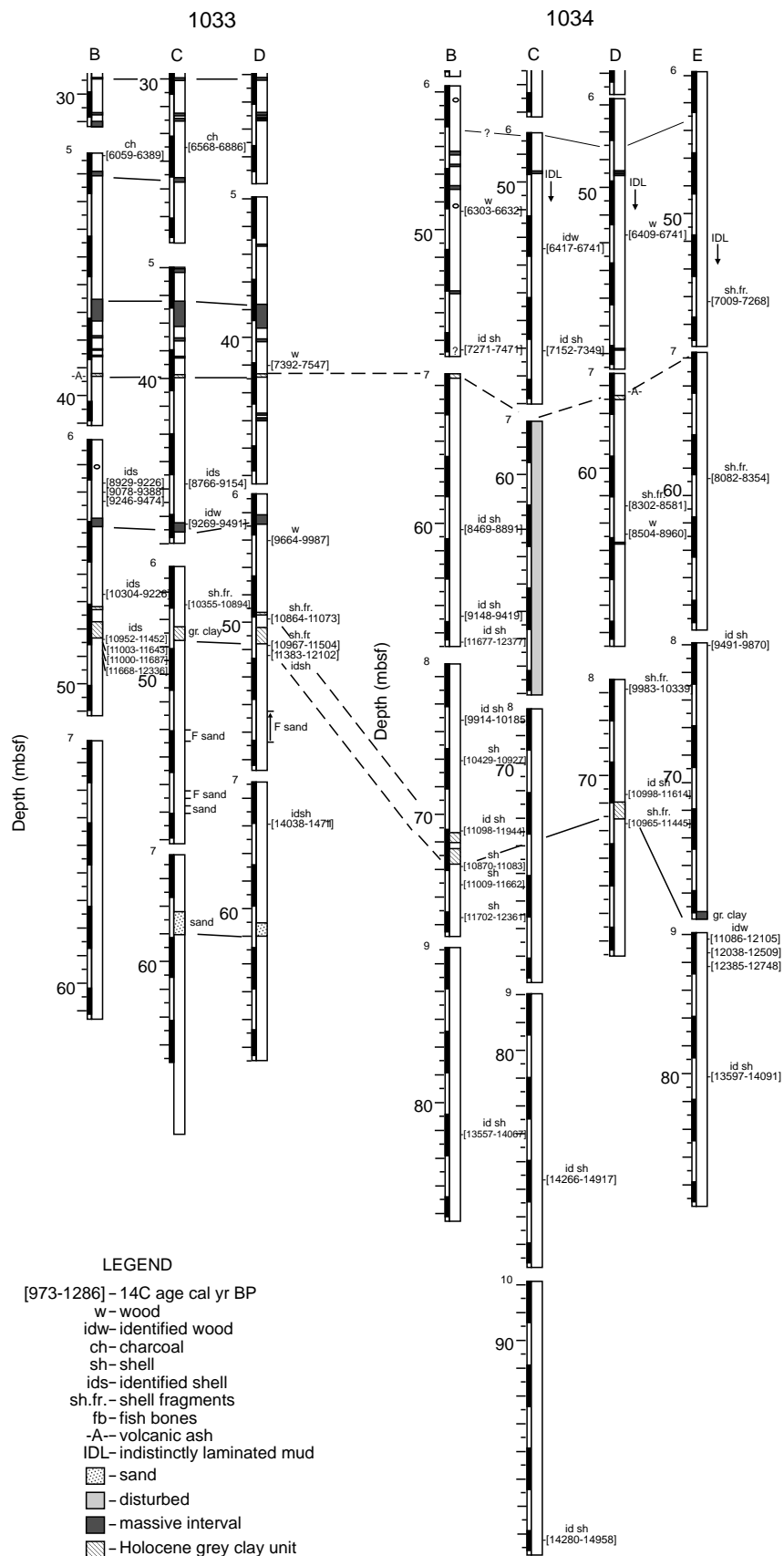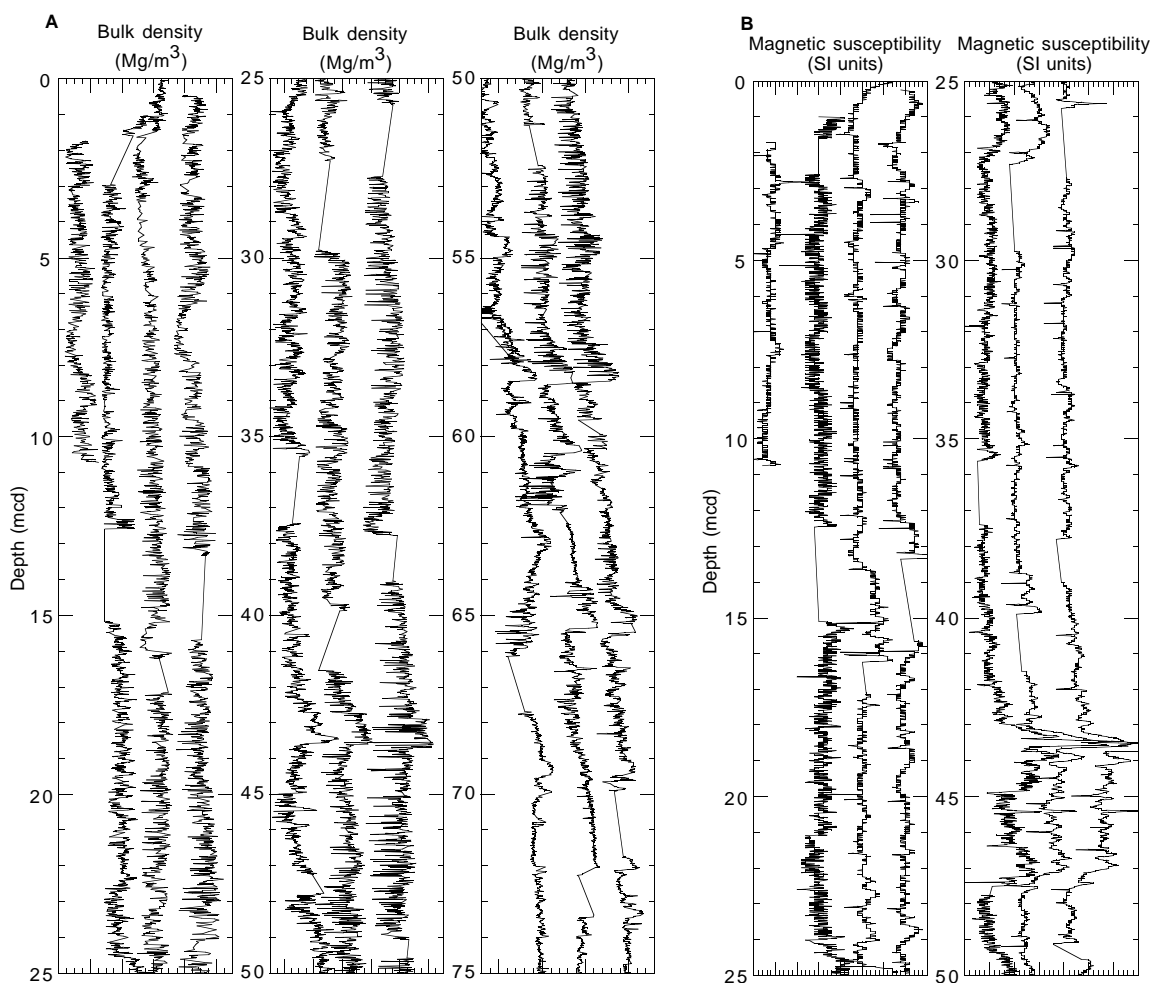
Figure 19 (continued).

Figure 20. **A.** GRAPE bulk density data vs. depth for all holes at Site 1033. The density scale has a range of 1.0 Mg/m³ for 0–25 mcd and 50–75 mcd; the range is 1.2 Mg/m³ for 25–50 mcd. **B.** Magnetic susceptibility vs. depth for all holes at Site 1033. The scale has a range of 40 SI units for 0–25 mcd and 70 SI units for 25–50 mcd. **C.** Color reflectance value L* vs. depth for all holes at Site 1033. The scale has a range of 100 L* units for 0–25 mcd, and 50 L* units for 25–50 mcd and 50–75 mcd. The data from each hole are shifted so that plots from each hole are not overwritten.

This diagenetic sequence "reversal," that is, oxidized beneath reduced sediments, is a situation not commonly encountered in marine settings (e.g., Whiticar et al., 1995). The combination of changes in organic supply and oxygenation in the overlying water column are likely responsible for this situation.

Methods Overview

During Leg 169S, the compositions and concentrations of hydrocarbons and other gases were monitored in the sediments generally at intervals of one per core. Because of the rigorous stratigraphic requirements of the Saanich Inlet leg, the gas geochemistry was restricted to samples from the core catcher only or from the cuts between liner sections. Vacutainers were taken where expansion void gas (EVG) was observed, typically in sediments <70 mbsf. The two methods used are (1) headspace (HS) method and (2) vacutainer (V) method (see "Sanaach Inlet Explanatory Notes" chapter, this volume for details).

Concentration Notation

The headspace and vacutainer gases measured by the HC and NGA methods are reported on a gas volumetric basis, that is, percent by volume (vol%) or as parts per million by volume (ppmv), especi-

ally μL CH₄/L sample (STP). In the case of the vacutainer (EVG) samples, the partial pressures of the gases measured are similar to those in the gas pocket of the sediment core liner. Inherent in the sampling for the headspace measurement, there is considerable contamination of air in the vial prior to sealing. This air contamination is not detected or quantified by the FID-GC. Correction for the atmospheric contribution will be possible with shore-based differential weight measurements to follow carbon isotope measurements of the gases. However, because the Wheaton sample bottle volumes are known to be quite constant, and the amounts of sediment taken are similar, the air contribution is roughly consistent. The gas contents reported for abundances, therefore, especially for the HC method, should be considered only in relative terms at this stage.

Furthermore, the ambient temperature and pressure sampling technique is unable to determine if the interstitial fluids at depth are saturated with respect to gas. However, if the gases are undersaturated at the surface conditions, it is reasonable to assume that the in situ conditions were undersaturated as well.

Site 1033 Gas Samples

Of the four holes cored at Site 1033, only the sediments of Holes 1033A and 1033B were analyzed for their gas composition. In the case of Hole 1033A, only three HS and V samples were collected in
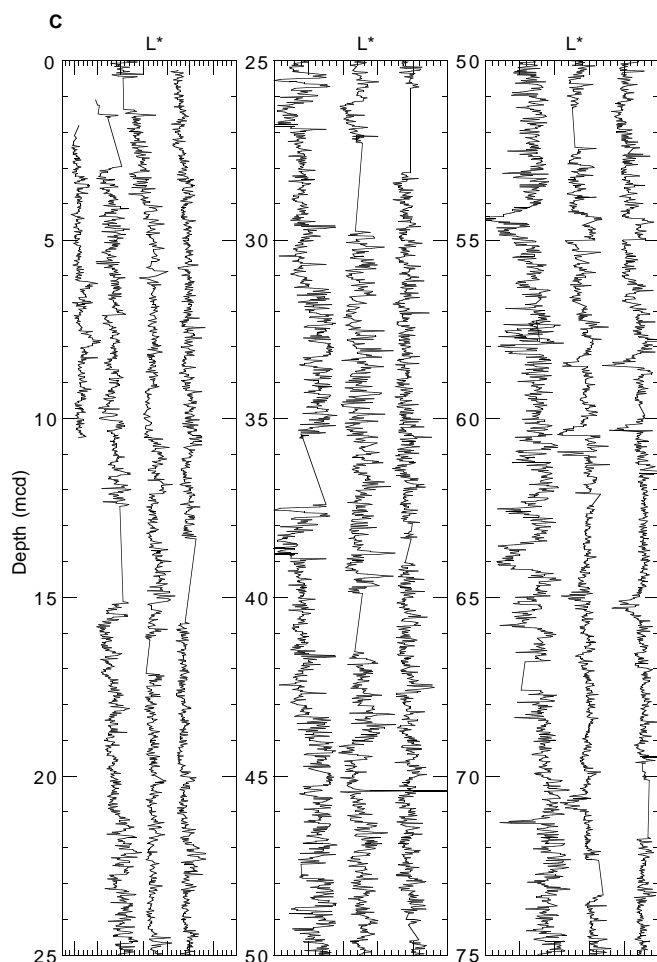
C

Figure 20 (continued).

Table 8. Offset depths for all cores at Site 1033.

Core	Depth (mbsf)	Offset	Depth (mcd)
169S-1033-			
A-1*	0	1.7	1.7
B-1	0	1	1
B-2	0.6	2	2.6
B-3*	10.1	5	15.1
B-4*	19.6	5.8	25.4
B-5*	29.1	8.3	37.4
B-6*	38.6	9.15	47.75
B-7*	48.1	8.5	56.6
B-8	57.6	10	67.6
B-9*	67.1	10.07	77.17
B-10*	76.6	9.98	86.58
B-11	86.1	9.6	95.7
B-12	95.5	8.4	103.9
C-1*	0	0	0
C-2*	6.2	−0.05	6.15
C-3	15.7	1.4	17.1
C-4*	25.2	4.55	29.75
C-5*	34.7	6.8	41.5
C-6	44.2	8.2	52.4
C-7*	53.7	8.7	62.4
C-8	63.2	10.1	73.3
D-1*	0	0.25	0.25
D-2	3.2	0.1	3.3
D-3	12.7	2.95	15.65
D-4	22.2	5.9	28.1
D-5	31.7	7.3	39
D-6	41.2	8.35	49.55
D-7	50.7	9.2	59.9
D-8*	60.2	11.5	71.7

Notes: * = cores used in composite splice. The offsets are simple linear shifts, calculated from the mbsf depth scale.

The distribution of methane has a clear inverse correspondence to the presence of dissolved sulfate (Fig. 27A). This strongly suggests that the methane encountered is of bacterial origin and has been generated following the removal of dissolved sulfate by SRBs. That the low sulfate is due to SRBs and not because of freshwater dilution is confirmed by the chloride data, which show little variation with depth (Fig 27C). The resultant low sulfate/chloride ratios in the shallow section of Site 1033 (Fig. 27D) indicates a preferential loss of sulfate explained by SRBs.

Vacutainer Samples

Similar to the headspace samples, the greatest amounts of methane in the void spaces were recorded in the uppermost 40 mbsf at Site 1033 (Table 13; Fig. 26B). However, the strong methane excursion observed in the headspace at 51 mbsf (Fig. 26A) is not tracked by the vacutainer sampling. In many instances, methane is the dominant gas in the vacutainers, constituting up to a maximum of 91.6% at 32.28 mbsf. With the exception of a low of 29% at 5.6 mbsf, the vacutainer gas hovered ~88% down to 40 mbsf. Below this depth, the amount of methane decreased rapidly to low levels of 600 ppmv at 69.5 mbsf (Fig. 26B). No vacutainer samples were recovered at depths greater than 69.5 mbsf as there were no apparent voids in the liners at greater depth.

The remaining gases in the vacutainers were identified to be molecular nitrogen (N_2), oxygen (O_2), carbon dioxide (CO_2), or hydrogen sulfide (H_2S; Table 13). Nitrogen and oxygen track very closely with a volume mixing ratio suggesting atmospheric gas (Fig. 28A, 28B). Certainly in the anaerobic sediments, free or dissolved oxygen is not expected and is most probably contamination. This would also mean that most of the molecular nitrogen is air contamination as well.

In contrast, the carbon dioxide in the upper 40 mbsf is present in amounts far exceeding the 350 ppmv mixing ratio expected for atmospheric CO_2 (Fig. 26C). In fact, CO_2 roughly tracks the methane contents in the vacutainers, suggesting a causal relationship with the diagenetic remineralization of organic matter. The measured titration

the shallowest core (169S-1033-1H) down to 8.88 mbsf (Tables 12, 13). In Hole 1034B, 16 HS and 11 V samples were taken down to 95.5 mbsf (Tables 12, 13).

Headspace Samples

The Saanich Inlet sediments were very gassy. Rapid degassing of the cores led to pressure build-up in the liners that was relieved by drilling a series of holes at ~5 cm intervals down the length of the core. This led to considerable sediment loss as the gas, interstitial fluids, and sediments were extruded by the overpressure through the relief holes. Care was taken to locate the liner relief holes in expansion void spaces. Fortunately, this sample loss does not appear to affect the relative stratigraphy and merely diminishes the sample volume.

Methane was the sole hydrocarbon in the headspace detected by the HS method. The concentrations ranged from a low of 8.7 ppmv to a high of 29,510 ppmv (Table 12). The gases that are not reported, but constituting the remainder, would likely be N_2, O_2, CO_2, or H_2S. Figure 26A shows the dramatic changes in methane concentration with sediment depth at Site 1033. The shallowest sample in Hole 1033A (0.03 mbsf) has a methane concentration value of 15,896 ppmv. Immediately below this, the methane drops to 3,195 ppmv, then gradually rises to ~8,000 ppmv by 50 mbsf. At 51.08 mbsf, methane rises sharply to the maximum of 29,510 ppmv, then drops sharply to and remains at very low levels, ~10 ppmv, below 60 mbsf (Fig. 26A).
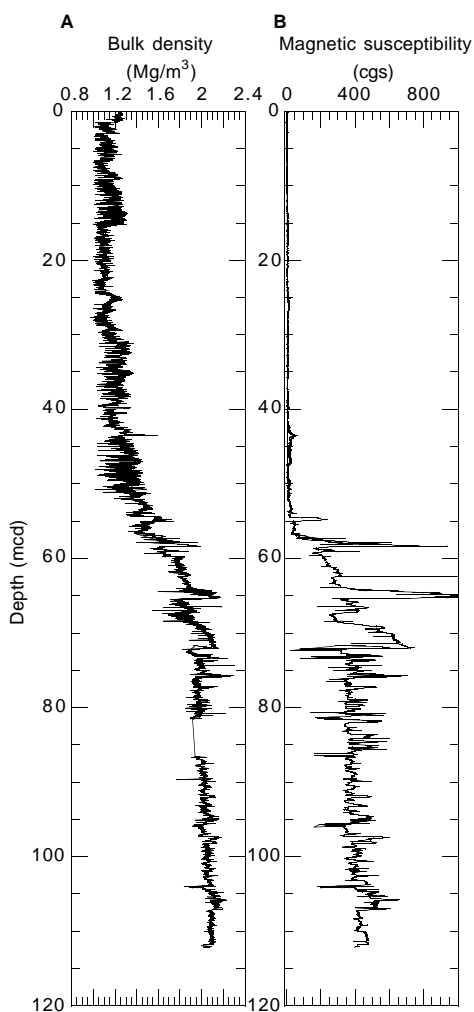
Figure 21. **A.** Composite of the spliced bulk density record vs. depth for Site 1033. **B.** Composite of the spliced magnetic susceptibility record vs. depth for Site 1033.

Table 9. Uncorrected and corrected acoustic velocity measured on discrete intervals for Hole 1033B.

Core, section, interval (cm)	Depth (mbsf)	Traveltime (μs)	Uncorrected velocity (km/s)	Temperature (°C)
169S-1033B-				
8H-6, 9	57.69	48.05	1.55	13.9
9H-1, 20	67.3	49.5	1.51	14.5
9H-2, 20	67.3	49.2	1.52	14.5
9H-3, 52	67.62	49.2	1.52	14.5
9H-4, 70	67.8	49.2	1.52	14.5
9H-5, 20	67.3	49.2	1.52	14.5
9H-6, 10	67.2	48.8	1.53	14.5
10H-1, 20	76.8	49.2	1.52	7.8
10H-2, 20	76.8	49.05	1.52	10.1
10H-3, 20	76.8	49.1	1.52	11.7
10H-4, 20	76.8	48.9	1.53	16.8
10H-5, 20	76.8	46.95	1.59	18.2
10H-6, 20	76.8	48.15	1.55	20.3
11H-1, 20	86.3	48.5	1.54	13.2
11H-2, 20	86.3	46.7	1.60	10.2
11H-3, 20	86.3	47.3	1.58	15.5
11H-4, 20	86.3	47.55	1.57	14.9
11H-5, 20	86.3	48.85	1.53	16
11H-6, 20	86.3	48.05	1.55	14.1
12H-1, 20	95.7	48.5	1.54	16.3
12H-2, 20	95.7	47.45	1.57	13.7
12H-3, 20	95.7	46.95	1.59	13.6
12H-4, 20	95.7	48.3	1.54	14.8
12H-5, 20	95.7	47.8	1.56	17
12H-6, 20	95.7	47.65	1.57	15.5

Note: Temperature measurements are provided so corrected velocity values can be calculated.
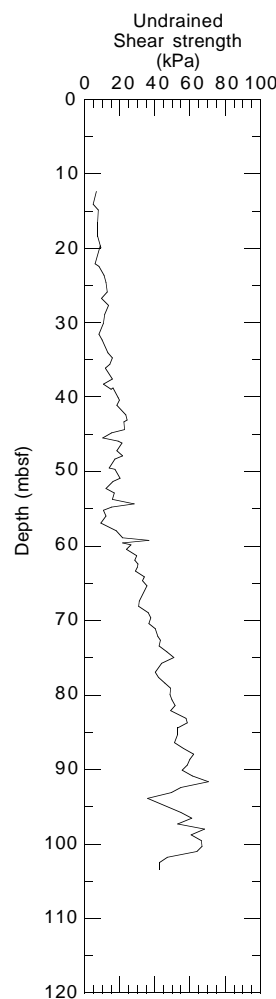
Figure 22. Undrained shear strength vs. depth for Hole 1033B.

alkalinity shown in Figure 26B confirms the high remineralization levels in the uppermost 40 mbsf.

Hydrogen sulfide accumulation, a consequence of bacterial sulfate reduction, is particularly high in the vacutainer samples taken near-surface: 225 and 102 ppmv at 1.18 and 5.60 mbsf, respectively (Fig 28C). Sulfide drops quickly to a level ~30 ppmv by 7 mbsf, where it persists at that level downhole to the last interval sampled (69.50 mbsf).

Organic Carbon, Nitrogen, Sulfur, and Carbonate

The key to the observed gas and nutrient profiles is the distribution and level of nonrefractory organic matter in the hole. As seen in Figure 29A, %C_{org}, is above 2 wt% in the upper 20 mbsf. It then gradually decreases to very low levels ~0.2 wt% by 50 mbsf (Table 14). Below that depth, the %C_{org} remained constant at this low level.

This dramatic change in organic matter contents in the sediments above and below 50 mbsf is mirrored by the %N_{org} and %S_{org} depth distributions (Table 14; Fig. 29A–C). Organic nitrogen at Site 1033 decreases gradually from ~0.4 wt% at the surface to 0.05 wt% at 50 mbsf, with the exception of the single sample of 0.75 wt% at 6 mbsf.

Similarly, sulfur decreases from 1.15 wt% to below the detection limit at 50 mbsf.

This strong demarcation between organic-rich and organic-poor sediments controls the diagenetic behavior expressed by the dissolved nutrients, especially alkalinity (Fig 27B), the reducible species (e.g., sulfate; Fig. 27A), and by the carbon- and sulfur-bearing gases.

Carbonate contents at Site 1033 remained relatively constant with depth between 1 and 1.5 wt%, with the exceptions of two samples with 8.1 and 4.1 wt% at depths 31.99 and 47.49 mbsf, respectively. Aggregates of calcite carbonate were encountered at Site 1033. These ~2-cm, yellow, granular crystals are thought to be decomposed "ikaite," or calcium carbonate hexahydrate (see Fig. 14). Carbonate indurated and nodule intervals were encountered (see "Lithostratigraphy" section, this chapter).

Site 1034 Gas Samples

The depth distribution profiles of the basic geochemical parameters (i.e., gases, nutrients, and organic matter) at Site 1034 are very similar to those described above for Site 1033. For this reason, Site 1034 will not be discussed in detail here, and the reader is referred to Site 1033. The data are listed in Tables 15 (headspace gases), 16 (vacutainer gases), and 17 (solid C, N, S).

Headspace and Vacutainer Gas

The gas composition was analyzed from the sediments cored at two of the four holes at Site 1034 (Holes 1034A and 1034B). In the case of Hole 1033A, one HS and two V samples were collected in the shallowest core (Core 1H) down to 5.39 mbsf (Figs. 30, 31). Nineteen headspace and 17 vacutainer samples were analyzed in Hole 1034B.

Methane in the headspace varied ~8,000 ppmv down to 65 mbsf. This was tracked by vacutainer methane and carbon dioxide (Fig 30). As in Hole 1033B, there was a single very prominent methane peak at depth, (19,308 ppmv at 83.18 mbsf, Hole 1034B; Fig. 30). At greater depth, CH_4 (HS and V) and CO_2 (V) dropped to low concentrations. These gas profiles correspond to the appearance of dissolved sulfate below 60 mbsf and its rise close to seawater values of 26 mM by 82.5 mbsf (Fig 32). The low and exhausted sulfate levels are inversely related to the titration alkalinity (Fig 32). As at Site 1033, the low sulfate is a result of bacterial sulfate reduction by SRBs and not because of dilution with freshwater. This interpretation is confirmed by the clear shift in the SO_4/Cl ratios (Fig 32). Hydrogen sulfide (V) was very high (371 ppmv) in the vacutainer sample at 0.39 mbsf and, analogous to Site 1033, decreases to a relatively constant level of ~30 ppmv with depth (Fig 31).

Organic Carbon, Nitrogen, Sulfur, and Carbonate

The $\%C_{org}$, $\%N_{org}$, $\%S$, all decreased regularly from surface values of 2.5 wt%, 0.4 wt%, and 1.0 wt%, respectively, down to the geochemical break at 85 mbsf (Fig 33). Below that depth, as at Site 1033 (break at 50 mbsf), the C, N, and S contents dropped to very low levels (~0.2, 0.05, and 0.0 wt%, respectively).

The carbonate contents at Site 1034 were similar to Site 1033, hovering ~1.5 wt% (Fig. 33D). The two large carbonate excursions seen in Site 1033 (Fig 29D) are not observed at this site. However, an incredibly exquisite 15-mm carbonate crystal was encountered at 48 mbsf in Section 169S-1034D-7H-1. It is thought that this crystal is "glendonite," a pseudomorphic recrystalization of "ikaite" (calcium carbonate hexahydrate). Yellow, granular carbonate aggregates are also observed at Site 1034 as was the case at Site 1033.

The organic matter content clearly controls the extent of diagenesis and redox level at Site 1034 as it did at Site 1033. Low sulfate, high methane, and high carbon dioxide all corresponded to the intervals with high organic matter contents in the upper 80 mbsf. Below 80 mbsf, low organic matter leads to limited sulfate reduction and the low CH_4 and CO_2 contents. The redox level also controls the occurrence of infauna, and, hence, the degree of bioturbation and the presence or absence of laminated sediments in Saanich Inlet.

INORGANIC GEOCHEMISTRY

Introduction

The routine shipboard chemical analytical programs for interstitial waters of samples collected in the Saanich Inlet were undertaken during Leg 169S. With high alkalinity interstitial waters, immediate studies of the cationic components, especially calcium and magnesium, is necessary, because upon degassing precipitation of carbonates may compromise the data. The analyses reported here were all completed within a period of 2 weeks after Leg 169. Methodologies used are from the routine program on *JOIDES Resolution* as described by Gieskes et al. (1991).

The shipboard program consisted largely of the routine shipboard analyses: pH, alkalinity, salinity, chloride, calcium, magnesium, strontium, lithium, potassium, sodium (by difference of cation and anion charge balance), sulfate, alkalinity, ammonium phosphate, boron, and silica (Tables 18, 19).

The data presentation emphasizes various groups of constituents: chloride and sodium, nutrient related constituents (alkalinity, sulfate, ammonium, and phosphate), alkaline earth elements (magnesium, calcium, and strontium), alkali metals (lithium, sodium, and potassium), as well as boron and dissolved silica.

Hole 1033B

Nutrient Elements

Nutrient elements are presented in Figure 34. As expected in these organic carbon–rich sediments, the upper Holocene varved sediments are essentially devoid of dissolved sulfate, but a sharp gradient in dissolved sulfate occurs between 60 and 80 mbsf. Below 80 mbsf, concentrations are essentially equal to the seawater values. This can be understood in terms of lack of sulfate reduction in the glacial clay section (also low in organic carbon) and the short length scale for diffusive communication with the overlying sediments. The profile of alkalinity indicates a very sharp increase to a maximum of ~90 mM. This value is well above that to be expected from simple sulfate reduction processes. Ammonium concentrations also exceed those expected from sulfate reduction processes alone. Finally, phosphate concentrations reach values as high as 350 μM, although with some variability in the concentration depth profile.

The most interesting observation, of course, is the sharp increase in dissolved sulfate below 60 mbsf, reaching constant values at ~80 mbsf. Organic carbon contents in the lower glaciomarine sediments are low, which explains the essential lack of sulfate reduction in this zone (see "Organic Geochemistry" section, this chapter). As a result of the rapid deposition of the upper sediments, the communication length is ~11 m, as discussed above. This is indeed the length of the principal part of the sulfate gradient. Both the alkalinity and the ammonium concentration gradients show more gradual decreases below their respective maxima. In part, this can be understood in terms of more important organic carbon diagenesis in the upper, more organic-rich sediments.

Alkaline Earth Elements

The concentration-depth profiles for alkaline earth elements are presented in Figure 35. The data for dissolved calcium indicate a

removal in the upper sediment section as a result of calcium carbonate precipitation. Again below 60 mbsf, a sharp increase in dissolved calcium occurs, but the concentrations exceed those of seawater by ~10 mM. Dissolved magnesium shows a sharp increase from the overlying bottom-water value, estimated at 48 mM from a chloride content of 495 mM. Below 40 mbsf, magnesium concentrations indicate a minimum at ~60 mbsf, below which the concentrations increase to ~3 mM less than present-day bottom water. Dissolved strontium indicates a minimum at ~30 mbsf below which a gradual increase occurs to 60 mbsf to reach concentrations about 25 μM higher than bottom water.

The data in the lowermost glaciomarine sediments suggest that reactions involving diagenesis of these sediments lead to slight increases in dissolved calcium and strontium, with a concomitant decrease in magnesium.

Chloride and Alkali Metals

Dissolved chloride (Fig. 36) shows a complex concentration depth distribution, with a maximum at ~10 mbsf, and similar high values in the glaciomarine section.

Dissolved sodium (as well as the Na/Cl ratio) shows a maximum in the sodium concentrations in the upper sediment section, similar to the magnesium profile. In the glaciomarine section, sodium and Na/Cl values drop to below those in the bottom waters, suggesting the uptake of sodium in the same process that led to the decrease in magnesium and increases in calcium and strontium.

Dissolved lithium and potassium concentrations are presented in Figure 37. Immediately below the sediment/water interface, lithium must have been removed, as concentrations appreciably less than those of bottom waters (24 μM) are observed in the top of Core 169S-1033B-1H. Further appreciable decreases occur in the glaciomarine section, mostly as a result of lithium uptake in these sediments. Dissolved potassium shows a slight maximum in concentration. Below 40 mbsf the potassium concentrations decrease to 5 mM, again as a result of diagenetic reactions in these lower lying sediments.

Silica and Boron

Dissolved silica (Fig. 38) typically is representative of the local lithology of the sample. In the upper section the average concentration is ~1100 μM, probably reflecting the presence of biogenic silica. Below 60 mbsf, in the glaciomarine sediments, values drop abruptly to ~250 μM, mostly reflecting the absence of biogenic silica, thus allowing dissolved silica control by detrital clay sediments.

Boron concentrations (Fig. 38) show a gradual increase in the varved sediment section to reach a maximum at ~25 mbsf. Below this, the concentrations decrease gradually to reach fairly constant values of 200 μM in the glaciomarine sediments.

Hole 1034B

Nutrient Elements

Nutrient elements are presented in Figure 39. Sedimentation rates at this site are higher than in Hole 1033B. As a result, it appears that increases in alkalinity and ammonium exceed those in Hole 1033B to a small extent. Dissolved phosphate concentration increases, however, are slightly less than in Hole 1033B.

Again, as in Hole 1033B, a sharp increase in sulfate occurs in dissolved sulfate below the 80 mbsf level, to reach almost constant concentrations below 100 mbsf (values only slightly less than in Hole 1033B).

Alkaline Earth Elements

The concentration-depth profiles of calcium, magnesium, and strontium are similar in nature to the profiles of Hole 1033B, with the exception that the maximum in dissolved magnesium in the upper sediments is larger. The minimum in magnesium at the boundary with the glaciomarine sediments observed at Hole 1033B is much less pronounced in this hole. As in Hole 1033B, the concentrations of dissolved calcium are ~10 mM higher than in bottom waters, whereas magnesium concentrations are slightly lower.

Chloride and Alkali Metals

As in Hole 1033B, the chloride concentrations are variable with depth, with a small maximum at 35 mbsf, a more pronounced minimum at 70 mbsf, and an increase to ~510 mM (Hole 1033B, ~505 mM) in the glaciomarine section. Concentration profiles of sodium (and Na/Cl) show increases in the upper sediments (maximum at ~35 mbsf, followed by a gradual decrease to ~410 μM in the glaciomarine sediments). Dissolved lithium shows a strong similarity to the profile in Hole 1033B, with a rapid depletion near the surface, followed by a maximum of ~20 μM at ~30 mbsf, and a decrease to well below seawater concentration in the glaciomarine section.

Silica and Boron

Concentration-depth profiles of dissolved boron and dissolved silica are very similar to the profiles of Hole 1033B, although the concentration maximum in dissolved boron is less pronounced in this borehole.

SUMMARY

There is a clear difference in the nature of the chemical compositional gradients in the rapidly deposited, organic carbon-rich Holocene sediments of the Saanich Inlet and those of the underlying glaciomarine sediments.

Of importance to note is that the chemical composition of the interstitial waters of the glaciomarine sediments is distinct from that of seawater. The chloride concentrations in the lower lying sediments are ~507 ± 3 mM, and their sulfate concentrations are ~25−26 mM, that is, within the expected value of 26.3 using the modern seawater concentration ratio of sulfate/chloride. No significant sulfate reduction therefore has affected these pore waters. On the other hand, concentrations in dissolved potassium, sodium, and magnesium drop below expected concentrations. These decreases appear to be balanced by increases in calcium and strontium. The rapidly deposited varved sediments of post-glacial age, on the other hand, indicate very large deviations from the chemical composition of the overlying seawater.

PALEONTOLOGY

Preliminary diatom analyses from Hole 1034B (Cores 169S-1034B-3H, 4H, and 8H) show similar species abundance, composition, and diversity to previously collected cores and phytoplankton records. Dominant species include *Paralia sulcata, Thalassionema nitzschoides, Skeletonema costatum, Thalassiosira gravida, Chaetoceros radicans* (spores), and *Thalassiosira eccentrica.* Cores 169S-1034B-9H through 13H in this hole are devoid of diatoms.

Bivalves and wood fragments were collected from all holes drilled and were identified at the University of Victoria and at the

Pacific Forestry Centre, Natural Resources Canada, respectively (Table 20). Whole bivalves, including some paired specimens, were particularly abundant in the lowermost part of the Holocene; *Macoma calcarea* and *Axinopsida serricata* dominate. Interestingly, of the wood samples identified, many were Pacific Yew (*Taxus brevifolia*), a relatively rare component of today's forests in the region (Fig. 40).

REFERENCES

Abella, S.E.B., 1988. The effect of Mt. Mazama ashfall on the planktonic community of Lake Washington. *Limnol. Oceanogr.,* 33:1376–1385.

Allen, G.B., 1995. Vegetation and climate history from the CDF and CDF/CWH transition on south east Vancouver Island [Master's thesis]. School of Earth and Ocean Sciences, University of Victoria, Victoria, BC, Canada.

Alley, N.F., and Chatwin, S.C., 1979. Late Pleistocene history and geomorphology, southwestern Vancouver Island, British Columbia. *Can. J. Earth Sci.,* 16:1645–1657.

Anderson, J.J., and Devol, A.H., 1973. Deep water renewal in Saanich Inlet, an intermittently anoxic basin. *Estuarine Coastal Mar. Sci.,* 1:1–10.

Bacon, C.R., 1983. Eruptive history of Mount Mazama and Crater Lake Caldera, Cascade range, U.S.A. *J. Volcanol. Geotherm. Res.,* 18:57–115.

Blais, A., 1995. Foraminiferal biofacies and Holocene sediments from Saanich Inlet, British Columbia: implications for environmental and neotectonic research [Ph.D. thesis]. Carleton University, Ottawa, ON, Canada.

————, 1992. Holocene sediments from Saanich Inlet, British Columbia and their neotectonic significance. *Pap.[0151] Geol. Surv. Can.,* 92-1A:195–198.

Blyth, H.E., and Rutter, N.W., 1993. *Surficial geology of the Sidney area.* Min. Energy, Mines, Petrol. BC., Open file map 1993-24, NTS 92B/11.

Blyth, H.E., Rutter, N.W., and Sankeralli, L.M., 1993. *Surficial geology of the Shawnigan Lake area.* Min. Energy, Mines, Petrol. BC., Open file map 1993-26, NTS 92B/12.

Bobrowsky, P.T., Clague, J.J., and Blais, A., 1993. Late Holocene earthquakes: the geological record from Saanich Inlet, southern Strait of Georgia. Proc., Conference on Large Earthquakes and Active Faults in the Puget Sound Region, University of Washington, Seattle, Washington, May 13-14, 1993.

Bobrowsky, P.T., and Clague, J.J., 1990. Holocene sediments from Saanich Inlet, British Columbia, and their neotectonic implications. *Pap.[0151]Geol. Surv. Can.,* 90-1E, 251–256.

British Columbia Ministry of Environment, Lands and Parks, 1996. *Saanich Inlet study. Synthesis report: technical version:* Victoria (B.C. Min. Environ., Lands, Parks).

Brown, F.S., Baedecker, M.J., Nissenbaum, A., and Kaplan, I.R., 1972. Early diagenesis in a reducing fjord, Saanich Inlet, British Columbia, III. Changes in organic constituents of sediment. *Geochim., Cosmochim. Acta,* 36:1185–1203.

Buddemeier, R.W., 1969. Radiocarbon study of varved marine sediments of Saanich Inlet, British Columbia [Ph.D. dissert.]. Univ. of Washington, Seattle.

Clague, J. J., 1994. Quaternary stratigraphy and history of south-coastal British Columbia: geology and geological hazards of the Vancouver region, southwestern British Columbia. *Bull.[0151] Geol. Surv. Can.,* 481:181–192.

Clague, J.J., Harper, J.R., Hebda, R.J., and Howes, D.E., 1982. Late Quaternary sea levels and crustal movements, coastal British Columbia. *Can. J. Earth Sci.,* 19:597–618.

Claypool, G.E., and Kaplan, I.R., 1974. The origin and distribution of methane in marine sediments. *In* Kaplan, I.R. (Ed.), *Natural Gases in Marine Sediments:* New York (Plenum), 99–139.

Cwynar, L.C., 1987. Fire and the forest history of the North Cascade Range. *Ecology,* 68:791–802.

Drinnan, R.W., Emmett, B., Humphrey, B., Austin, B., and Hull, D.J., 1995. *Saanich Inlet study: water use inventory and water quality assessment.* Rep. for Water Qual. Branch, Environ. Protection Department, B.C. Ministry of Environment, Lands and Parks.

EnviroEd Consultants Limited, 1995. Saanich Inlet study synthesis workshop, information package. Ministry Lands and Parks of British Columbia, April 25-26: Saanich Native Heritage Soc., (Inst. Ocean Sci.), 1–46.

Gieskes, J.M., Gamo, T., and Brumsack, H., 1991. Chemical methods for interstitial water analysis aboard *JOIDES Resolution. ODP Tech. Note,* 15.

Gross, M.G., Gucluer, S.M., Creager, J.S., and Dawson, W.A., 1963. Varved marine sediments in a stagnant fjord. *Science,* 141:918–919.

Gucluer, S.M., and Gross, M.G., 1964. Recent marine sediments in Saanich Inlet, a stagnant marine basin. *Limnol. Oceanogr.,* 9:358–376.

Hebda, R.J., 1983. Late glacial and postglacial vegetation history at Bear Cove Bog, northeast Vancouver Island, British Columbia. *Can. J. Bot.,* 61:3172–3192.

————, 1995. British Columbia vegetation and climate history with focus on 6 Ka B.P. *Geog. Phys. Quat.,* 49:55–79.

Hebda, R.J., and Whitlock, C., 1997. Environmental history. *In* Schoonmaker, P.K., von Hagen, P. and Wolf, E.C. [Eds.], *The Rainforest of Home: Profile of a North America Bioregion.* Island Press (Covelo), 227–254.

Herlinveaux, R.H., 1962. Oceanography of Saanich Inlet in Vancouver Island, British Columbia. *J. Fish. Res. Board Can.,* 19:1–37.

Heusser, C.J., 1983. Vegetational history of the Northwestern United States, including Alaska. *In* Porter, S.C. (Ed.), *Late Quaternary Environments of the United States*: Minneapolis (Univ. of Minnesota Press).

Hobson, L.A., and McQuoid, M.R., 1997. Temporal variations among planktonic diatom assemblages in a turbulent environment of the southern Strait of Georgia, British Columbia, Canada. *Mar. Ecol.: Prog. Ser.,* 150: 263–274.

Holland, S.S., 1964. Landforms of British Columbia: A physiographic outline. *Bull.—BC Dept. Mines Petrol. Resources,* 48:1–138.

Linden, R.H., and Schurer, P.J., 1988. Sediment characteristics and sea-level history of Royal Roads anchorage, Victoria, British Columbia. *Can. J. Earth Sci.,* 25:1800–1810.

Mathewes, R.W., 1993. Evidence for Younger Dryas-age cooling on the North Pacific coast of America. *Quat. Sci. Rev.,* 12:321–331.

Mathewes, R.W., 1985. Paleobotanical evidence for climatic change in southern British Columbia during late-glacial and Holocene time. *In* Harrington, C.R. (Ed), *Climate Change in Canada 5: Critical Periods in the Quaternary Climatic History of Northwestern North America.* Syllogeus, 55:397–422.

Muller, J.A., 1981. Geology of Victoria. *Geol. Surv. Can.,* Map 1553A.

Nissenbaum, A., Presley, B.J., and Kaplan, I.R., 1972. Early diagenesis in a reducing fjord, Saanich Inlet, British Columbia, I. Chemical and isotopic changes in major components of interstitial water. *Geochim. Cosmochim. Acta,* 36:1007–1027.

Pickard, G.L., 1975. Annual and longer term variations of the deepwater properties in the coastal waters of southern British Columbia. *J. Fish. Res. Board Can.,* 32:1561–1587.

Powys, R.I.L., 1987. The geochemistry and diatom assemblages of varved sediments from Saanich Inlet, B.C. [Ph.D. Dissertation]. University of British Columbia, Victoria, BC, Canada.

Presley, B.J., Kolodny, Y., Nissenbaum, A., and Kaplan, I.R., 1972. Early diagenesis in a reducing fjord, Saanich Inlet, British Columbia, II. Trace element distribution in interstitial water and sediment: *Geochim. Cosmochim. Acta,* 36:1073–1090.

Robinson, S.W., and Thompson, G., 1981. Radiocarbon corrections for marine shell dates with application to southern Pacific Northwest Coast prehistory. *Syesis,* 14:45–57.

Sancetta, C., 1989. Processes controlling the accumulation of diatoms in sediments: a model derived from British Columbian fjords. *Paleoceanography,* 4:235–251.

Sancetta, C., and Calvert, S.E., 1988. The annual cycle of sedimentation in Saanich Inlet, British Columbia: implications for the interpretation of diatom fossil assemblages. *Deep-Sea Res.,* 35:71–90.

Sims, J.D., 1975. Determining earthquake recurrence intervals from deformational structures in young lacustrine sediments. *Tectonophysics,* 29:141–152.

Stucchi, D.J., and Giovando, L., 1983. Deep water renewal in Saanich Inlet. *In* Juniper, S.K., and Brinkhurst, R.O. (Eds.), *Proc. Multidiscipl. Symp. Saanich Inlet, February 2, 1983.* Can. Tech. Rep. Fish. Aquat. Sci., 38:7–16.

Thomson, R.E., 1994. Physical oceanography of the Strait of Georgia-Puget Sound-Juan de Fuca Strait system. *In* Wilson, R.C.H., Beamish, R.J., Aitkens, F., and Bell, J. (Eds.), *Review of the Marine Environment and Biota*

of the Strait of Georgia, Puget Sound and Juand de Fuca Strait: Proceedings of the BC/Washington Symposium on the Marine Environment, January 13-14, 1994. Can. Tech. Rep. Fish. Aquat. Sci., 1948:36–100.

Whiticar, M.J., Hovland, M., Kastner, M., and Sample, J.C., 1995. Organic geochemistry of gases, fluids, and hydrates at the Cascadia accretionary margin. In Carson, B., Westbrook, G.K., Musgrave, R.J., and Suess, E. (Eds.), Proc. ODP, Sci. Results, 146 (Pt. 1): College Station, TX (Ocean Drilling Program), 385–397.

Ms 169IR-102

NOTE: For all sites drilled, core-description forms ("barrel sheets") can be found in Section 3, beginning on page 63.
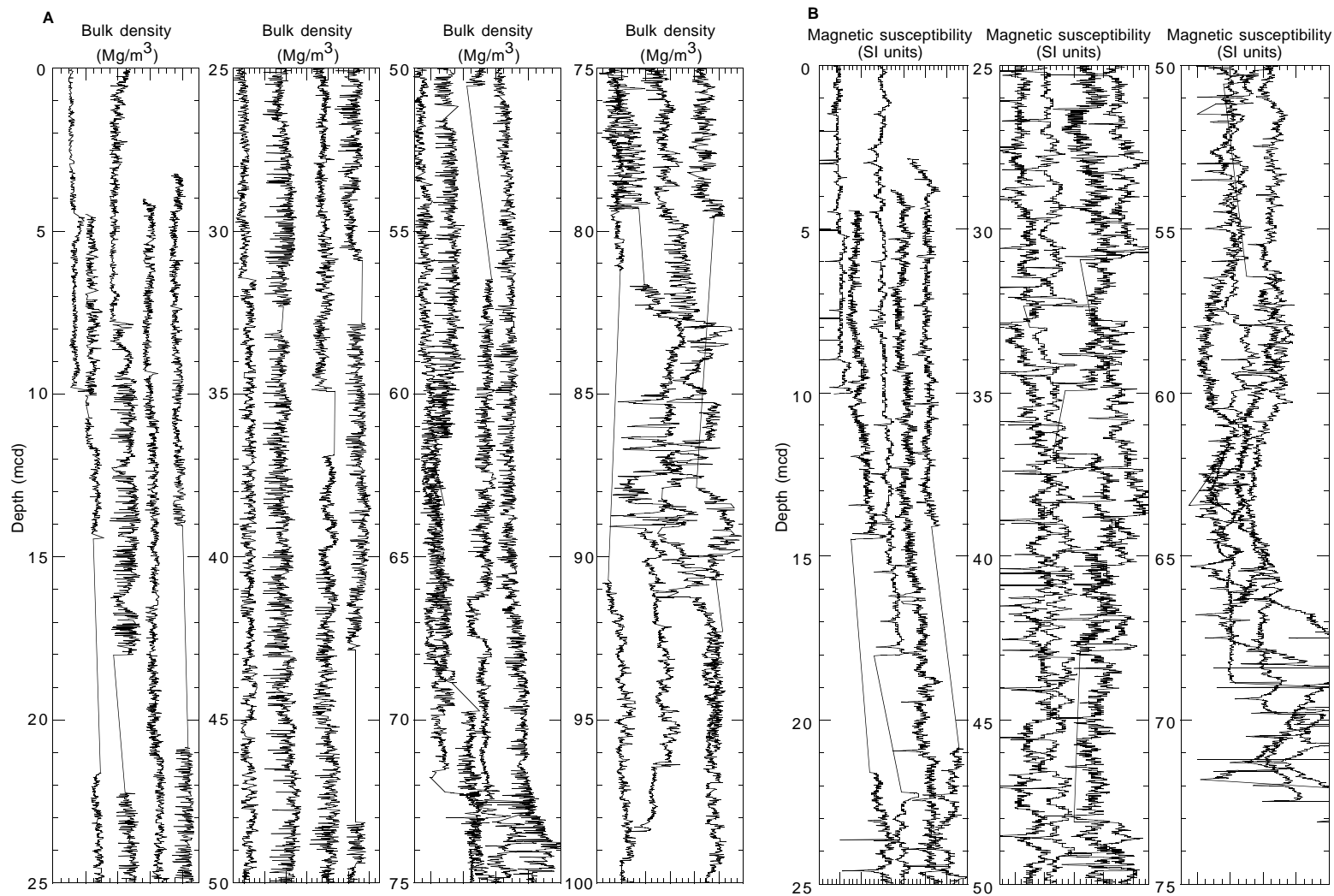
Figure 23. **A.** GRAPE bulk density data vs. depth for all holes at Site 1034. The density scale has ranges of 1.6 Mg/m³ for 0–25 mcd, 1.4 Mg/m³ for 25–50 mcd, 1.9 Mg/m³ for 50–75 mcd, and 1.2 Mg/m³ for 75–100 m. **B.** Magnetic susceptibility vs. depth for all holes at Site 1034. The scale has ranges of 75 SI units for 0–25 mcd and 50–75 mcd, and 70 SI units for 25–50 mcd. (continued on next page).
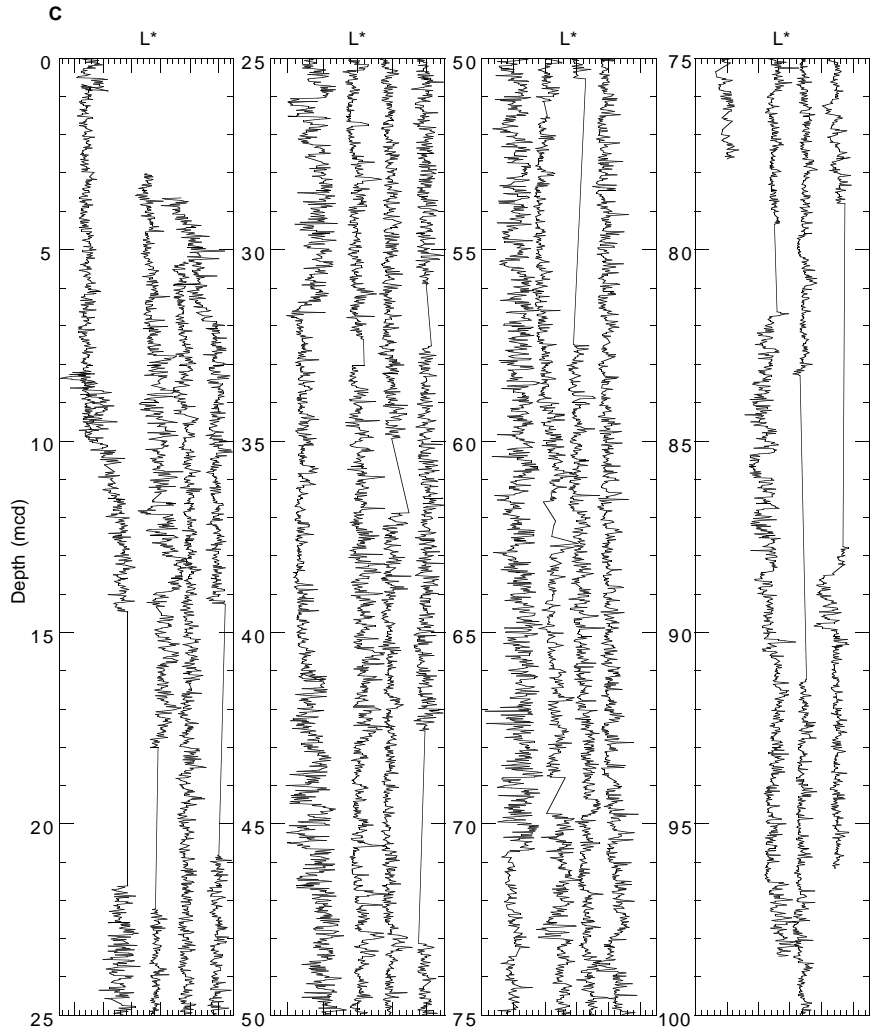
Figure 23 (continued). **C.** Color reflectance value L* vs. depth for all holes at Site 1034. The scale has ranges of 55 L* values for 0−25 mcd, 45 for 25−50 mcd, 50 for 50−75 mcd, and 60 for 75−100 mcd. The data from each hole are shifted so that plots from each hole are not overwritten.

Table 10. Offset depths for all cores at Site 1034.

Core	Depth (mbsf)	Offsets	Depth (mcd)
169S-1034A-			
1H*	0	0	0
169S-1034B-			
1H	0	7.6	7.6
2H	4.2	0.25	4.45
3H*	13.7	7.9	21.6
4H*	23.2	8.2	31.4
5H*	32.7	8.35	41.05
6H*	42.2	8.05	50.25
7H*	51.7	1.8	53.5
8H*	61.2	1.1	62.3
9H	70.7	0	70.7
10H	80.2	–8	72.2
11H	89.7	1	90.7
12H	99.2	0	99.2
13H	108.7	0	108.7
169S-1034C-			
1H	0	0	0
2H*	8	0	8
3H	17.5	4.7	22.2
4H	27	6	33
5H	36.5	4.6	41.1
6H	46	5.5	51.5
7H	55.5	4.5	60
8H*	65	5	70
9H	74.5	–4.8	69.7
10H	84	–2.4	81.6
11H	93.5	–4.4	89.1
169S-1034D-			
1H	0	0.25	0.25
2H	5.7	0.1	5.8
3H*	15.2	2.95	18.15
4H	24.7	5.9	30.6
5H	34.2	7.3	41.5
6H	43.7	8.35	52.05
7H	53.2	9.2	62.4
8H	62.7	11.5	74.2
9H*	72.2	0	72.2
10H*	81.7	0	81.7
11H*	91.2	0	91.2
169S-1034E-			
1H	0	2.85	2.85
2H	4	0.35	4.35
3H	13.4	7.9	21.3
4H	23	–2.2	20.8
5H	32.5	0.3	32.8
6H	42	6.1	48.1
7H	51.5	4.9	56.4
8H	61	2.35	63.35
9H*	70.5	–0.7	69.8
10H	80	7.75	87.75

Notes:* = cores used in composite splice. The offsets are simple linear shifts, calculated from the mbsf depth scale.
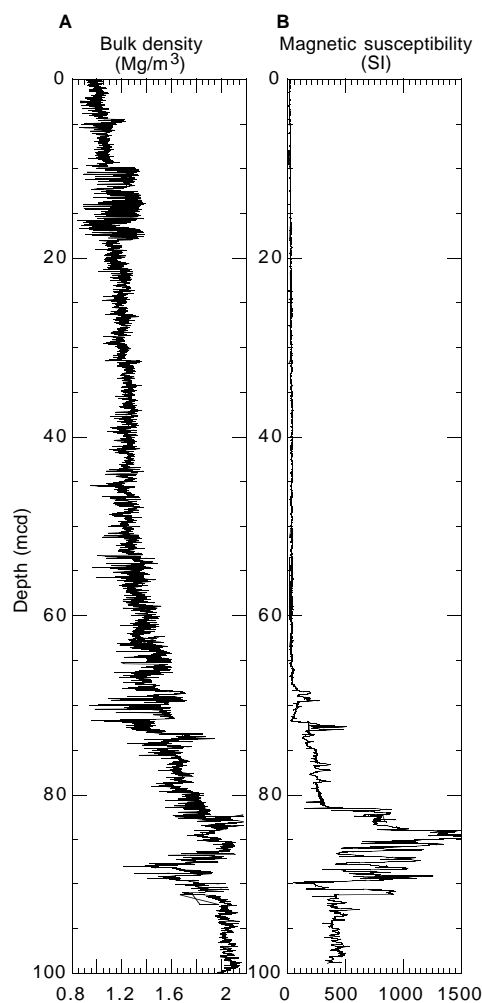
Figure 24. **A.** Composite of the spliced bulk density record vs. depth for site 1034. **B.** Composite of the spliced magnetic susceptibility record vs. depth for Site 1034.

Table 11. Uncorrected acoustic velocity measurements on discrete intervals for Hole 1034B.

Core, section, interval (cm)	Depth (mbsf)	Traveltime (µs)	Uncorrected velocity (km/s)	Temperature (°C)
169S-1034B-				
2H-1, 23	4.43	78.25	0.95	8.4
10H-6, 35	80.55	49.2	1.52	16.4
10H-7, 10	80.3	51.4	1.45	16.5
11H-1, 20	89.9	49.55	1.51	15.0
11H-2, 20	89.9	48.7	1.53	15.9
11H-3, 20	89.9	49.1	1.52	17.6
11H-4, 15	89.85	48.75	1.53	17.6
11H-5, 14	89.84	48.7	1.53	17.4
11H-6, 10	89.8	48.7	1.53	19.5
11H-7, 20	89.9	48.7	1.53	18.5
12H-1, 20	99.4	48.2	1.55	14.0
12H-2, 10	99.3	46.55	1.60	13.8
12H-3, 20	99.4	48.7	1.53	8.9
12H-4, 20	99.4	47.3	1.58	13.0
12H-5, 18	99.38	48.2	1.55	13.3
12H-6, 20	99.4	48.2	1.55	10.9
13H-1, 20	108.9	46.95	1.59	15.3
13H-2, 20	108.9	47.4	1.57	15.6
13H-3, 20	108.9	46.35	1.61	16.2
13H-4, 20	108.9	46.4	1.61	17.1
13H-4, 50	109.2	46.75	1.60	17.6
13H-5, 20	108.9	46.5	1.60	19.5
13H-6, 10	108.8	46.7	1.60	18.5
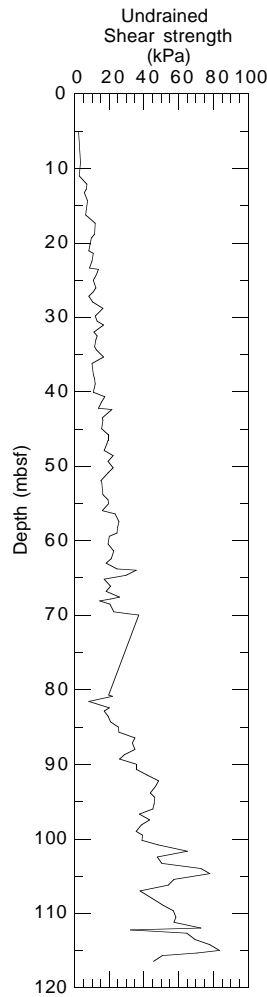
Figure 25. Undrained shear strength vs. depth for Hole 1034B.

Table 12. Headspace gas chromatographic results of Site 1033.

Core, section, interval (cm)	Uncorrected top core (mbsf)	Depth estimate (mbsf)	O_2	N_2	C_1	$C_2=$	C_2	H_2S	$C_3=$	C_3	C_1/C_2
169S-1033A-											
1H-2, 145–150	0	2.98	0	0	3,485	0	0	—	—	0	100,000
1H-4, 145–150	0	5.98	0	0	4,842	0	0	—	—	0	100,000
1H-6, 135–140	0	8.88	0	0	6,448	0	0	—	—	0	100,000
169S-1033B-											
1H-1, 0–5	0	0.03	0	0	15,896	0	0	—	—	0	100,000
2H-2, 145–150	0.06	3.04	0	0	3,195	0	0	—	—	0	100,000
2H-4, 145–150	0.06	6.04	0	0	5,578	0	0	—	—	0	100,000
2H-6, 145–150	0.06	9.04	0	0	7,696	0	0	—	—	0	100,000
3H-2, 145–150	10.1	13.08	0	0	9,997	0	0	—	—	0	100,000
3H-4, 145–150	10.1	16.08	0	0	7,971	0	0	—	—	0	100,000
3H-6, 145–150	10.1	19.08	0	0	10,145	0	0	—	—	0	100,000
4H-2, 145–150	19.6	22.58	0	0	8,147	0	0	—	—	0	100,000
5H-2, 145–150	29.1	32.08	0	0	6,703	0	0	—	—	0	100,000
6H-2, 145–150	38.6	41.58	0	0	7,721	0	0	—	—	0	100,000
7H-2, 145–150	48.1	51.08	0	0	29,510	0	0	—	—	0	100,000
8H-2, 145–150	57.6	60.58	0	0	1,858	0	0	—	—	0	100,000
9H-2, 145–150	67.1	70.08	0	0	19.4	0	0	—	—	0	100,000
10H-2, 145–150	76.6	79.58	0	0	9.44	0	0	—	—	0	100,000
11H-2, 145–150	86.1	89.08	0	0	14.52	0	0	—	—	0	100,000
12H-2, 145–150	95.5	98.48	0	0	8.74	0	0	—	—	0	100,000

Notes: — = no results. 100,000 = default value if C_2 is not present. All values are in ppmv.

Table 13. Vacutainer gas chromatographic results of Site 1033.

Core, section, interval (cm)	Uncorrected top core (mbsf)	Depth estimate (mbsf)	O₂	N₂	C₁	CO	CO₂	C₂=	C₂	H₂S	C₁/C₂
169S-1033A-											
1H-1, 118–118	0	1.18	1,735	18,561	912,566	—	54,086	—	—	225.0	100,000
1H-4, 110–110	0	5.60	127,327	536,073	294,706	—	15,516	—	—	102.0	100,000
1H-5, 118–118	0	7.18	3,257	20,246	876,422	—	84,782	—	—	27.0	100,000
169S-1033B-											
1H-1, 60–60	0.06	0.66	170,235	731,605	17,703	—	1,261	—	—	87.7	100,000
2H-3, 50–50	0.06	3.56	4,275	26,570	880,531	—	72,491	—	—	23.2	100,000
2H-5, 50–50	0.06	6.56	136,253	563,257	247,227	—	27,939	—	—	24.7	100,000
3H-7, 50–50	10.1	19.60	884	11,745	916,391	—	75,639	—	—	31.0	100,000
4H-3, 50–50	19.6	23.10	5,064	65,429	866,517	—	44,210	—	—	31.9	100,000
4H-6, 50–50	19.6	27.60	40,828	168,285	716,770	—	50,038	—	—	31.9	100,000
5H-3, 18–18	29.1	32.28	2,587	54,373	912,769	—	35,470	—	—	27.7	100,000
5H-6, 52–52	29.1	37.12	6,933	51,026	880,636	—	44,335	—	—	3.6	100,000
6H-1, 68–68	38.6	39.28	1,934	50,282	899,475	—	35,950	—	—	33.0	100,000
7H-3, 28–28	48.1	51.38	98,941	738,159	142,621	—	2,659	—	—	26.4	100,000
9H-2, 90–90	67.1	69.50	132,811	836,973	598.1	—	660	—	—	27.9	100,000

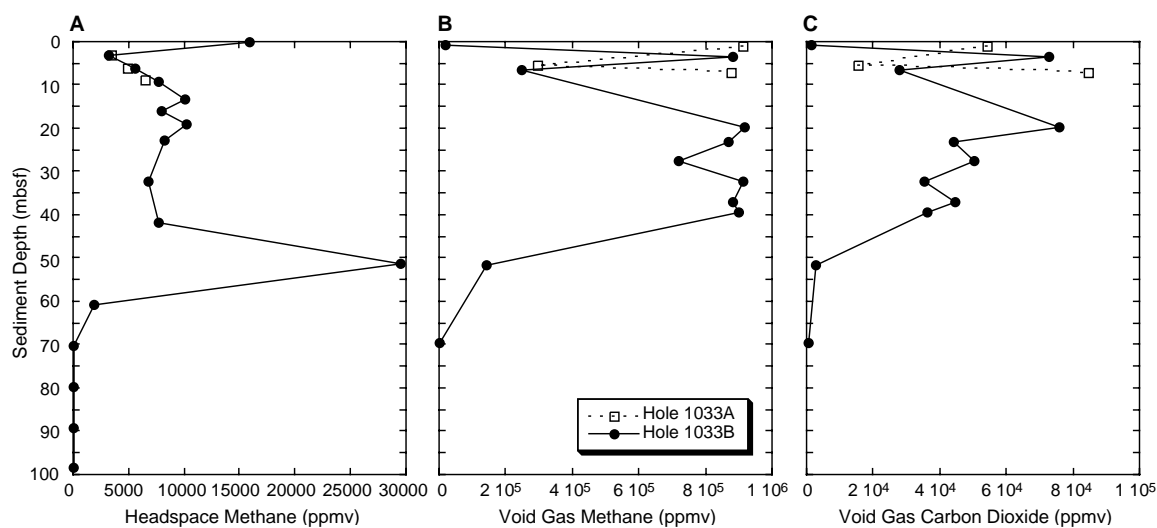Notes: — = no results. 100,000 = default value if C₂ is not present. All values are in ppmv.

Figure 26. Depth distribution of (**A**) headspace CH₄, (**B**) vacutainer CH₄, and (**C**) vacutainer CO₂ gases at Site 1033.
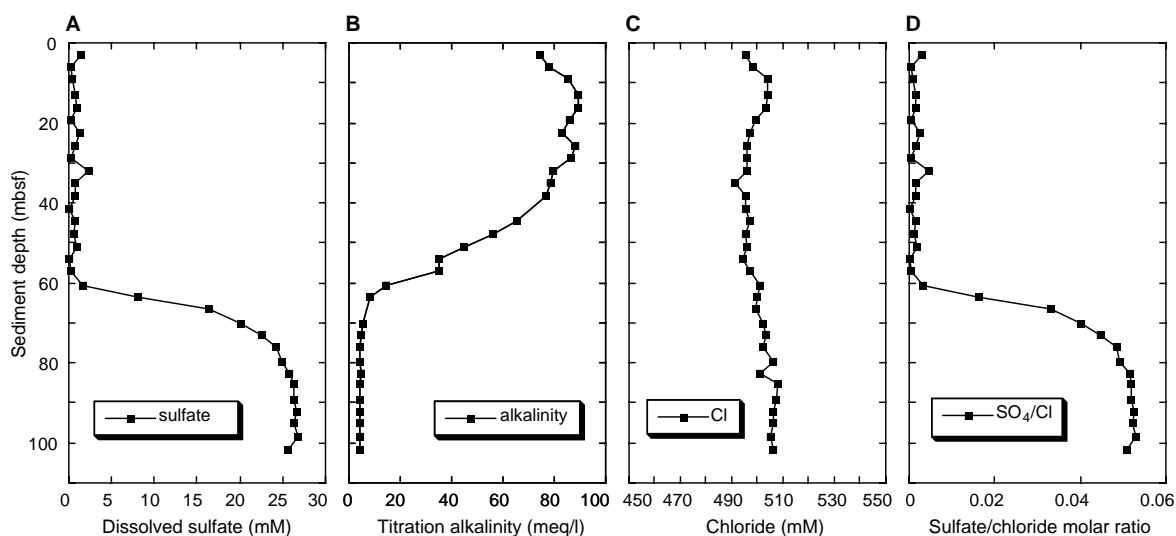

Figure 27. Depth distribution of dissolved (**A**) sulfate titration, (**B**) alkalinity, (**C**) chloride, and (**D**) sulfate/chloride ratio at Site 1033.
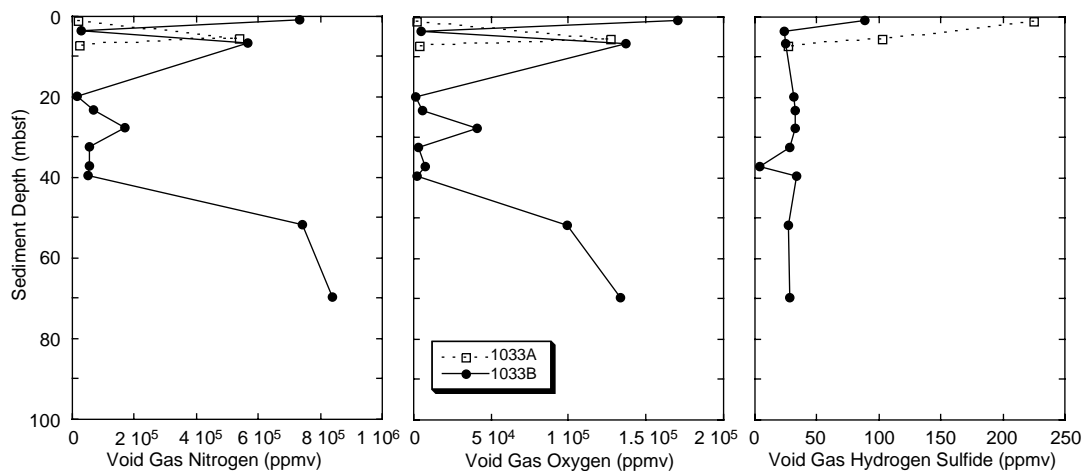
Figure 28. Depth distribution of vacutainer (**A**) N$_2$, (**B**) O$_2$, and (**C**) H$_2$S gases at Site 1033.

Table 14. C, N, and S analyses of organic matter and carbonate carbon at Site 1033.

| Core, section, interval (cm)	Depth (mbsf)	CaCO$_3$ (wt%)	C$_{org}$ (wt%)	S (wt%)	N$_{org}$ (wt%)
169S-1033B-					
2H-2, 139−145	3.5	1.00	2.50	1.15	0.42
2H-4, 139−145	6.5	1.75	2.25	1.13	0.75
2H-6, 139−145	9.5	1.75	2.31	0.98	0.45
3H-2, 139−145	13.0	1.33	2.35	0.97	0.38
3H-4, 139−145	16.0	0.00	2.77	1.27	0.36
3H-6, 139−145	19.0	1.58	2.18	1.39	0.34
4H-2, 139−145					
4H-4, 139−145	25.5	1.92	1.73	0.98	0.38
4H-6, 139−145	28.5	1.92	1.93	1.11	0.35
5H-2, 139−145	32.0	8.08	1.69	1.58	0.25
5H-4, 139−145	35.0	2.50	1.80	1.22	0.24
5H-6, 139−145	38.0	1.75	1.50	1.59	0.33
6H-2, 139−145	41.5	0.92	1.10	0.84	0.21
6H-4, 139−145	44.5	1.00	1.35	1.28	0.23
6H-6, 139−145	47.5	4.08	1.44	1.00	0.24
7H-2, 139−145	51.0	0.75	0.50	0.52	0.12
7H-4, 139−145	54.0	0.75	0.24	0.00	
7H-6, 139−145	57.0	0.75	0.31	0.07	0.05
8H-2, 139−145	60.5	1.58	0.26	0.00	
8H-4, 139−145	63.5	1.00	0.25	0.00	
8H-6, 139−145	66.5	1.33	0.24	0.00	
9H-2, 139−145	70.0	1.00	0.23	0.00	
9H-4, 139−145	73.0	1.33	0.21	0.00	0.05
9H-6, 139−145	76.0	1.17	0.18	0.00	0.08
10H-2, 131−145	79.5	1.08	0.27	0.00	0.05
10H-4, 131−145	82.5	1.25	0.21	0.00	0.09
10H-6, 131−145	85.5	1.08	0.16	0.00	0.05
11H-2, 131−145	89.0	1.58	0.19	0.00	0.05
11H-4, 133−147	92.0	1.08	0.25	0.00	0.05
11H-6, 57−71	95.0	1.25	0.19	0.00	0.06
12H-2, 131−145	98.4	0.58	0.30	0.00	0.06
12H-4, 131−145	101.4	1.17	0.21	0.00	0.10
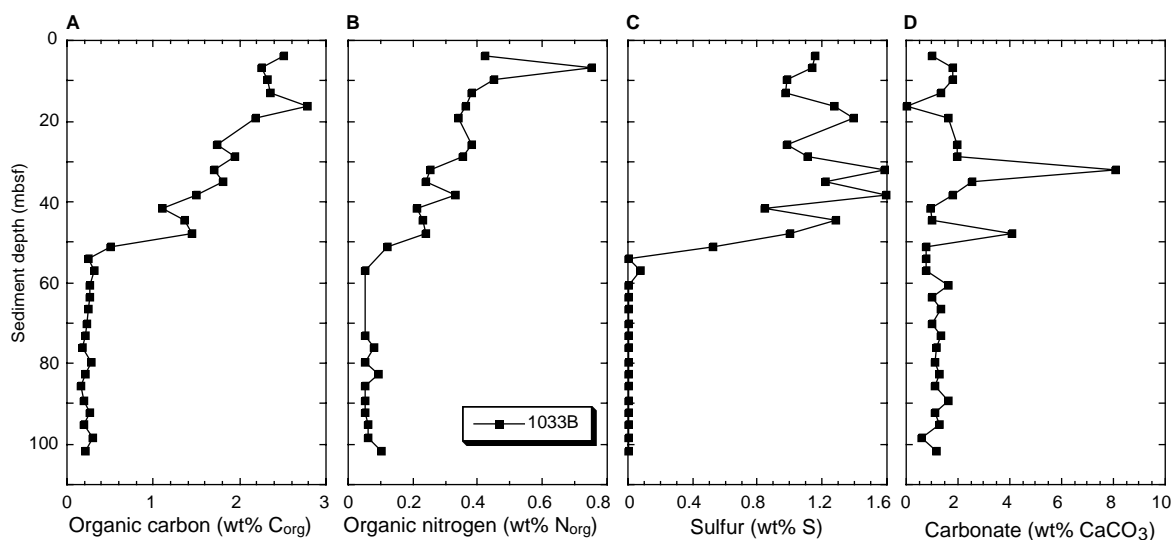
Figure 29. Depth distribution of (**A**) wt% organic carbon, (**B**) wt% organic nitrogen, (**C**) wt% sulfur, and (**D**) wt% carbonate at Site 1033.

Table 15. Headspace gas chromatographic results of Site 1034.

Core, section, interval (cm)	Uncorrected top core (mbsf)	Depth estimate (mbsf)	O_2	N_2	C_1	$C_2=$	C_2	H_2S	$C_3=$	C_3	C_1/C_2
169S-1034A-											
1H-2, 145–150	0	2.98	0	0	5,296	0	0	—	—	0	100,000
169S-1034B-											
1H-1, 60–60	0	0.60	0	0	8,997	0	0	—	—	0	100,000
1H-2, 145–150	0	2.98	0	0	4,352	0	0	—	—	0	100,000
2H-2, 145–150	4.2	7.18	0	0	7,820	0	0	—	—	0	100,000
2H-4, 145–150	4.2	10.18	0	0	11,338	0.6	0	—	—	0	100,000
2H-6, 145–150	4.2	13.18	0	0	4,442	0	0	—	—	0	100,000
3H-2, 145–150	13.7	16.68	0	0	7,800	0	0	—	—	0	100,000
3H-4, 145–150	13.7	19.68	0	0	4,649	0	0	—	—	0	100,000
3H-6, 145–150	13.7	22.68	0	0	5,399	0.5	0	—	—	0	100,000
4H-2, 145–150	23.2	26.18	0	0	6,564	0	0	—	—	0	100,000
4H-4, 145–150	23.2	29.18	0	0	8,034	0	0	—	—	0	100,000
4H-6, 145–150	23.2	32.18	0	0	7,839	0	0	—	—	0	100,000
5H-2, 145–150	32.7	35.68	0	0	7,372	0	0	—	—	0	100,000
6H-2, 145–150	42.2	45.18	0	0	8,017	0	0	—	—	0	100,000
7H-2, 145–150	51.7	54.68	0	0	4,784	0	0	—	—	0	100,000
8H-2, 145–150	61.2	64.18	0	0	6,192	0	0	—	—	0	100,000
10H-2, 145–150	80.2	83.18	0	0	19,308	0	0	—	—	0	100,000
11H-2, 145–150	89.7	83.18	0	0	681	0	0	—	—	0	100,000
12H-2, 145–150	99.2	92.68	0	0	45.8	0	0	—	—	0	100,000
13H-2, 145–150	108.7	102.18	0	0	13.6	0	0	—	—	0	100,000

Notes: — = no results. 100,000 = default value if C_2 is not present. All values are in ppmv.

Table 16. Vacutainer gas chromatographic results of Site 1034.

Core, section, interval (cm)	Uncorrected top core (mbsf)	Depth estimate (mbsf).	O_2	N_2	C_1	CO	CO_2	$C_2=$	C_2	H_2S	C_1/C_2
169S-1034A-											
1H-4, 0–1	0	4.51	124,073	508,350	315,601	—	32,406	—	—	26.0	100,000
1H-4, 89–89	0	5.39	27,880	113,147	873,883	—	60,048	—	—	28.0	100,000
169S-1034B-											
1H-1, 39–39	0	0.39	109,313	497,551	365,214	—	5,543	—	—	371.0	100,000
2H-1, 86–86	4.2	5.06	2,331	25,724	858,811	—	99,636	—	—	28.8	100,000
2H-5, 29–29	4.2	10.49	97,518	423,682	419,235	—	40,296	—	—	20.6	100,000
3H-4, 43–43	13.7	18.63	84,080	396,558	455,461	—	46,140	—	—	30.6	100,000
3H-6, 66–66	13.7	21.86	179,422	733,036	56,142	—	6,990	—	—	29.2	100,000
4H-1, 100–100	23.2	24.20	92,995	393,650	437,821	—	60,818	—	—	25.4	100,000
4H-6, 135–135	23.2	32.05	53,318	219,947	586,008	—	128,563	—	—	22.5	100,000
5H-3, 52–52	32.7	36.22	67,412	338,632	525,465	—	59,158	—	—	30.5	100,000
5H-4, 16–16	32.7	37.36	27,848	337,283	579,907	—	45,768	—	—	20.1	100,000
6H-2, 50–50	42.2	44.20	85,300	406,177	462,295	—	46,729	—	—	34.7	100,000
7H-2, 126–126	51.7	54.46	617	14,482	937,693	—	44,912	—	—	31.4	100,000
7H-3, 132–132	51.7	56.02	46,967	199,550	701,273	—	35,460	—	—	30.8	100,000
8H-2, 35–35	61.2	63.05	1,711	28,067	915,046	—	46,870	—	—	22.1	100,000
8H-5, 50–50	61.2	67.70	55,076	232,566	641,156	—	51,849	—	—	27.7	100,000
10H-1, 100–100	80.2	81.20	95,739	680,959	201,554	—	4,718	—	—	35.4	100,000
11H-6, 45–45	89.7	97.65	101,568	877,571	1,629	—	288	—	—	29.7	100,000
12H-6, 50–50	99.2	107.20	152,016	823,183	51.7	—	553	—	—	29.7	100,000

Notes: — = no results. 100,000 = default value if C_2 is not present. All values are in ppmv.

Table 17. C, N, and S analyses of organic matter and carbonate carbon at Site 1034.

Core, section, interval (cm)	Depth (mbsf)	$CaCO_3$ (wt%)	C_{org} (wt%)	S (wt%)	N_{org} (wt%)
169S-1034B-					
1H-1, 139–145	1.4	1.58	2.27	1.00	0.38
1H-3, 139–145	3.3	1.58	2.25	0.90	0.36
2H-2, 139–145	7.1	0.67	2.05	1.00	0.32
2H-4, 139–145	10.1	1.42	1.90	0.96	0.31
2H-6, 139–145	13.1	1.42	2.02	0.99	0.32
3H-2, 139–145	16.6	1.67	1.80	0.84	0.32
3H-4, 139–145	19.6	1.25	1.93	0.99	0.29
3H-6, 139–145	22.6	1.42	1.70	0.80	0.27
4H-2, 139–145	26.1	2.67	1.64	0.93	0.26
4H-4, 139–145	29.1	1.75	1.61	0.85	0.30
4H-6, 139–145	32.1	1.67	1.56	0.77	0.28
5H-2, 139–145	35.6	1.50	1.67	0.81	0.07
5H-4, 139–145	38.6	1.56	1.61	0.93	0.25
5H-6, 139–145	41.6	1.67	1.49	0.89	0.26
6H-2, 139–145	45.1	1.58	1.61	0.78	0.26
6H-4, 139–145	48.1	1.67	1.29	1.06	0.24
6H-6, 139–145	51.1	1.33	1.37	1.04	0.23
7H-2, 139–145	54.6	1.75	1.34	1.02	0.22
7H-4, 139–145	57.6	1.50	1.26	0.96	0.20
7H-6, 139–145	60.6	0.92	1.09	0.96	0.19
8H-2, 139–145	64.1	1.33	1.07	0.65	0.20
8H-4, 139–145	67.1	0.83	0.97	0.93	0.17
8H-6, 139–145	70.1	0.67	1.33	0.80	0.19
10H-2, 139–145	83.1	1.25	0.22	0.00	0.06
10H-4, 139–145	86.1	1.00	0.18	0.12	0.06
10H-6, 121–127	89.0	1.50	0.29	0.00	0.05
11H-2, 139–145	92.6	1.00	0.32	0.00	0.06
11H-4, 139–145	95.6	2.00	0.19	0.00	0.05
11H-6, 139–145	98.5	1.67	0.21	0.00	0.07
12H-2, 131–145	102.1	1.00	0.19	0.00	0.06
12H-4, 131–145	105.1	1.42	0.22	0.00	0.06
12H-6, 63–77	107.4	1.08	0.21	0.00	0.00
13H-2, 131–145	111.6	1.33	0.14	0.00	0.05
13H-4, 131–145	114.6	1.33	0.22	0.00	0.06
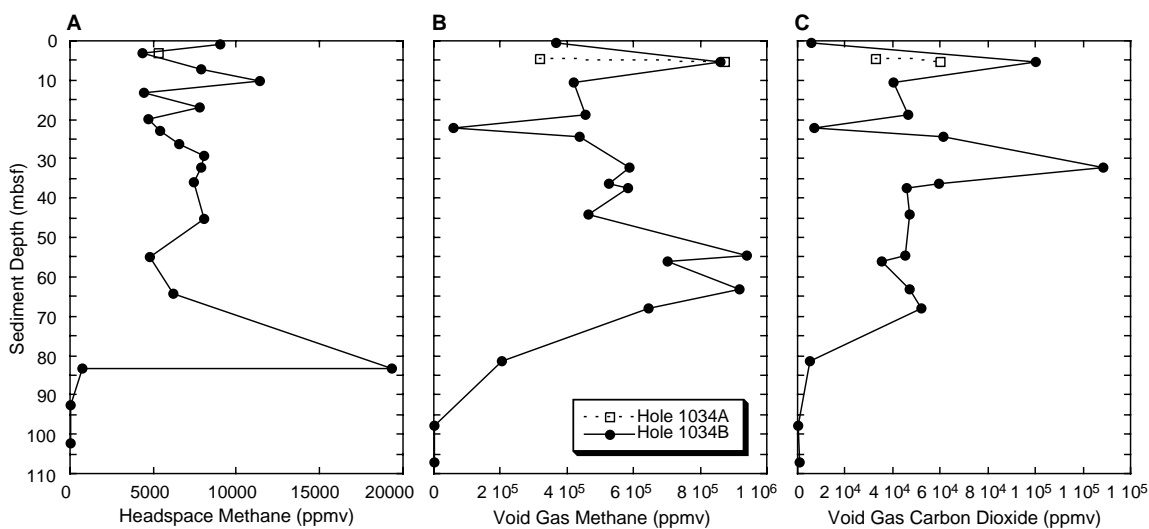
Figure 30. Depth distribution of (**A**) headspace CH$_4$, (**B**) vacutainer CH$_4$, and (**C**) vacutainer CO$_2$ gases at Site 1034.
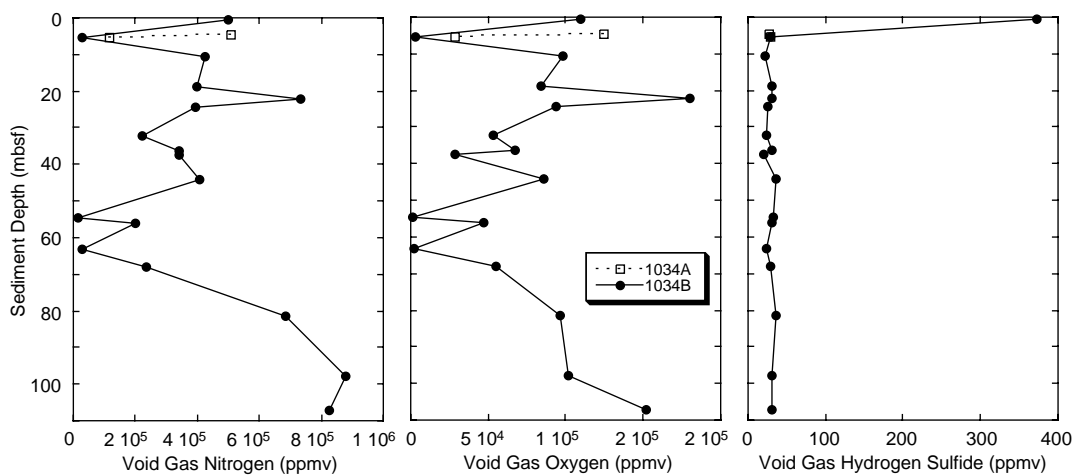
Figure 31. Depth distribution of vacutainer (**A**) N$_2$, (**B**) O$_2$, and (**C**) H$_2$S gases at Site 1034.
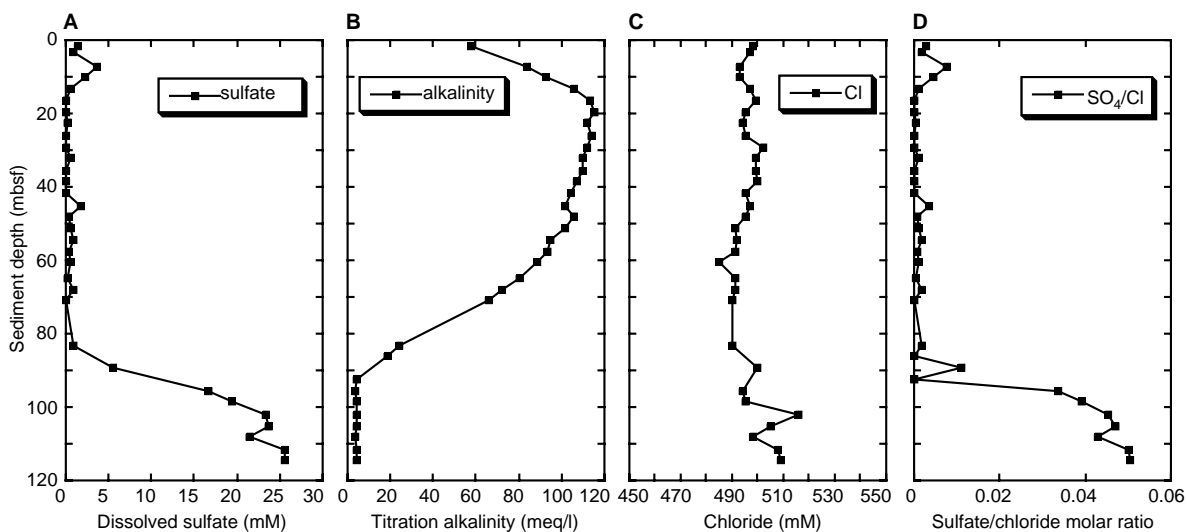
Figure 32. Depth distribution of (**A**) dissolved sulfate ratio, (**B**) titration alkalinity, (**C**) chloride, and (**D**) sulfate/chloride ratio at Site 1034.
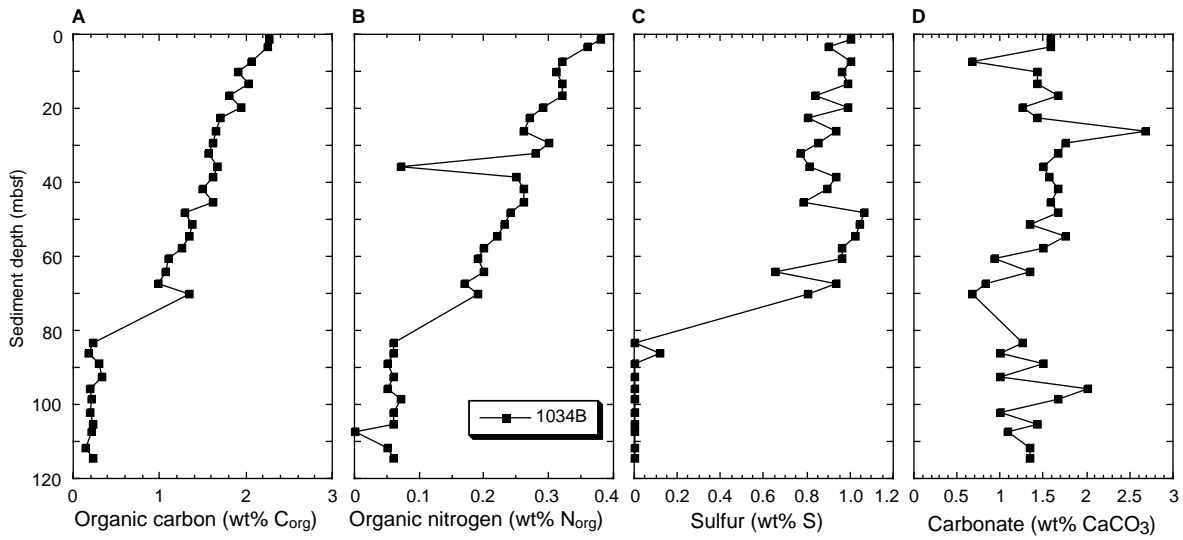
51

Figure 33. Depth distribution of (**A**) wt% organic carbon, (**B**) wt% organic nitrogen, (**C**) wt% sulfur, and (**D**) wt% carbonate at Hole 1034B.

Table 18. Results of interstitial water analyses at Site 1033.

Core, section, interval (cm)	Depth (mbsf)	pH	Alkalinity (mM)	Cl (mM)	Ca (mM)	Mg (mM)	Sr (µM)	K (mM)	Li (µM)	SO$_4$ (mM)	PO$_4$ (µM)	B (µM)	NH$_4$ (mM)	H$_4$SiO$_4$ (mM)	Na (mM)	Na/Cl
169S-1033B-																
2H-2, 139–145	3.5	7.83	74.2	495	8.90	49.4	74.3	10.5	16.7	1.4	301	583	10.5	1.03	435	0.88
2H-4, 139–145	6.5	7.85	77.7	498	9.50	51.8	72.4	10.8	17.7	0.2	382	719	12.7	1.03	430	0.86
2H-6, 139–145	9.5	7.92	84.9	504	8.65	52.9	83	11.4	19.6	0.4	325	743	14.0	1.05	441	0.88
3H-2, 139–145	13.0	7.93	89.1	504	7.40	53.8	69.2	11.4	20.1	0.7	192		15.3	1.06	446	0.88
3H-4, 139–145	16.0	7.88	89.0	503	6.22	54.0	74.2	11.2	20.4	0.8	247	827	16.5	1.02	445	0.89
3H-6, 139–145	19.0	8.06	86.0	499	5.43	52.7	62.2	11.3	20.5	0.2	179		15.9	0.93	442	0.89
4H-2, 139–145	22.5	7.87	82.8	497	4.82	53.1		10.8	21.8	1.2	206		15.1	1.07	441	0.89
4H-4, 139–145	25.5	7.92	88.2	496	4.52	55.3		11.1	20.2	0.7	344	1109	14.9	1.05	440	0.89
4H-6, 139–145	28.5	8.09	86.1	496	3.90	55.2	60.2	11.7	18.5	0.1	252		14.3	0.90	438	0.88
5H-2, 139–145	32.0	7.96	79.4	496	3.43	56.0		10.7	20.7	2.2	333		13.7	1.14	436	0.88
5H-4, 139–145	35.0	8.00	78.5	491	2.75	55.8		10.7	17.1	0.7	341	990	13.8	1.00	429	0.87
5H-6, 139–145	38.0	8.08	76.4	495	2.53	55.8	73.4	11.0	16.6	0.6	305		13.9	1.15	431	0.87
6H-2, 139–145	41.5			495	2.30	54.3		10.2	15.7	0.0	360		12.0	1.22		
6H-4, 139–145	44.5	7.98	65.1	497	2.82	52.0		10.4	14.2	0.7	236	839	9.8	0.99	433	0.87
6H-6, 139–145	47.5	7.96	56.0	495	2.77	50.5	85.9	9.32	11.4	0.4	152		8.3	1.10	427	0.86
7H-2, 139–145	51.0	7.93	44.4	496	3.32	47.0		7.81	8.4	0.8	104		5.6	1.06	428	0.86
7H-4, 139–145	54.0	7.92	34.9	494	3.55	44.3		6.76	6.2	0.0	73	405	4.1	0.59	422	0.85
7H-6, 139–145	57.0	7.96	34.8	497	3.64	45.0	84.3	7.25	6.6	0.2	59		4.1	0.65	424	0.85
8H-2, 139–145	60.5	8.03	14.4	501	3.69	40.8	107.7	5.24		1.6	0		1.7	0.29	423	0.84
8H-4, 139–145	63.5	7.97	8.3	500	8.12	42.0		5.26		8.0	44	257	1.1	0.27	418	0.84
8H-6, 139–145	66.5	8.03		499	13.7	43.5	100.3	4.60	9.7	16.4	0		0.7	0.30		
9H-2, 131–145	70.0	7.96	4.92	502	16.6	44.8	104.2	4.56	9.6	20.1	0		0.6	0.31	419	0.84
9H-4, 131–145	73.0	7.96	4.61	503	18.5	45.2	107.1	4.58	10.1	22.4	15	190	0.5	0.29	420	0.84
9H-6, 131–145	76.0	7.95	4.28	502	19.9	46.1		4.75	9.8	24.2			0.6	0.22	417	0.83
10H-2,131–145	79.5	7.93	4.20	506	20.2	45.7	107.2	4.79	10.5	24.8			0.6	0.21	423	0.84
10H-4, 131–145	82.5	8.00	4.32	501	20.5	46.1		4.69	10.6	25.8		160	0.5	0.21	418	0.84
10H-6, 131–145	85.5	8.05	4.19	508	20.4	45.4		4.86	10.5	26.3			0.5	0.20	428	0.84
11H-2, 131–145	89.0	7.98	3.95	507	20.5	44.3		4.63	10.3	26.2			0.5	0.25	428	0.85
11H-4, 133–147	92.0	7.96	3.98	506	21.1	44.5	110.7	5.20	10.0	26.6	0	156	0.5	0.27	427	0.84
11H-6, 57–71	95.0	8.03	3.98	506	20.8	44.7		4.92	9.9	26.3			0.5	0.23	426	0.84
12H-2, 131–145	98.4	8.03	4.01	505	22.0	43.4		4.52	9.2	26.7		114	0.5	0.23	426	0.84
12H-4, 131–145	101.4	8.03	3.75	506	22.3	43.1	113.2	4.58	8.9	25.6		62	4.0	0.21	422	0.83

Table 19. Results of interstitial water analyses at Site 1034.

| Core, section, interval (cm)	Depth (mbsf)	pH	Alkalinity (mM)	Cl (mM)	Ca (mM)	Mg (mM)	Sr (μM)	K (mM)	Li (μM)	SO₄ (mM)	PO₄ (μM)	B (μM)	NH₄ (mM)	H₄SiO₄ (mM)	Na (mM)	Na/Cl
169S-1034B-																
1H-1, 139–145	1.4	8.08	57.3	498	8.5	45.1	72.7	10.1	13	1.3	220	419	5.5	1.27	435	0.874
1H-3, 139–145	3.3			497	9.5	48.3	71.7	10.7	14	0.8	192	661	9.4	1.41		
2H-2, 139–145	7.1	7.93	83.4	493	9.3	51.7	72.0	11.0	20	3.7	220		12.2	0.93		
2H-4, 139–145	10.1	7.93	92.8	493	9.2	53.6		12.3		2.2	197	685	15.2	1.0	437	0.887
2H-6, 139–145	13.1	7.92	105.7	497	9.2	56.4	75.7	12.3	26	0.4	243		17.4	0.95	443	0.891
3H-2, 139–145	16.6	7.88	113.0	499	8.9	57.5	73.5	12.2		0.0	208		17.7	0.96	449	0.900
3H-4, 139–145	19.6	7.93	115.0	495	9.15	56.9	72.8	11.9	21	0.0	254	752	18.6	1.03	447	0.904
3H-6, 139–145	22.6	7.93	112.0	494	8.7	58.6	69.8	11.8		0.2	167		18.7	0.88	441	0.893
4H-2, 139–145	26.1	7.93	114.0	495	7.45	58.4	70.9	12.4	21	0.0	200		18.6	0.92	446	0.902
4H-4, 139–145	29.1	7.92	112.0	502	7.4	58.8		12.7		0.0	128	887	19.4		450	0.895
4H-6, 139–145	32.1	7.96	110.0	499	7.0	58.8		12.3	20	0.6	149		20.7	0.83	446	0.893
5H-2, 139–145	35.6	7.93	110.0	499	6.8	60.1	62.2	11.4		0.0	171		19.1	0.93	445	0.891
5H-4, 139–145	38.6	7.96	107.0	500	5.5	60.9		12.7	20	0.1	122	828	19.0	0.78	442	0.885
5H-6, 139–145	41.6	8.06	104.0	495	4.9	61.0	61.8	12.6		0.0	135		17.6	0.80	437	0.883
6H-2, 139–145	45.1	7.88	101.8	497	4.8	62.6		12.1	21	1.7	151	796	18.1	0.96	437	0.880
6H-4, 139–145	48.1	7.90	105.5	495	4.7	62.3		12.0		0.4	364		16.3	1.00	439	0.887
6H-6, 139–145	51.1	8.10	101.6	491	4.4	62.1	63.8	12.4		0.6	318		16.2	0.85	432	0.880
7H-2, 139–145	54.6	8.01	94.4	492	4.0	61.1		11.6	19	0.9	282	679	15.8	0.88	431	0.875
7H-4, 139–145	57.6	8.06	93.4	491	3.7	61.2		11.8		0.4	307		14.1	0.99	430	0.875
7H-6, 139–145	60.6	8.10	88.7	485	3.9	59.6	65.9	11.3		0.5	315		11.8	0.94	425	0.876
8H-2, 139–145	64.1	7.93	80.1	491	4.4	57.6		11.4	17	0.2	184	563	11.4	0.92	425	0.865
8H-4, 139–145	67.1	7.98	72.0	491	3.6	57.0	68.7	10.6		0.8	84		10.7	0.70	422	0.860
8H-6, 139–145	70.1	7.87	66.0	490	4.0	55.1	72.8	9.5	15	0.1	182	230	9.8	1.06	419	0.854
10H-2, 139–145	83.1	7.93	24.2	490	4.8	43.2	89.5	5.3	5	0.9	44		2.8	0.33	412	0.841
10H-4, 139–145	86.1	8.13	18.3													
10H-6, 121–127	89.0	7.98		500	7.3	41.9	90.3	4.55	8	5.5	0		1.1	0.22		
11H-2, 139–145	92.6	7.89	4.47													
11H-4, 139–145	95.6	8.13	3.79	494	16.2	41.7	98.9	4.54	7	16.6	0	171	0.6	0.16	410	0.830
11H-6, 139–145	98.5	7.77	3.9	495	18.0	42.2	102	4.55		19.4	0		0.7	0.18	412	0.832
12H-2, 131–145	102.1	7.96	3.89	516	21.5	43.3	111.3	4.38		23.4	0		0.5	0.18	432	0.838
12H-4, 131–145	105.1	8.23	4.03	505	22.3	43.0	110.8	4.78	9	23.7	0	139	0.4	0.16	421	0.833
12H-6, 63–77	107.4	7.95	3.46	498	20.9	42.8	110.5	4.63		21.4	0		0.4	0.19	412	0.827
13H-2, 131–145	111.6	8.01	3.91	508	22.4	43.7	113.5	4.57		25.5	0		0.5	0.18	426	0.838
13H-4, 131–145	114.6	8.05	3.89	509	22.4	42.5	111.3	4.49	8	25.6	0	155	0.3	0.2	430	0.844
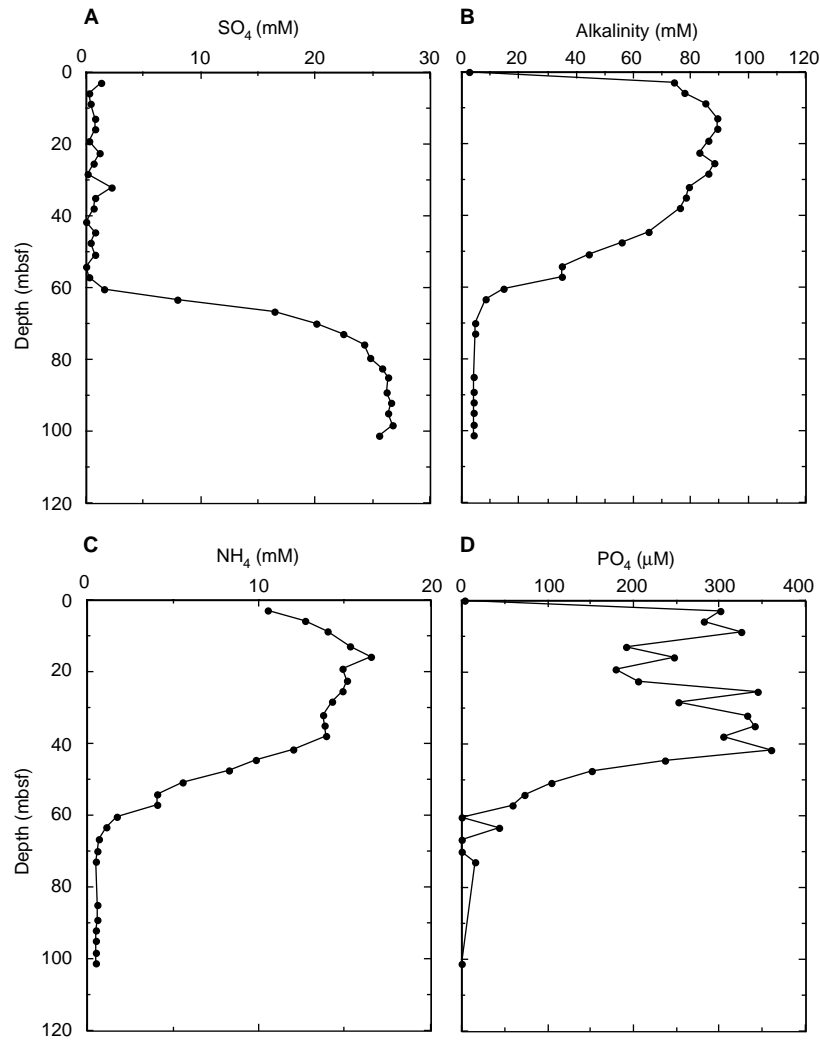
Figure 34. Depth distribution of major nutrients at Hole 1033B. **A**. Dissolved sulfate. **B**. Alkalinity. **C**. Ammonia. **D**. Phosphate.
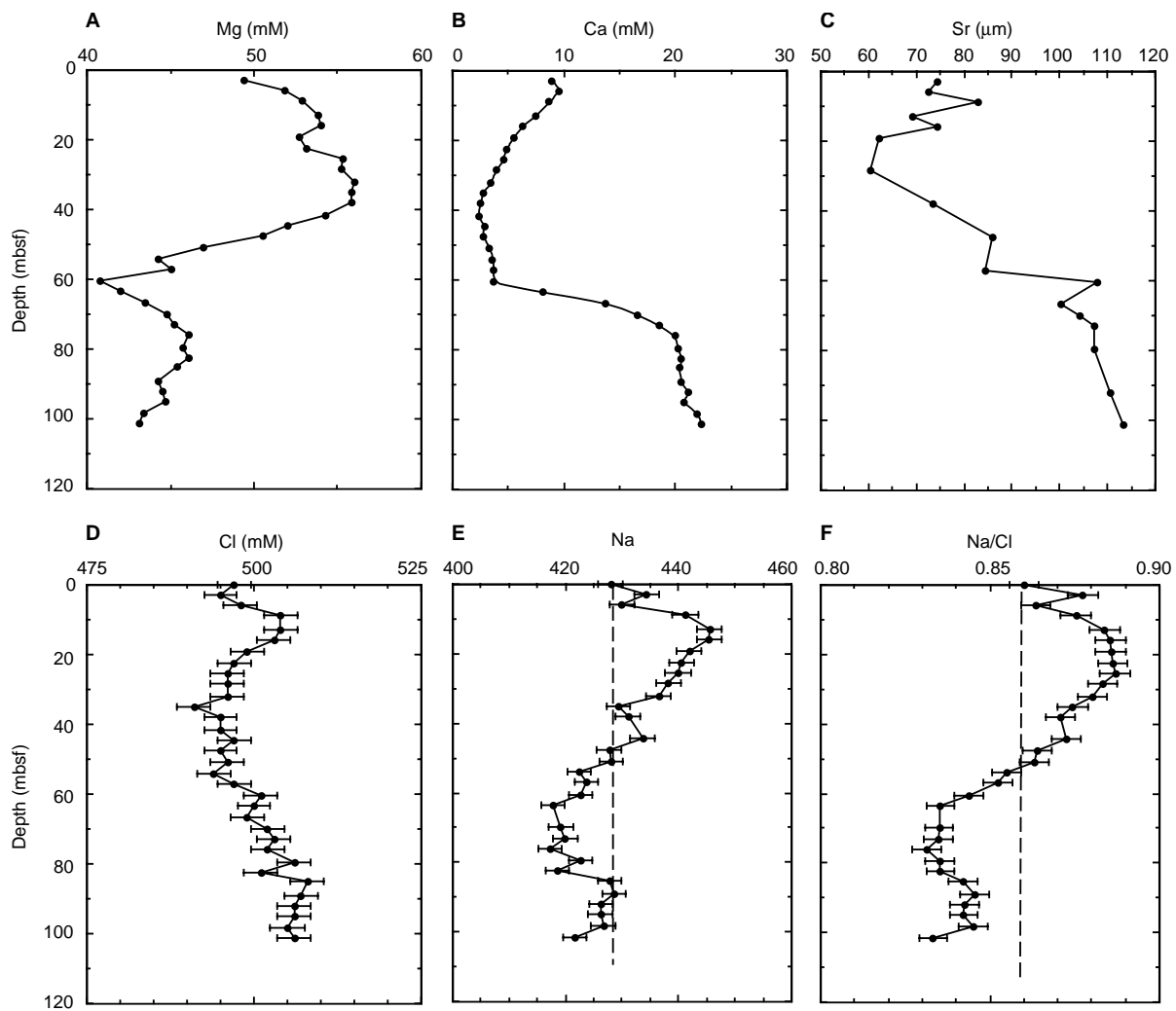
Figure 35. Depth distribution of (**A**) dissolved magnesium, (**B**) calcium, (**C**) strontium, (**D**) chlorine, (**E**) sodium, and (**F**) sodium/chloride ratio at Hole 1033B.
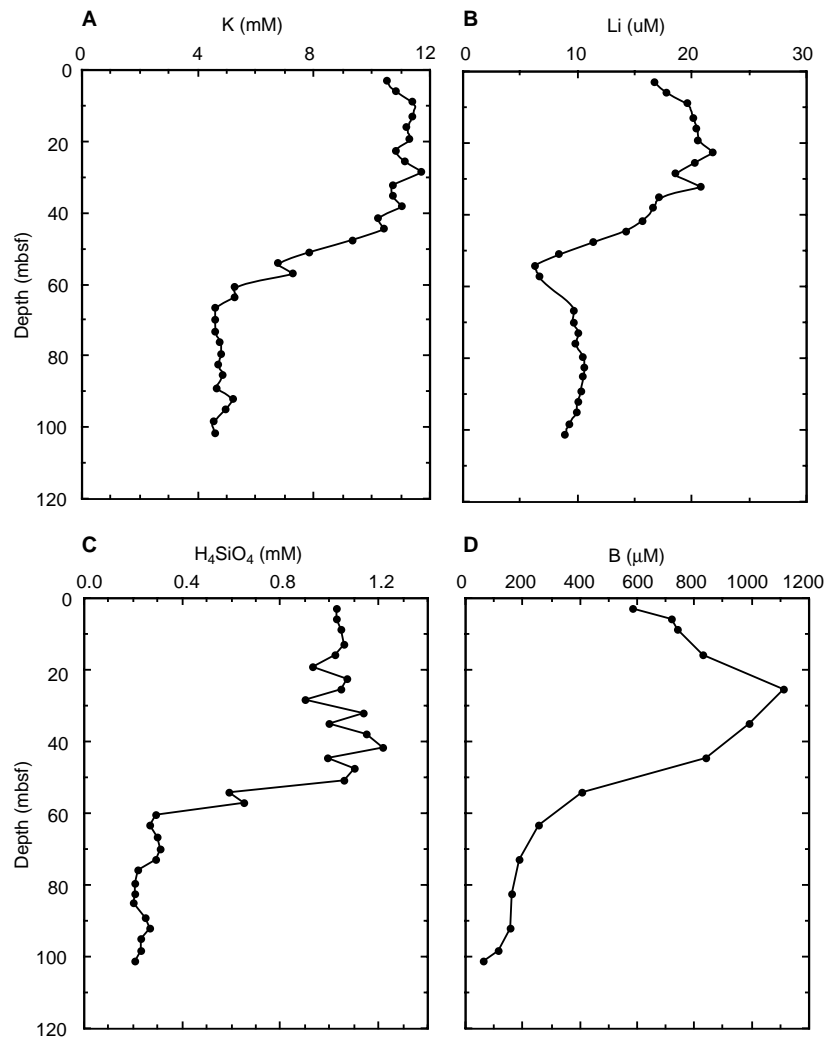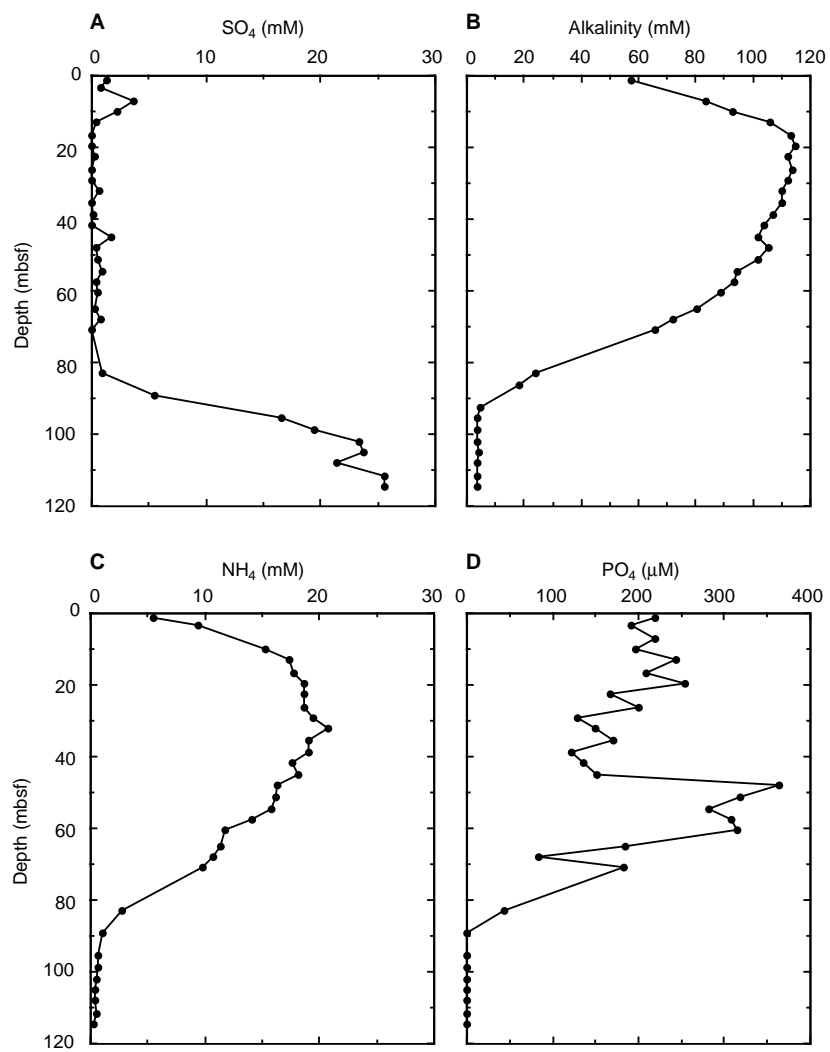
Figure 36. Depth distribution of dissolved (**A**) potassium, (**B**) lithium, (**C**) silica, and (**D**) boron at Hole 1033B.

Figure 37. Depth distribution of major nutrients at Hole 1034B. **A**. Dissolved sulfate. **B**. Alkalinity. **C**. Ammonia. **D**. Phosphate.
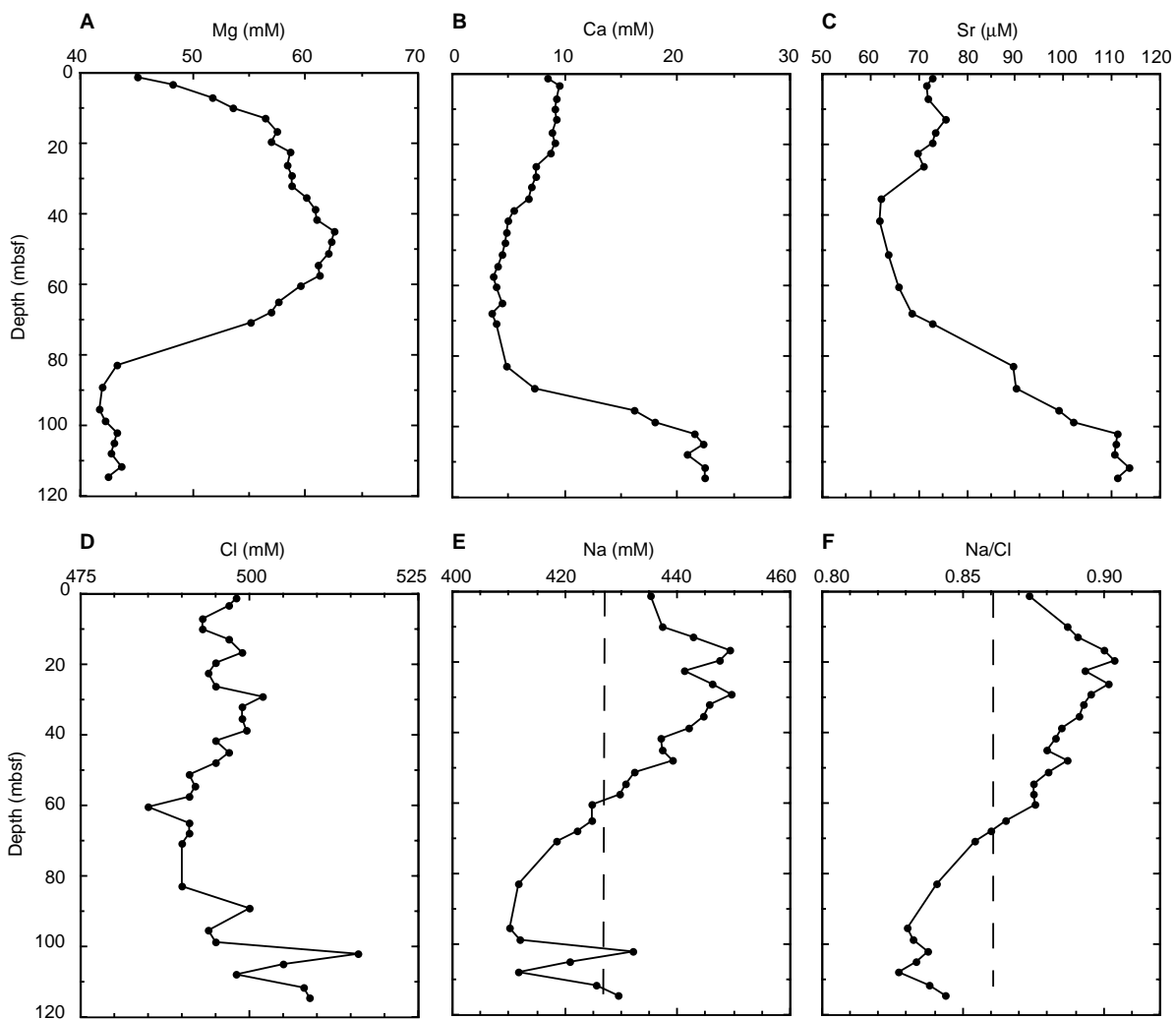
Figure 38. Depth distribution of dissolved (**A**) magnesium, (**B**) calcium, (**C**) strontium, (**D**) chlorine, (**E**) sodium, and (**F**) sodium/chloride ratio at Hole 1034B.
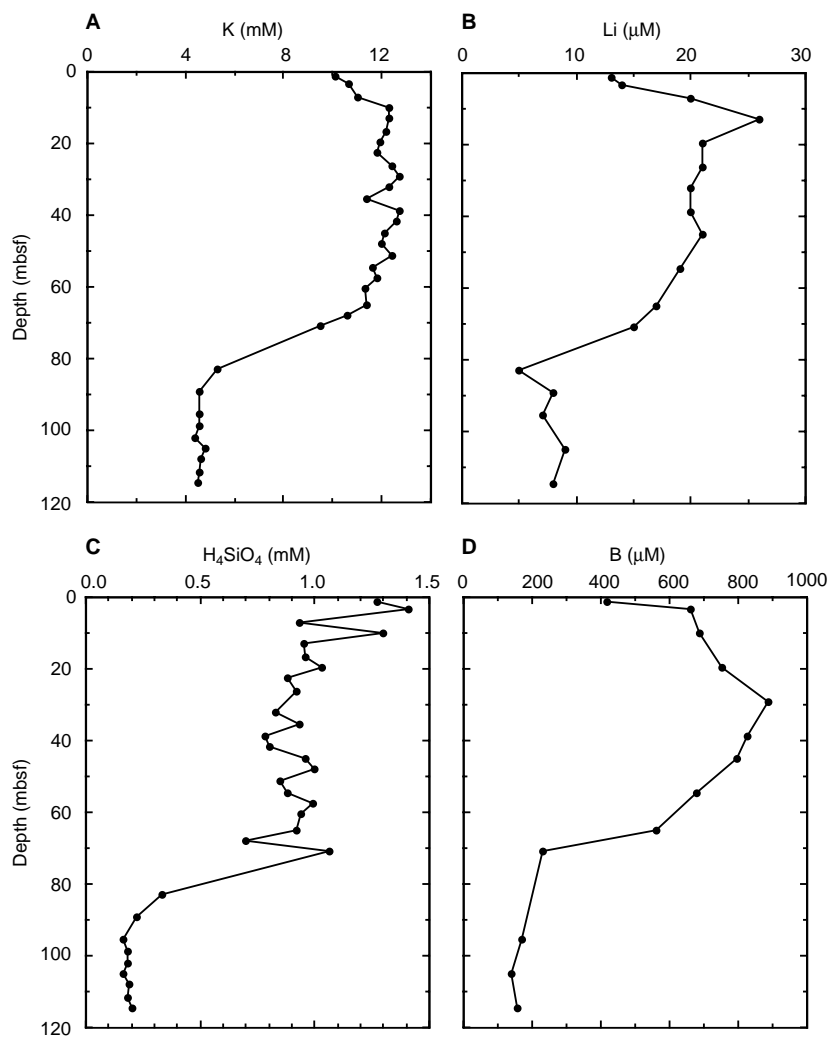
Figure 39. Depth distribution of dissolved (**A**) potassium, (**B**) lithium, (**C**) silica, and (**D**) boron at Hole 1034B.

Table 20. Identified shell and plant material from Sites 1033 and 1034.

Core, section, interval (cm)	Depth (mbsf)	Sample	Taxon
169S-1033B-			
2H-7, 28	9.88	Shell	Bivalvia *Compsomyax subdiaphana**
6H-2, 15	40.25	Shell	Bivalvia *Macoma calcarea**
6H-2, 60	40.70	Shell	Bivalvia *Axinopsida serricata**
6H-2, 90	41.00	Shell	Bivalvia *Axinopsida serricata**
6H-4, 110	44.20	Shell	Bivalvia *Axinopsida serricata**
6H-5, 135	45.95	Shell	Bivalvia *Macoma calcarea**
6H-5, 141	46.01	Shell	Bivalvia *Macoma calcarea**
6H-6, 13	46.23	Shell	Bivalvia *Macoma calcarea**
6H-6, 88	46.98	Shell	Bivalvia *Macoma calcarea**
169S-1033C-			
2H-5, 113	13.33	Shell	Cirripedia *Balanus nubilus*
3H-1, 37	16.07	Wood	Pacific Yew *Taxus brevifolia**
5H-6, 51	42.63	Shell	Cirripedia *Balanus nubilus**
5H-7, 56	43.95	Wood	Pacific Yew *Taxus brevifolia**
6H-3, 91	48.11	Shell	Bivalvia *Macoma calcarea*
6H-4, 20	48.90	Shell	Bivalvia *Macoma calcarea*
6H-6, 58	52.28	Shell	Bivalvia *Nuculana fossa*
4H-1, 124	23.44	Shell	Cirripedia *Balanus nubilus**
5H-3, 4	34.74	Shell	Bivalvia *Axinopsida serricata*
5H-3, 51	35.21	Shell	Bivalvia *Axinopsida serricata*
5H-4, 55	36.75	Wood	Moss *Isothecium stoloniferum*
6H-2, 100	43.70	Shell	Bivalvia *Macoma calcarea*
6H-2, 132	44.02	Shell	Bivalvia *Macoma calcarea*
6H-3, 3	44.16	Shell	Bivalvia *Macoma calcarea*
6H-4, 137	47.00	Shell	Bivalvia *Macoma carlottensis**
6H-5, 42	47.55	Shell	Bivalvia *Macoma calcarea*
6H-5, 75	47.88	Shell	Bivalvia *Macoma calcarea*
7H-2, 5	52.25	Shell	Gastropoda *Cylichna alba**
169S-1034B-			
2H-4, 118	9.88	Shell	Bivalvia *Mytilus edulis**
6H-1, 36	42.56	Shell	Bivalvia *Clinocardium nuttalli**
6H-CC, 0	52.10	Shell	Bivalvia *Macoma calcarea**
7H-4, 107	57.27	Shell	Bivalvia *Macoma calcarea**
8H-2, 57	63.27	Shell	Bivalvia *Macoma calcarea**
8H-5, 16	67.36	Shell	Bivalvia *Macoma calcarea**
9H-5, 21	76.49	Shell	Bivalvia *Nuculana fossa**
169S-1034C-			
2H-3, 61	11.61	Shell	Gastropoda *Littorina sitkana*
6H-3, 110	50.10	Wood	Western Red Cedar *Thuja plicata**
6H-5, 125	53.25	Shell	Bivalvia *Axinopsida serricata*
6H-5, 141	53.41	Shell	Bivalvia *Axinopsida serricata*
6H-6, 72	54.22	Shell	Bivalvia *Axinopsida serricata*
9H-5, 60	81.10	Shell	Scaphopoda *Rhabdus rectius**
10H-5, 112	91.12	Shell	Bivalvia *Yoldia martyria*
10H-7, 4	92.54	Shell	Bivalvia *Yoldia martyria*
10H-7, 36	92.86	Shell	Bivalvia *Yoldia martyria*
10H-7, 49	92.99	Shell	Bivalvia *Yoldia martyria**
169S-1034D-			
8H-3, 143	67.13	Shell	Bivalvia *Nuculana fossa**
8H-7, 7	71.77	Shell	Bivalvia *Macoma calcarea*
9H-1, 50	72.70	Shell	Bivalvia *Compsomyax subdiaphana*
9H-2, 75	74.45	Shell	Bivalvia *Macoma lipara*
9H-4, 147	78.17	Shell	Bivalvia *Nuculana fossa*
9H-5, 24	78.44	Shell	Bivalvia *Compsomyax subdiaphana*
169S-1034E-			
8H-1, 12	61.12	Shell	Bivalvia *Macoma calcarea*
8H-3, 114	65.14	Shell	Bivalvia *Macoma calcarea*
8H-4, 35	65.85	Shell	Bivalvia *Macoma calcarea*
8H-4, 78	66.28	Shell	Bivalvia *Macoma calcarea*
8H-6, 100	69.50	Shell	Bivalvia *Macoma calcarea*
9H-1, 19	70.69	Wood	Pacific Yew *Taxus brevifolia**
9H-1, 133	71.83	Shell	Bivalvia *Macoma calcarea**
9H-2, 118	73.18	Shell	Bivalvia *Macoma calcarea*
9H-4, 64	75.64	Shell	Bivalvia *Nuculana fossa**

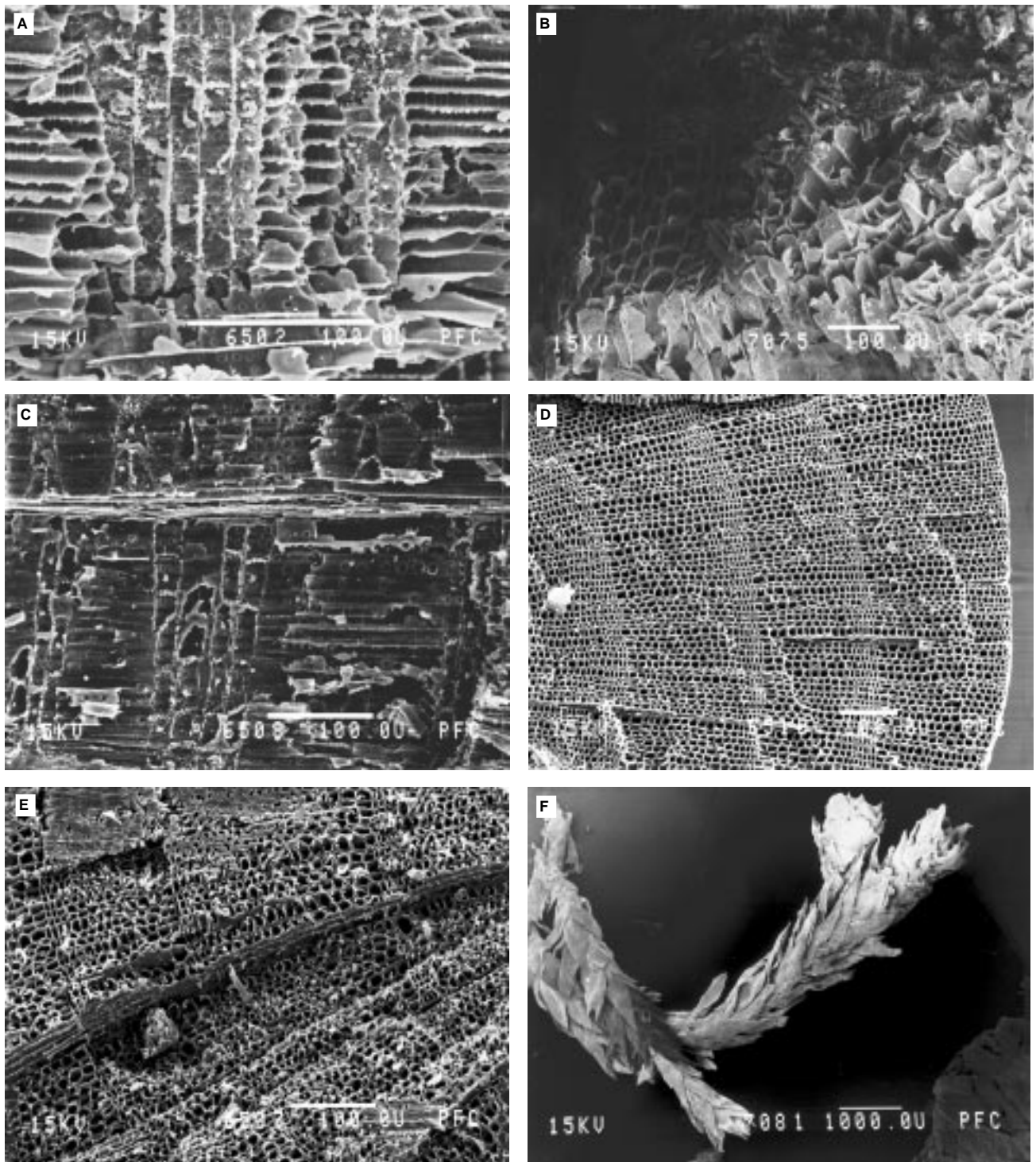Note: * = radiocarbon dated by AMS.

Figure 40. Scanning electron micrographs of identified plant fragments from Sites 1033 and 1034. A, B, and E = *Taxus brevifolia* (Pacific Yew). C and D = *Thuja plicata* (Western Red Cedar). F = *Isothecium stoloniferum.* Scale bar in micrometers.